THESIS
2
(1998)

MICHIGAN STATE UNIVERSITY LIBRARIES
3 1293 01706 9810

This is to certify that the

thesis entitled

Studies on Polymer Alloying
using Reactive Extrusion

presented by

Dimitrios Argyropoulos

has been accepted towards fulfillment
of the requirements for

M.S. degree in Chem. Eng.

Ramani Narayan
Major professor

Date 2/28/92

O-7639 *MSU is an Affirmative Action/Equal Opportunity Institution*

LIBRARY
Michigan State
University

PLACE IN RETURN BOX
to remove this checkout from your record.
TO AVOID FINES return on or before date due.

DATE DUE	DATE DUE	DATE DUE
JUL 2 9 2006 052009		

1/98 c:/CIRC/DateDue.p65-p.14

STUDIES ON POLYMER ALLOYING
USING REACTIVE EXTRUSION

By

Dimitrios Christos Argyropoulos

A THESIS

Submitted to
Michigan State University
in partial fulfillment of the requirements
for the degree of

MASTER OF SCIENCE

DEPARTMENT OF CHEMICAL ENGINEERING

1992

ABSTRACT

STUDIES ON POLYMER ALLOYING
USING REACTIVE EXTRUSION

By

Dimitrios Christos Argyropoulos

Polysaccharides and functionalized synthetic polymers have been blended by reactive extrusion processing to prepare filled composites or polymer alloys. The effect of various reaction parameters on the morphology, interfacial adhesion, and properties of the resulting materials was studied. In the first part of the work, high amylose starch filled SMA (random styrene maleic anhydride copolymer) composites were prepared. The maleic anhydride (MA) functionality provided for better adhesion to the starch granules. An acceptable reduction of the tensile strength, a retention of the Izod impact strength and an increase of the modulus was generally observed compared to the base resin. In the second part of the work, cellulose acetate (CA) alloys with SMA were prepared. In the presence of catalyst, CA-SMA graft copolymer was generated in situ by reaction of the anhydride groups on the SMA with the hydroxyls on CA, and interfacial adhesion was improved. Reduction of the dispersed phase size was the main morphological result of the compatibilization. The tensile strength, elongation and Izod impact strength of the blends were significantly improved. The maximum tensile strength observed was ~11,000 psi.

Copyright by
DIMITRIOS CHRISTOS ARGYROPOULOS
1992

... to my parents

ACKNOWLEDGMENTS

Many people helped me in different ways during my work. I want to thank them all, and specially my advisor, Dr. Ramani Narayan, for his guidance and support. I would prefer, however, not to mention other names, because I am afraid of forgetting someone. I just want to say that the people of the Composite Materials and Structures Center, the Center for Electron Optics, Michigan Biotechnology Institute and the Chemical Engineering Department, not only helped me, but also provided an excellent working environment. Special thanks to my friends who helped in their own way.

TABLE OF CONTENTS

Chapter Page

LIST OF TABLES ix

LIST OF FIGURES x

ABBREVIATIONS xvi

1 INTRODUCTION 1

Terminology 2

The problem and the solution 3

The work and the thesis 4

2 BACKGROUND - LITERATURE REVIEW 7

POLYMER BLENDS 7

Basic thermodynamics 9

Blend preparation 10

Miscibility determination 11

Blend morphology 13

COMPATIBILIZATION 16

FILLED POLYMERS 20

REACTIVE EXTRUSION 23

3 MATERIALS 26

STARCH 26

CELLULOSE ACETATE 31

Chapter Page

STYRENE MALEIC ANHYDRIDE COPOLYMER 35
CATALYST 38
4 PROCESSING AND CHARACTERIZATION 39
BLENDS OR COMPOSITES PREPARATION 39
Grinding 39
Drying 42
Extrusion 43
MATERIALS CHARACTERIZATION 48
Preparation for injection molding 48
Injection molding 48
Compression molding 50
Tensile and Izod impact tests 51
Transmission electron microscopy (TEM) 52
Scanning electron microscopy (SEM) 57
Other tests 57
5 AMYLOSE COMPOSITES 59
MORPHOLOGY 59
MECHANICAL PROPERTIES 70
6 CELLULOSE ACETATE BLENDS 82
MORPHOLOGY 82
CA/SMA blends - No catalyst 82
Addition of potential catalysts 92
Morphology after reaction 97
Dispersed phase size 122
MECHANICAL PROPERTIES 127

Chapter Page

7 CONCLUSIONS AND RECOMMENDATIONS 142

Amylose composites 142

Cellulose acetate blends 143

APPENDIX 146

BIBLIOGRAPHY 150

LIST OF TABLES

Table Page

1 The sets of experiments. 6

2 Data for CA. 34

3 Data for SMA. 36

4 Extrusion conditions. 47

5 Injection molding conditions. 49

6 Mechanical properties of the amylose composites. 71

7 Size of dispersed phase (SMA) in CA/SMA blends. 123

8 Mechanical properties of the CA blends. 128

9 Tensile and Izod impact strength of unfilled-unreinforced commercially available plastics (from *Modern Plastics Encyclopedia '92*, McGraw-Hill, 1991). 146

LIST OF FIGURES

Figure Page

1 Property relationship in polymer blends. 8

2 Effect of composition and viscosity on phase morphology. 13

3 Droplet breakup. 14

4 Ideal location of a block or graft copolymer at the interface between two polymer phases. 16

5 Structural components of starch. 27

6 SEM picture of amylose granules. 28

7 Amylose particle size distribution. 29

8 Cellulose and cellulose acetate. 32

9 SEM picture of CA particles. 34

10 Styrene maleic anhydride copolymer. 35

11 Grafting reaction between the hydroxyl group of cellulose acetate and the anhydride functionality of styrene maleic anhydride copolymer. 37

12 4-dimethylaminopyridine. 38

13 Experimental procedure. 40

14 SMA-8 wiley milled using a 1 mm sieve. 42

15 Baker-Perkins extruder (Composite Materials and Structures Center, Michigan State University). 44

16 Co-rotating intermeshing (closely self-wiping) twin-screws. 45

Figure Page

17 ASTM D638 type I specimen (actual size). The points where it was cut and notched for ASTM D256A (Izod) impact test are also indicated. 52

18 Block trimming (not on scale). 54

19 SEM picture of amylose/PS 15/85 after extrusion. No matrix/filler adhesion. 60

20 SEM picture of amylose/PS 15/85 after extrusion. No matrix/filler adhesion. 61

21 SEM picture of amylose/PS 15/85 after injection (Izod impact fracture surface). No matrix/filler adhesion. 61

22 SEM picture of amylose/SMA-8 15/85 after extrusion. Good interfacial adhesion. 62

23 SEM picture of amylose/SMA-8 15/85 after extrusion. Good interfacial adhesion. 63

24 SEM picture of amylose/SMA-8 30/70 after extrusion. Good interfacial adhesion. 64

25 SEM picture of amylose/SMA-8 45/55 after extrusion. Good interfacial adhesion. 64

26 SEM picture of amylose/SMA-4 15/85 after extrusion. Good interfacial adhesion. 65

27 SEM picture of amylose/SMA-14 15/85 after extrusion. Good interfacial adhesion. 65

28 SEM picture of amylose/SMA-8 15/85 after extrusion (amylose was vacuum oven dried before it was mixed with SMA-8). Good interfacial adhesion. 66

29 SEM picture of amylose/SMA-8 15/85 after extrusion. One of the few amylose granules which broke. 67

30 TEM picture of amylose/SMA-8 after extrusion. For (a) the composition is 15/85 and for (b) is 45/55. 68

31 TEM picture of amylose/SMA-8 15/85 after extrusion. The lighter part is amylose, and the darker part is SMA-8. 68

32 SEM picture of an amylose/SMA-8 36/64 compression molded specimen (fracture in tension). Amylose had before extrusion 33% moisture. 69

Figure Page

33 SEM picture of an amylose/SMA-8 20/80 compression molded specimen, soaked in water for 31 days (fracture in tension). 70

34 Stress-strain curves of amylose composites. 72

35 Stress-strain curves of amylose composites. 73

36 Relative Young's modulus (composite/matrix) as a function of the MA level (a) and the amylose content (b). 75

37 Tensile strength of the composites containing 15% amylose and of their corresponding matrixes (a), and relative tensile strength (composite/matrix) as a function of the MA level (b) and the amylose content (c). 77

38 Relative Izod impact strength (composite/matrix) as a function of the MA level (a) and the amylose content (b). 80

39 SEM picture of CA/SMA-8 70/30 after extrusion (fracture perpendicular to the flow direction). 83

40 SEM picture of CA/SMA-8 70/30 after extrusion (fracture perpendicular to the flow direction). 83

41 TEM picture of CA/SMA-8 70/30 after extrusion (sectioning perpendicular to the flow direction). 85

42 TEM picture of CA/SMA-8 70/30 after two extrusion passes (sectioning perpendicular to the flow direction). 85

43 TEM picture of CA/SMA-8 70/30 after three extrusion passes (sectioning perpendicular to the flow direction). 86

44 TEM picture of CA/SMA-8 70/30 after extrusion (sectioning parallel to the flow direction). 87

45 SEM picture of CA/SMA-14 70/30 after extrusion (fracture perpendicular to the flow direction). 88

46 TEM picture of CA/SMA-14 70/30 after extrusion (sectioning perpendicular to the flow direction). 88

47 SEM picture of CA/SMA-8 70/30 injection molded specimen (fracture in tension, surface perpendicular to the flow direction). 89

48 SEM picture of CA/SMA-8 70/30 injection molded specimen (fracture parallel to the flow direction). 90

Figure Page

49 SEM picture of CA/SMA-8 30/70 after extrusion (fracture perpendicular to the flow direction). 90

50 Droplet deformation in uniform shear flow for viscosity ratio between 0.7 and 2.2. 91

51 SEM picture of CA/SMA-8/KCl 30/70/1 after extrusion (fracture perpendicular to the flow direction). 92

52 SEM picture of CA/SMA-8/KCl 50/50/1 after extrusion (fracture perpendicular to the flow direction). 93

53 SEM picture of CA/SMA-8/KCl 30/70/2 after extrusion (screw speed 15 rpm, fracture perpendicular to the flow direction). 94

54 SEM picture of a KCl particle in a CA/SMA-8/KCl 50/50/1 system after extrusion (fracture perpendicular to the flow direction). ... 95

55 SEM picture of Dexel/SMA-8/poly(4-vinylpyridine-co-styrene) 70/30/0.5 after extrusion (fracture between parallel and perpendicular to the flow direction). 96

56 SEM picture of Dexel/SMA-8/poly(2-vinylpyridine) 70/30/2 after extrusion (fracture perpendicular to the flow direction). 96

57 TEM picture of CA/SMA-8/DMAP 70/30/0.1 after three extrusion passes, the catalyst added before the third extrusion (sectioning perpendicular to the flow direction). 97

58 SEM picture of CA/SMA-8/DMAP 70/30/0.1 after three extrusion passes, the catalyst added before the third extrusion (fracture perpendicular to the flow direction). 99

59 SEM picture of CA/SMA-8/DMAP 70/30/0.1 after three extrusion passes, the catalyst added before the third extrusion (fracture perpendicular to the flow direction). 100

60 SEM picture of CA/SMA-8/DMAP 70/30/0.1 after three extrusion passes, the catalyst added before the third extrusion (fracture perpendicular to the flow direction). 100

61 SEM picture of extracted CA/SMA-8/DMAP 70/30/0.1 after three extrusion passes, the catalyst added before the third extrusion (fracture perpendicular to the flow direction). 101

62 SEM picture of extracted CA/SMA-8/DMAP 70/30/0.1 after three extrusion passes, the catalyst added before the third extrusion (fracture parallel to the flow direction). 102

Figure Page

63 TEM picture of CA/SMA-8/DMAP 70/30/0.05 after two extrusion passes, the catalyst added before the second extrusion (sectioning perpendicular to the flow direction). 103

64 SEM picture of CA/SMA-8/DMAP 70/30/0.05 after two extrusion passes, the catalyst added before the second extrusion (fracture perpendicular to the flow direction). 103

65 TEM picture of CA/SMA-8/DMAP 70/30/0.05 after three extrusion passes, the catalyst added before the second extrusion (sectioning perpendicular to the flow direction). 104

66 SEM picture of CA/SMA-8/DMAP 70/30/0.05 after three extrusion passes, the catalyst added before the second extrusion (sectioning perpendicular to the flow direction). 104

67 TEM picture of CA/SMA-8/DMAP 70/30/0.1 after extrusion (sectioning perpendicular to the flow direction). 105

68 SEM picture of CA/SMA-8/DMAP 70/30/0.1 after extrusion (fracture perpendicular to the flow direction). 106

69 SEM picture of CA/SMA-8/DMAP 70/30/0.1 after extrusion (fracture perpendicular to the flow direction). 106

70 SEM picture of CA/SMA-8/DMAP 70/30/0.1 after extrusion and extraction (fracture perpendicular to the flow direction). 107

71 SEM picture of CA/SMA-8/DMAP 70/30/0.1 after extrusion and extraction (fracture parallel to the flow direction). 108

72 TEM picture of CA/SMA-8/DMAP 70/30/0.05 after extrusion (sectioning perpendicular to the flow direction). 109

73 TEM picture of CA/SMA-8/DMAP 70/30/0.05 after two extrusion passes, the catalyst added before the first extrusion (sectioning perpendicular to the flow direction). 110

74 TEM picture of CA/SMA-8/DMAP 70/30/0.01 after extrusion (sectioning perpendicular to the flow direction). 110

75 SEM picture of CA/SMA-8/DMAP 70/30/0.05 after extrusion (fracture perpendicular to the flow direction). 111

76 SEM picture of CA/SMA-8/DMAP 70/30/0.1 after two extrusion passes, the catalyst added before the first extrusion (fracture perpendicular to the flow direction). 112

77 SEM picture of CA/SMA-8/DMAP 70/30/0.01 after extrusion (fracture perpendicular to the flow direction). 112

Figure Page

78 SEM picture of CA/SMA-8/DMAP 70/30/0.05 after injection (fracture in tension, surface perpendicular to the flow direction). 114

79 SEM picture of CA/SMA-8/DMAP 70/30/0.05 after injection (fracture in tension, surface parallel to the flow direction). 114

80 SEM picture of CA/SMA-8/DMAP 70/30/0.01 after injection (fracture in tension, surface perpendicular to the flow direction). 115

81 TEM picture of CA/SMA-14/DMAP 70/30/0.01 after extrusion (sectioning perpendicular to the flow direction). 116

82 SEM picture of CA/SMA-14/DMAP 70/30/0.01 after extrusion (fracture perpendicular to the flow direction). 117

83 TEM picture of CA/SMA-R/DMAP 70/30/0.01 after extrusion (sectioning perpendicular to the flow direction). 118

84 SEM picture of CA/SMA-R/DMAP 70/30/0.01 after extrusion (fracture perpendicular to the flow direction). 118

85 TEM pictures of (a): CA/SMA/KCl 30/70/2 (screw speed 15 rpm), (b), (c) and (d): CA/SMA-8/DMAP 70/30/0.1, after extrusion, pelletization, extraction and epoxy embedding. 121

86 Size distributions for the dispersed phase (SMA) of CA/SMA blends (refer to table 7). 124

87 Size distributions for the dispersed phase (SMA) of CA/SMA blends (refer to table 7). 125

88 Size distributions for the dispersed phase (SMA) of CA/SMA blends (refer to table 7). 126

89 Stress-strain curves for CA blends. 129

90 Stress-strain curves for CA blends. 130

91 Stress-strain curves for CA blends. 131

92 Tensile strength comparisons for the CA/SMA blends. 134

93 Elongation comparisons for the CA/SMA blends. 136

94 Tensile modulus comparisons for the CA/SMA blends. 138

95 Izod impact strength comparisons for the CA/SMA blends. 140

ABBREVIATIONS

Symbolism

A/B: Blend or composite of A and B.

A-B: Copolymer of A and B.

A-co-B: Copolymer of A and B.

A-b-B: Block copolymer of A and B.

A-g-B: Graft copolymer of A and B.

Polymers

ABS: Acrylonitrile-butadiene-styrene.

CA: Cellulose acetate.

EPDM: Ethylene propylene diene monomer rubber.

HIPS: High impact polystyrene.

LDPE: Low-density polyethylene.

MMA: Methyl methacrylate.

PBT: Polybutylene terephthalate.

PC: Polycarbonate.

PE: Polyethylene.

PET: Polyethylene terephthalate.

PMMA: Polymethyl methacrylate.

PP: Polypropylene.

PPO: Polyphenylene oxide.

PS: Polystyrene.

PVDF: Polyvinylidene fluoride.

PVC: Polyvinyl chloride.

SAN: Styrene-acrylonitrile.

SMA: Styrene maleic anhydride copolymer.

SMA-4: SMA with 4% maleic anhydride.

SMA-8: SMA with 8% maleic anhydride.

SMA-14: SMA with 14% maleic anhydride.

SMA-R: Rubber modified SMA.

Other abbreviations

DEP: Diethyl phthalate.

DMAP: 4-dimethylaninopyridine.

DS: Degree of substitution.

DSC: Differential scanning calorimetry.

FTIR: Fourier transform infra-red.

GPC: Gel permeation chromatography.

IPN: Interpenetrating network.

MA: Maleic anhydride.

MW: Molecular weight.

rpm: Revolutions per minute.

RTD: Residence time distribution.

SEM: Scanning electron microscopy (or microscope).

TEM: Transmission electron microscopy (or microscope).

INTRODUCTION

The interest in using renewable resources to make polymeric materials has intensified in recent years. The main reasons for this interest are [Narayan (1991)]:

- Environmental concerns, requiring polymeric materials to be environmentally compatible.
- Alternate feedstocks to non-renewable imported petroleum feedstocks.
- The need to find new industrial uses for the nation's abundant agricultural feedstocks.

Natural biopolymers (specially polysaccharides, like starch and cellulose) and their derivatives are being considered as a replacement (partially or in full) for synthetic polymers derived from petroleum in many applications. Legislation, in the form of the 1990 Farm Bill is seeking to expedite the development and market penetration of industrial products that use agricultural materials.

This thesis is devoted to the study of combining natural polymers, starch and cellulosics, with synthetic polymers, to create new composite materials and polymer alloys.

Terminology

Some of the terms used in this text have been used with different meaning in the literature. The following is the description of these terms as used in this text.

- Polymer blend: A general term used for the mixture of two or more polymers. Polymer blends are often referred to by the word “polyblends”.
- Miscible blend: When a mixture of polymers forms a single, thermodynamically compatible phase.
- Immiscible-incompatible blend: Phase separation with no or minimal interfacial contact, generally resulting in poor mechanical properties.
- Immiscible-compatibilized blend: The term “compatibility” is often used synonymously with miscibility. However, compatibility is also used when the blend of two or more materials has a desired or beneficial characteristic. This is how we will use it in the thesis. Generally, an immiscible but compatibilized polymer blend offers a unique combination or enhancement of the resultant blend properties, due to strong interfacial adhesion.
- Polymer alloy: Many times the terms “alloy” and “blend” are used interchangeably. According to the definition adopted here, the term “alloy” describes an immiscible but compatibilized blend.
- Polymer composite: A combination of a polymer with a reinforcing element or a filler. Normally the components can be physically identified, there is an interface between them, each component retain it’s identity, and does not dissolve or merge completely into the other(s).

The problem and the solution

Most polymer pairs are not miscible (although many more miscible polymer pairs have been identified in the last few years) [Paul (1978a)]. For many purposes miscibility in polymer blends is neither a requirement nor desirable, since immiscible but compatibilized blends usually offer a synergistic combination of important characteristics of both blend components. However, adhesion between the components is necessary to obtain this synergistic enhancement in properties. Adhesion is also a very important factor in the case of composites.

The mixing of a natural polymer with a synthetic one results in a two phase morphology with high interfacial tension and poor adhesion between the components. This results in an incompatible blend or a composite with poor adhesion between the matrix and the reinforcing element or the filler. In both cases the resultant material has poor mechanical properties.

There are two ways of improving adhesion between the phases:

- Use of a compatibilizing agent. This can be a material which interacts/reacts with both components, or is miscible in both phases. Block and graft copolymers of the form A-B are common compatibilizers which have been used to reduce interfacial tension between A-rich and B-rich phases.
- Modification of the components (surface modification or molecular level modification). This consists of incorporating segments capable of specific interactions and/or chemical reactions with the other phase, resulting in the desired adhesion.

Reactive extrusion process

Extrusion is the process traditionally used to melt, homogenize and pump polymers through certain dies, but it is also the most common way of mixing two thermoplastics, or a thermoplastic with a filler or a reinforcing element. If a reaction occurs during the extrusion, then the process is called reactive extrusion. It would be advantageous and beneficial if the formation of the compatibilizer (block or graft copolymer), through a reaction between the components, occurs during the mixing step in the extruder. Thus, reactive extrusion offers a continuous, low cost and high speed process to mix two materials with in situ compatibilization.

The work and the thesis

The work is divided into two parts (sections). In the first part, the use of high amylose starch as a filler in a synthetic polymer matrix has been examined. Starch has been combined with thermoplastics in different ways. However, not much work has been reported on the use of starch in its particulate solid form. Although there are no measurements or calculations in the literature for the mechanical properties of starch, it is reported [Griffin (1985)] that dry starch granules are stronger than many synthetic polymers. This suggests that they can be a used successfully as a rigid particulate filler. Also, the physical integrity of the granules is not expected to change, because the theoretical glass transition temperature of starch is higher than its decomposition temperature (unless plasticized). The fine particle size and narrow particle size distribution of some starches (like maize starch), together with the lower price and density compared to other spherical fillers (like glass spheres), are major advantages. In addition, starch is very inexpensive as compared to synthetic polymers, and will contribute to the overall reduction of the composite's cost.

In the second part, cellulose acetate (CA - polymer derived from the chemical modification of cellulose) alloys with synthetic polymers was the focus of the study. CA is a thermoplastic, but its processing and extrusion rates are slow. It requires a plasticizer for processing, which reduces the tensile strength and stiffness of the material. CA is also relatively expensive in comparison to many synthetic thermoplastics. The objective was to blend CA with a synthetic polymer, to form a CA alloy (immiscible but compatibilized blend) which had improved properties, was easily processible and required no plasticizer.

For both sets of experiments, the synthetic polymers used were commercially available styrene maleic anhydride copolymers (SMA's). Maleic anhydride (MA) is a commonly used functionality for polymer modification in order to promote adhesion, because of its ability to react with hydroxyl or amino groups [Tsubokawa et al. (1991)]. In our case MA is expected to react with the hydroxyl of starch or cellulose acetate through an esterification reaction.

A twin-screw extruder was used for mixing the natural and synthetic polymers, with in situ reactive compatibilization as the main objective. Table 1 summarizes the two parts of the thesis work.

Table 1: The sets of experiments.

	Natural polymer		Synthetic polymer		
Set 1	Starch	Filler ≤ 30% Lower cost	SMA	Matrix ≥ 70%	No catalyst is needed for reaction
Set 2	CA	Blend component 70%	SMA	Blend component 30% Lower cost	Catalyst is needed for reaction

The thesis is divided into seven chapters. In chapter 2, basic knowledge about polymer blends, compatibilization, filled plastics and reactive extrusion is given. Selected previous works related to the above topics is presented. Information about the materials used (starch, CA and SMA), the reaction mechanism, and the catalysts used is given in chapter 3. Chapter 4 describes the experiments conducted and the techniques used for materials characterization. The results are presented and discussed in chapter 5 for the first set of experiments and in chapter 6 for the second set. Chapters 5 and 6 are divided into two parts: the first part refers to the morphology of the composites or blends, and the second part refers to the mechanical properties. Conclusions and recommendations are presented in chapter 7.

Chapter 2

BACKGROUND - LITERATURE REVIEW

POLYMER BLENDS

There has been a tremendous scientific and commercial development in the area of polymer blends during the last ten years. Among the reasons for this development are the following [Meier (1991)]:

- Invention of new classes of materials (thermoplastic elastomers).
- Better processibility (ABS/PC, PPO/PS).
- Impact resistance (HIPS, ABS, rubber-modified epoxies).
- Better mechanical properties (polymeric plasticizers/PVC).
- Solvent resistance (PC/PBT), oxidative resistance (unsaturated elastomers/ EPDM), flame resistance (ABS/PVC).
- Lower cost (PPO/PS).
- 7-10 years are needed for the development of a new polymer, but only 2-4 years for a new blend.

In general, two component polymer mixtures can be described by the following equation [Kienzle (1988)]:

$$P = P_1C_1 + P_2C_2 + IP_1P_2 \tag{1}$$

where P is a property value of the blend, P_1 and P_2 are the property values of the components, C_1 and C_2 are the concentrations of the components and I is an interaction coefficient. If I equals zero there is an additive result, and the property of the blend is the weighted arithmetic average of the constituents properties. For incompatible blends, I has most of the times a negative value, which basically is the result of poor interfacial adhesion. For polymer alloys, however, the compatibilization achieved results in positive values of I, which means that the properties of the polymer combination are better than the weighted arithmetic average of the constituents' properties. Figure 1 describes graphically the above effects of the interaction coefficient.

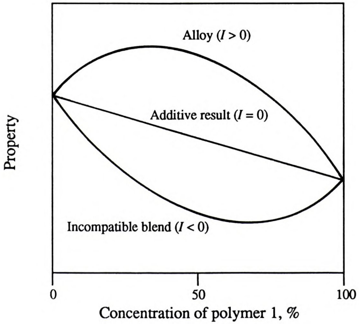

Figure 1: Property relationship in polymer blends.

Basic thermodynamics

The behavior of mixtures at equilibrium is governed by the expression [Paul *et al.* (1988)]:

$$\Delta G_{\mathrm{mix}} = \Delta H_{\mathrm{mix}} - T\,\Delta S_{\mathrm{mix}} \qquad (2)$$

where ΔG_{mix} is the free energy of mixing, ΔH_{mix} the enthalpy of mixing, T the temperature and ΔS_{mix} the entropy of mixing. For miscibility, ΔG_{mix} must be negative and also satisfy the requirement:

$$\left(\frac{\partial^2}{\partial \phi_i^2}\Delta G_{\mathrm{mix}}\right)_{T,P} > 0 \qquad (3)$$

which ensures stability against phase segregation. ϕ_i is the volume fraction of component i and P the pressure. According to Boltzman law for the entropy of mixing [Olabisi (1979)]:

$$\Delta S_{\mathrm{mix}} = k\,\ln\Omega \qquad (4)$$

where k is a constant and Ω is the total number of ways of arranging N_1 and N_2 molecules on a regular lattice comprising $N = N_1 + N_2$ cells. Applying the above law for polymers yields the Flory-Higgins expression:

$$\Delta S_{\mathrm{mix}} = -\,k\,(N_1\ln\phi_1 + N_2\ln\phi_2) \qquad (5)$$

Because of the small number of moles of each polymer in the blend (as a result of their large molecular weights (MWs)), ΔS_{mix} is very small. It can not, therefore, contribute substantially to a negative free energy of mixing, and makes the enthalpy of mixing (ΔH_{mix}) the key for determining miscibility. The enthalpy of mixing can be modeled by the expression [Paul and Barlow (1982), Meier (1991)]:

$$\Delta H_{\mathrm{mix}} = V \phi_1 \phi_2 (\delta_1 - \delta_2)^2 \qquad (6)$$

where V is the volume and δ_1 and δ_2 are the Hildebrand solubility parameters. Note that in this approximation ΔH_{mix} is always positive (endothermic mixing), which results in a positive ΔG_{mix} since ΔS_{mix} is very small. This is why miscibility in polymer blends is limited to a rare occurrence. Specific interactions, like hydrogen bonding or intramolecular repulsion effects can also lead to miscibility by resulting in a negative ΔH_{mix} [Paul (1991)]. SMA and styrene acrylonitrile (SAN) copolymers, for example, are miscible when the MA and AN contents do not differ too much, because of an exothermic interaction between the MA and AN units [Kim *et al.* (1989)].

Blend preparation

The objective of mixing is to bring the components in close proximity by facilitating the relaxation of any non-equilibrium gradients. This is generally aided by heat, solvents, or both.

Melt mixing is the most common commercial method for preparing polymers blends, primarily because of economics. It offers simplicity, speed and does not require the use of solvents. Limitations of melt mixing are the potential for degradation due to the high temperature, the difficulty of mixing materials with large difference in melt viscosity, the difficulty in cleaning the machinery and the cost of the equipment. Brabender mixers, extruders and two-roll mills are commonly used for laboratory-scale mixing. Extruders and Banbury mixers are the devices mainly used in the industry.

Other methods for blend preparation are casting from common solvents, freeze drying, emulsion mixing and mixing via reaction. All these methods, however, are mainly used for laboratory-scale mixing [Shaw (1985b)].

Miscibility determination

The easiest way for establishing miscibility of a polymer blend is by simple optical examination, since a single phase results in a transparent material. Immiscibility usually results in a translucent or opaque material. However, an immiscible blend may appear transparent if the refractive indices are matched, or if the size of the dispersed phase becomes smaller than the wavelength of light (no scattering) [Meier (1991)]. It is also possible for a miscible amorphous phase containing a crystalline phase to reduce transparency by scattering the light [Paul *et al.* (1988)].

Methods based on glass transitions are commonly used for determining miscibility. Miscible blends have a single glass transition, whereas two-phase blends have two T_gs, each one characteristic of the respective phases. The T_g of miscible systems appears somewhere between the T_gs of the components, and usually depends on the composition. Empirical equations have been proposed for predicting the T_g-composition dependence. One of these (applying for several miscible blends) is the simple Fox relationship [MacKnight *et al.* (1978)]:

$$\frac{1}{T_g} = \frac{\phi_1}{T_{g_1}} + \frac{\phi_2}{T_{g_2}} \tag{7}$$

Dynamic mechanical tests can be conducted, for determining if a polymer blend has one or two T_gs. These are very sensitive (possibility of detecting 1%

of a non-miscible component), but it requires relatively complex equipment and the transitions must be separated by more than 20°C to distinguish them graphically. Thermal methods like differential scanning calorimetry (DSC) and differential thermal analysis can also be used for miscibility determination. They are quick, easy and require very small amounts of materials (~ 5 mg), but typically more than 10-20% of the second phase needs to be present in order to be detected. Also, if the size of the dispersed phase domain is very small (somewhere below 100 Å) it can not be detected by DSC [Meier (1991)].

Electron microscopy is another technique which can be used for determining miscibility, since the appearance of two phases would clearly show that the components are not miscible. Transmission electron microscopy (TEM) has the ability to detect very small phase sizes (resolution 0.2 nm). Disadvantages are the expensive equipment and the requirement of sectioning the sample. Poor contrast between the phases can also create problems, but it can be enhanced either by selective chemical reactions (e.g. staining with OsO_4 or RuO_4) [Sawyer and Grubb (1987)], or by annealing under the electron beam [Thomas and Talmon (1978)]. Scanning electron microscopy (SEM) can also be used for detecting a second phase, although its resolution is somewhat lower than that of TEM (3-6 nm). Again, expensive equipment is required, but the procedure is easier since microtomy is not needed. Electron microscopy is discussed in more details in chapter 3 [Shaw (1985a), Flegler *et al.* (1990), Meier (1991)].

Blend morphology

Immiscible polymer blends can be organized into a variety of morphologies. These morphologies may consist of a continuous phase (matrix), and a dispersed phase. The dispersed phase can be in the form of spheres, fibrils or platelets with varying aspect ratios. In this case the matrix phase dominates the properties of the blend. Another distinct morphology consists of both phases being simultaneously continuous and thereby forming an interpenetrating network (IPN) of phases. The type of morphology depends upon several factors, the most important being the composition and the viscosities of each component. Figure 2 shows the effect of those two parameters on the morphology of the blend. The component which is in higher proportion or is less viscous tends to form the continuous phase [Paul (1991)].

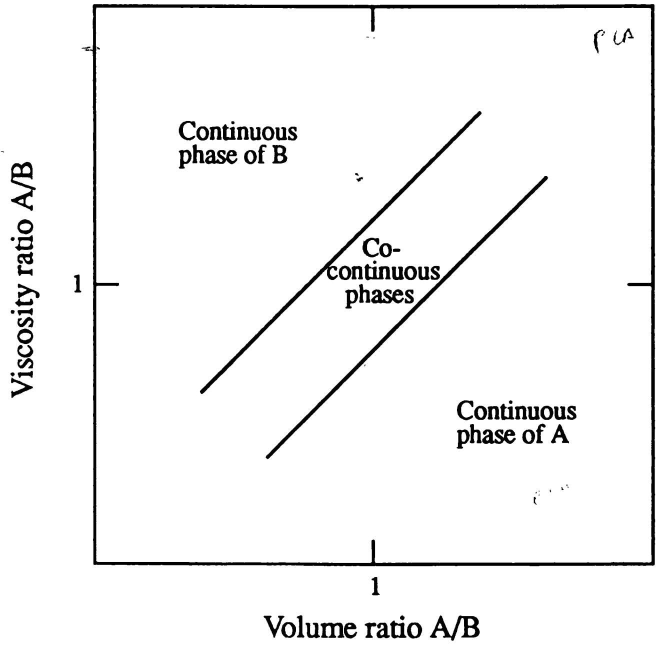
Continuous phase of B
Co-continuous phases
Continuous phase of A
Viscosity ratio A/B
1
1
Volume ratio A/B

Figure 2: Effect of composition and viscosity on phase morphology.

In the case where there is only one continuous phase, it is interesting to discuss how mixing is proceeding. Under the appropriate flow fields, droplets of the dispersed phase break-up as shown in Figure 3. Taylor was the first one to study the breakup of a single Newtonian liquid drop in a Newtonian liquid matrix under uniform and steady shear field [Taylor (1934)]. Of course in the case of polymer mixing the system is quite different from Taylor's, in many ways:

- The drop and the matrix are both viscoelastic.
- The strain field is much more complex.
- Since the properties of the materials change with the temperature, it is possible that they are not the same during the whole mixing process.

However, Taylor's analysis can provide a basis for analyzing dispersion.

Taylor showed theoretically that breakup occurs when the apparent deformation D of the droplet has the value 0.5. So a condition for breakup is:

$$D = \frac{L-B}{L+B} = 0.5 \tag{8}$$

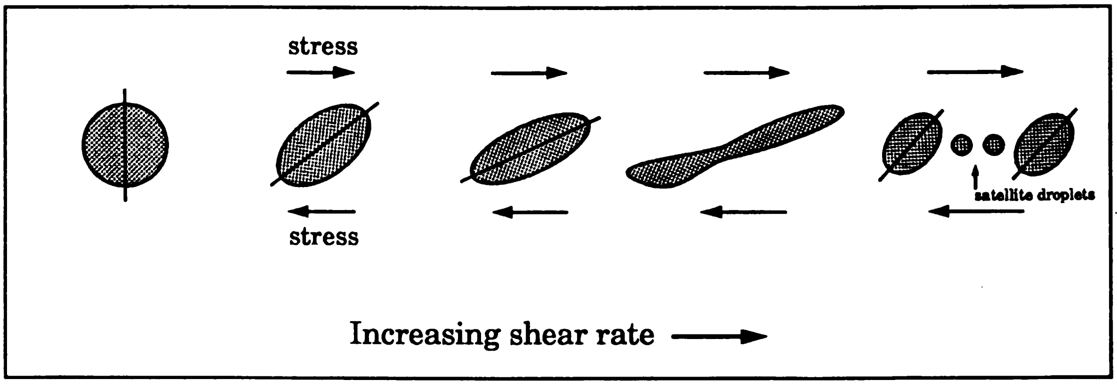

Figure 3: Droplet breakup.

where L is the major axis (length) and B is the minor axis (breadth) of the deformed droplet. Taylor also defined a dimensionless group E, given by:

$$E = R\left(\frac{19k + 16}{16k + 16}\right) \tag{9}$$

where R is a ratio of viscous to interfacial forces and k is the viscosity ratio:

$$R = \frac{G\eta_m r}{\gamma} \qquad \text{and} \qquad k = \frac{\eta_d}{\eta_m} \tag{10,11}$$

G is the shear rate, r is the droplet radius, γ is the interfacial tension, η_m is the matrix viscosity and η_d is the droplet viscosity. When the viscous forces tending to elongate and disrupt the droplet are greater than the interfacial forces tending to keep it in one piece, then breakup occurs. At this point, the theoretical value of E (for Taylor's system) also is 0.5. Therefore, the criterion for droplet breakup becomes:

$$\frac{G\eta_m a}{\gamma} \geq \frac{19k + 16}{16k + 16} \tag{12}$$

where a is the diameter of the droplet. The left side of the above equation is the Weber number (*We*, the ratio of viscous to interfacial forces) [Han (1981), Wu (1987)].

Another interesting phenomenon is the morphology occurring after converging (extensional) flow of a blend having a continuous and a dispersed phase (droplets). The shear and elongational viscosities of the two components and the interfacial tension are the main parameters which will determine if the dispersed phase will remain in droplet form or will be deformed into fibrils [Han (1981)].

COMPATIBILIZATION

As was mentioned before, simple blending of immiscible blends does not generally give a material with desired characteristics, because of the high interfacial tension typically existing between the two phases. The result of this is [Paul (1978b)]:

- Poor interfacial adhesion.
- Difficulty of attaining the desired degree of dispersion.
- Instability against gross segregation or stratification during later processing or use.
- Poor mechanical properties.

The general routes followed for altering this interfacial situation and compatibilizing the blend where cited in chapter 1. At this point more details will be given, and some selected examples will be briefly discussed.

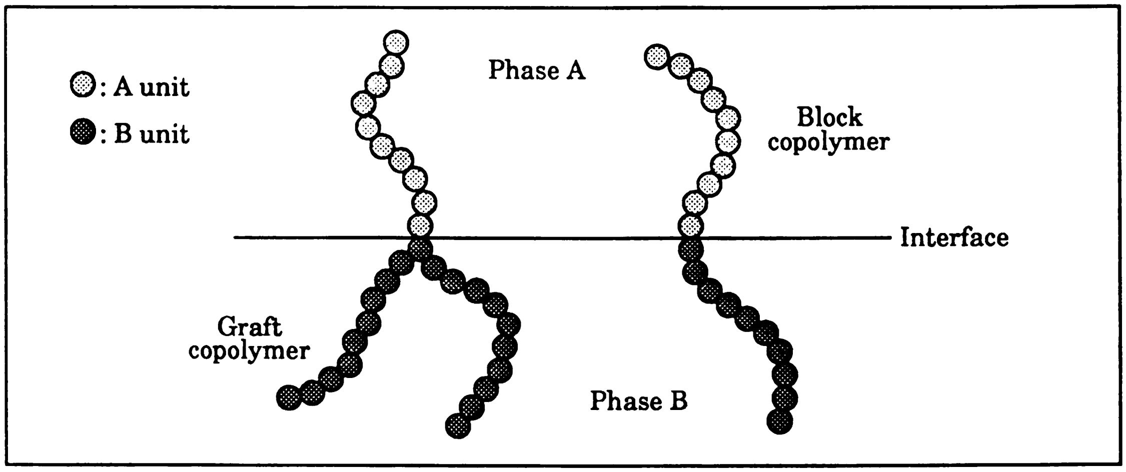

Figure 4: Ideal location of a block or graft copolymer at the interface between two polymer phases.

The first way of improving interfacial adhesion is by using a compatibilizing agent. This can be a block or graft copolymer which, if properly selected, will preferentially locate at the interface between the phases A and B, as shown in Figure 4. The compatibilizer can be an A-B copolymer, or any other copolymer where one of the arms is miscible or adhered to one of the phases, and the other arm is miscible or adhered to the other phase.

The system polystyrene (PS)/polyethylene (PE) is an example where the addition of a copolymer leads to improved properties. Better impact strength has been observed when a graft copolymer of PS and low-density polyethylene (LDPE) was added to a blend of the homopolymer [Barentsen et al. (1974)]. The copolymer was prepared by Friedel-Crafts alkylation of the aromatic rings of polystyrene with the olefinic groups in LDPE. Addition of a PS-LDPE copolymer prepared by a radiation technique also resulted in improved yield strength and elongation at break [Locke and Paul (1973)]. Another example is the compatibilization of CA/polyacrylonitrile (PAN) blends using a graft of PAN onto CA [Paul (1978b)].

For most PS-polyolefin systems, however, copolymers other than these of A-B type have been used, like hydrogenated butadiene-b-styrene [Fayt *et al.* (1986)] or a triblock copolymer with styrene end blocks and ethylene-butene-1 in between [Barlow and Paul (1984)]. It is also possible to use a copolymer of the A-C type, C being soluble in one of the phases. Styrene-b-methyl methacrylate (MMA) has, for example, been used as compatibilizer in a blend were one phase is a blend of high impact polystyrene (HIPS) and polyphenylene oxide (PPO) and the other is polyvinylidene fluoride (PVDF), since polymethyl methacrylate (PMMA) is soluble in PVDF [Fayt *et al.* (1987)].

In all the above examples, no reaction is expected between the compatibilizer added and the blend components. If a reaction occurs between the copolymer and the homopolymer(s), it will improve adhesion (the adhesive strength resulting from chemical bonding is about 35 times greater than that resulting from van der Waals attraction [Wu (1978)]). In order for a reaction to occur, the components of the blend need to be functionalized, i.e. specific segments need to be incorporated on the polymer chain, that can react with the copolymer. When the adhesion between two materials is due to the reaction between one of the materials and a functional group contained in the other, then the adhesive strength is given by the expression [Wu (1978)]:

$$f = aC^b \tag{13}$$

where f is the adhesive strength, C is the concentration of the functional group, and a and b are positive constants. The value of b has been found to be about 0.6.

Many reactive copolymers have been used as compatibilizers for polymer blends. Most of them contain anhydride or carboxyl functionalities, and the majority of blends employ polyamide as one of the components [Xanthos (1988)]. A graft copolymer of MA and polypropylene (PP) is used as a reactive compatibilizer for nylon 6/PP blends, due to the relatively fast reaction between the anhydride and the terminal -NH_2 group [Ide and Hasegawa (1974)]. PE modified with carboxyl or anhydride groups either by copolymerization or grafting is employed as compatibilizer of PE/polyamide blends [Subramanian and Mehra (1987)]. SMA and styrene glycidyl methacrylate were used as in situ reactive compatibilizers of PS/nylon 6,6 blends [Chang and Hwu (1991)]. Compounds other than block or graft copolymers are also used as coupling agents for reactive compatibilization of PS/PE blends [Ballegooie

and Rudin (1988)].

Functionalization of the blend components can also lead to adhesion through other specific interactions between the functionality incorporated and the copolymer, or directly between the functionality and the other blend component. The latter eliminates the addition of the copolymer, and is another way of improving adhesion in polymer blends [Xanthos (1988)].

Compatibilization is also possible through a copolymer formed in situ when mixing two polymers (or functionalized polymers). This is faster, easier and more economical than the two-step procedure of making a copolymer and then adding it to the blend. HIPS and acrylonitrile-butadiene-styrene (ABS) are classical examples of in situ compatibilization through free radical reactions [Manson and Sperling (1976)]. Functionalization of one or both components of a blends has many times as a goal an in situ compatibilization reaction. Reactive PS and reactive PE, functionalized with oxazoline and carboxylic acid respectively, have been found to give the desired reaction during melt mixing [Baker and Saleem (1987)]. The incorporation of carboxyl groups to ethylene-propylene rubbers which are mixed with nylon 6,6 resulted in much lower interfacial tension [Wu (1987)]. Functionalization of PP with acrylic acid also helped the compatibilization of PP/polyethylene terephthalate (PET) blends [Xanthos *et al.* (1990)]. MA grafted PPO was blended with nylon 6,6 by another research group, and improvement of blend ductility was observed [Campbell *et al.* (1990)]. Even more preferable would be the in situ functionalization of a blend component and its reaction with the other component to provide the desired compatibilization. An example of this from the area of composites, is the functionalization of PP with MA and reaction of the func-

tionalized material with wood fibers in a one step mixing process {Mohanakrishnan *et al.* (1991)].

In general many compatibilizing techniques have been developed (and many others are under investigation), providing the market with commercial alloys designed to meet precise user needs [Toensmeier (1988)].

FILLED POLYMERS

According to the definition given in the first chapter, when the physical integrity of a material which is mixed with a polymer remains the same after mixing, then this combination is called a composite. The polymer becomes the matrix, and the material added is considered a filler or a reinforcement (depending on its aspect ratio and the effect it has on the composite's properties). Most of the times, the materials added are inorganics like clay, mica, silica particles, glass spheres or fibers, carbon fibers etc. There are also, however, organic materials which have been used as fillers or reinforcements of a polymer matrix. These are either natural like wood flour, cotton, cellulose fibers, sisal, jute and hemp, or synthetic like polyacrylonitrile, nylon, aramid and polyester fibers, and rubber dust [Walker (1987)].

As was mentioned in chapter 1, one of the natural materials which has been combined with plastics is starch. Most of the times, however, starch was plasticized or modified before the mixing process (a common modification of starch is synthesis of starch graft copolymers from starch and monomers using mainly free-radical initiation [Fanta and Bagley (1977)]). For example, cross-

linked starch xanthate was mixed with polyvinyl chloride (PVC) and plasticizer [Westhoff *et al.* (1974)], a graft copolymer of starch and PS was synthesized and then mixed with PS homopolymer [Bagley *et al.* (1977)], cross-linked starch xanthate was incorporated into rubber to provide reinforcement [Doane (1978)], and starch was gelatinized with water and then mixed with polyethylene-acrylic acid copolymer [Otey *et al.* (1980)]. When, however, starch was blended in its original form with PVC and plasticizer, quite lower tensile strength was generally observed even for low starch content [Westhoff *et al.* (1974)]. On the other hand, remarkable retention of the tensile strength was reported for thermoplastic polyurethane elastomers extended with up to 35% starch. This is attributed to chemical bonding through a mechanochemical action [Griffin (1985)].

There are not many reports, however, on the use of starch in its original granular form. It is also not clear what happens to the properties of a starch filled synthetic polymer when the adhesion between the starch granules and the polymer is improved. It is possible that the results will be similar to those observed for polymers filled with other spherical fillers, like glass spheres. The effect of varying contents of rigid starch particles and levels of adhesion to a functionalized thermoplastic, on the morphology and properties of the resultant composites, and comparison with other filled polymer systems, is one part of the work included in this thesis.

The basic reasons for incorporating a rigid particle into a synthetic polymer are:

- Toughening by means of mechanisms such as crack front pinning.
- Reduction of cost.

- Increase of stiffness.
- Reduction of exothermic temperature rise and coefficient of thermal expansion, and increase in thermal conductivity [Young (1986)].

For rigid-particulate filled systems, matrix-filler adhesion can have a significant effect on the properties of the composite. Like in the case of polymer blends, the adhesion can be improved by modifying the matrix or the filler (basically at the surface), or by using a coupling agent (which is also usually applied on the surface of the filler).

An example of matrix modification is the compatibilization of PE/clay composites by in situ grafting MA on the PE in the presence of a peroxide. Reaction of the anhydride group with the filler surface resulted in the desired adhesion [Gaylord *et al.* (1980)]. Also, MA grafted ethylene propylene rubber (EPDM) resulted in encapsulation of the filler in a PE/EPDM/filler system. The fillers were oxidized silicon powder or calcium carbonate treated with silane coupling agents [Scott *et al.* (1987)]. There are also examples of filler surface modification. PMMA grafts were grown on the surface of glass beads, and then the beads were used as a filler of PMMA homopolymer [Eastmond and Mucciariello (1982)]. Anhydride groups were introduced onto inorganic ultrafine particles such as silica, titanium oxide and ferrite, and then polymers having hydroxyl and amino groups were grafted onto these surfaces with ester and amide bond, respectively [Tsubokawa and Kogure (1991)]. Different coupling agents have also been used for directly improving matrix-filler adhesion. A pre-treatment with silane coupling agent was used for glass beads filling an epoxy [Broutman and Sahu (1971)], PS [Abate and Heikens (1983)], or PC [Dekkers and Heikens (1984)] matrix. An elastomeric adduct was also used for coating glass beads filling an epoxy matrix [Amdouni *et al.* (1990)].

Invariably, the addition of rigid particles into a polymer matrix results in increase of the modulus. The tensile and impact strengths, however, are normally less than those of the pure matrix. The property which (for thermosetting polymers) is observed to improve by the inclusion of a rigid filler, is the materials toughness, expressed in terms of fracture energy. It has been proposed, that the reason for this improvement is a crack pinning process [Young (1986)]. However, the deformation mechanism of the matrix (crazing or shear yielding) may also play a significant role on the properties of filled composites. More details of what has been observed for particulate filled polymers will be given in chapter 5, so that they can be directly compared to the results of this work.

REACTIVE EXTRUSION

Reactive extrusion is the use of the extruder as a continuous flow reactor. In reactive extrusion a chemical reaction takes place simultaneously with the processing and shaping of a material. Many benefits are the result of this combination [Tzoganakis (1989)]:

- Processes such as polymerization or chemical modification of existing polymers, can done continuously, and together with shaping of the product.
- Mixing and compatibilization of polymers can be achieved in one step.
- Reactive agents can be introduced at optimum points in the reaction sequence, and homogenization of the ingredients achieved. Various liquid or gaseous reactants can also be introduced at specific points.

- There is good control over the temperature, the residence time distribution (RTD) and the extent of the reaction.
- Heat and mass transfer problems arising from the viscosity increase during polymerization, can be handled much easier than in a batch process.
- Lower residence times, compared to those required in batch processes, can help avoiding degradation.
- The use of a solvent is eliminated, resulting in dramatic cost reduction in raw materials and solvent recovery equipment.

Due to the high temperatures required, however, degradation can be a problem for thermally unstable materials. Also, the process can not be used for reactions needing very high residence times.

Different types of reaction can be performed in an extruder [Brown an Orlando (1988)]:

- Bulk polymerization reactions (both condensation and addition).
- Graft reactions of a molten polymer with a monomer or mixture of monomers.
- Interchain reactions of two (or more) polymers, forming a copolymer. They are usually used for compatibilization of the polymer blend. Most of the compatibilization reactions described earlier in this chapter are conducted in an extruder.
- Polymer functionalization or functional group modification reactions.
- Coupling reactions of a homopolymer resulting to an increase of the MW by chain extension or branching.
- Controlled degradation (basically MW reduction).

Heterogeneous polymerization and concentration, combined devolatilization-reaction and compatibilization of recycled plastic mixtures during extrusion, are some of the areas where reactive extrusion is expected to be useful in the near future [Kowalski (1990)].

The extruders commercially available are single or twin-screw. The twin-screw extruders can be intermeshing (fully or partially) or non-intermeshing, co-rotating or counter-rotating [Rauwendaal (1986)]. All these types have been used for reactive extrusion processes. However, co-rotating intermeshing twin screw extruders have been found to be suitable for most applications [Tzoganakis (1989)].

MATERIALS

STARCH

The natural polymer which was used as a filler for the first set of experiments, is starch. Starch is a granular mixture of two different high polymers: amylose and amylopectin. Both are homopolymers of α-D-glucopyranosyl units, except that amylose is a liner polymer where the units are linked with an α-D-(1→4) bond, and amylopectin is a branched polymer having both α-D-(1→4) and α-D-(1→6) bonds (Figure 5). The amount of amylose contained in starch depends on the source (plant) starch is coming from. Most native starches contain 20-30% by weight of amylose [Young (1984)]. The starch used in our experiments is coming from amylomaize (a variety of hybrid corn). It was supplied by National Starch and Chemical Corporation (Hylon VII), and the amylose content was 70-75%. Due to the high amylose content, we will refer to it as amylose instead of starch. It should be mentioned that high amylose starch is the material of choice for obtaining thermoplastic properties (after plasticization or modification), for example, for film forming. Amylopectin, which is highly branched, makes processing and film forming difficult. However, when starch is used as a filler, the high amylose content is not expected to affect the properties.

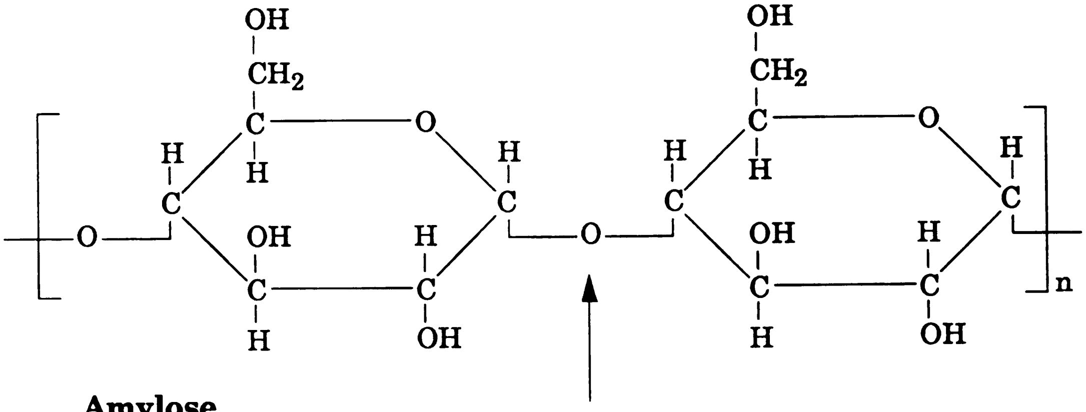

Amylose
Linear polymer

α-D-(1→4) bond

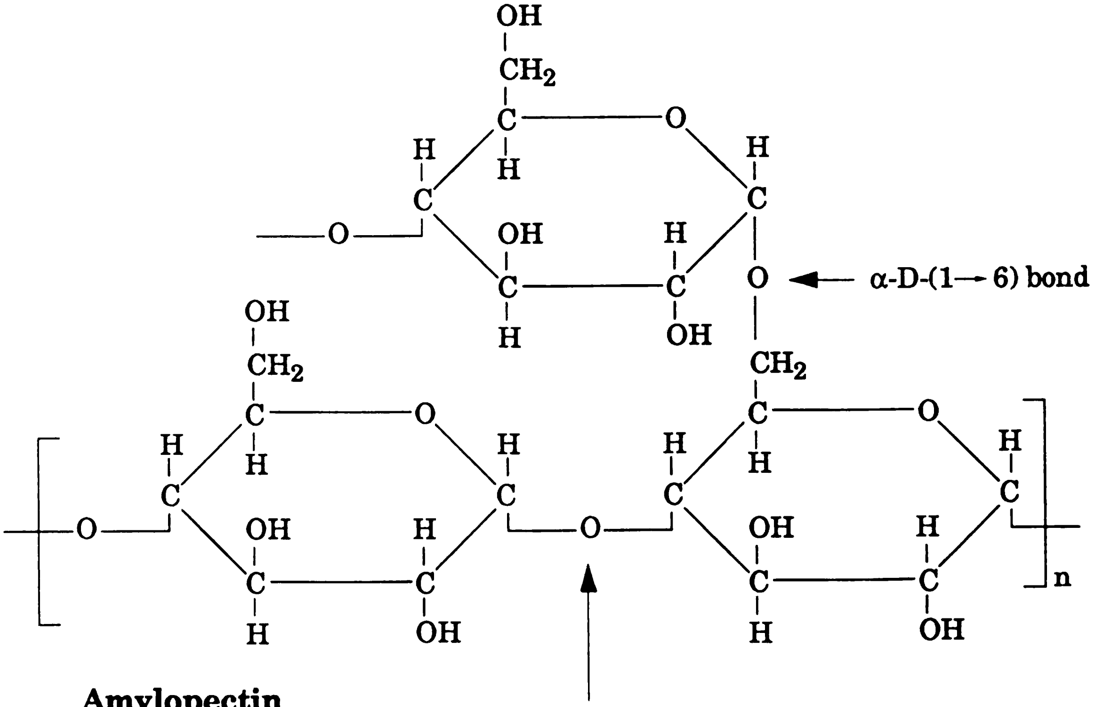
OH
CH2
C
O
H
α-D-(1→6) bond
n

Amylopectin
Branched polymer

α-D-(1→4) bond

Figure 5: Structural components of starch.

Figure 6 is an SEM picture of the amylose particles. Starches coming from different plants have different shapes. It can be noticed, that in this case the particles are almost spherical (the aspect ratio is very close to 1). Average particle diameters, also depend on the origin of the starch. Potato starch, for example, has particles with average diameters about 50 μm, whilst for rice starch the average diameters are about 5-6 μm [Griffin (1985)]. Figure 7 presents the amylose particle size distribution, based on measurements of 200 particles directly from SEM micrographs. The calculations were based on the form:

$$D = \frac{L+B}{2} \tag{14}$$

were D is the calculated diameter, L is the major axis (length) and D is the minor axis (breadth).

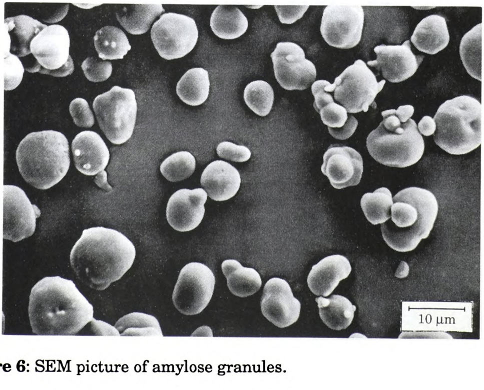

Figure 6: SEM picture of amylose granules.

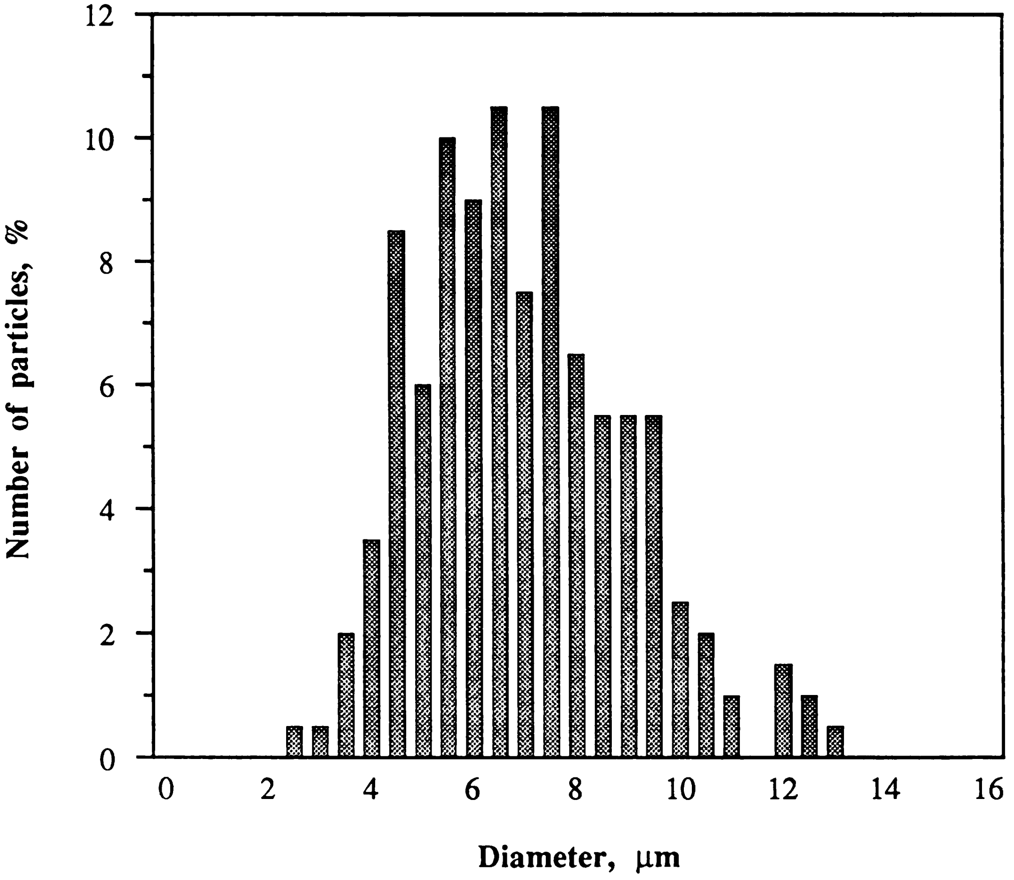

Figure 7: Amylose particle size distribution.

The weight average diameter ($\bar{D}_w$) is 7.4 µm, the number average diameter ($\bar{D}_n$) is 6.9 µm, and the sample standard deviation (σ_{n-1}) is 2.0 µm[1]. The distribution is showing one peak (some starches, such as potato and wheat show double-peaked distributions [Griffin (1985)]), all the particles are between 2 and 13 µm and 91% of the particles are between 4 and 10 µm.

We can, therefore, say that amylose particles are almost spherical, have very fine particle size and a narrow particle size distribution. Particle size distributions of fillers provided by the mineral industry is quite different, showing particles from an upper limit because of a sieve classification, to very fine dust due to brittle fracture. There are many advantages in using amylose as a potentially successful filler. These are:

- Natural origin (use of renewable resources).
- Much lower cost than the synthetic polymers.
- Fine particle size.
- Narrow particle size distribution.
- Strength of the particles (as will be also shown in chapter 5).
- Lower cost than other spherical fillers like glass spheres (cost of solid glass spheres ranges from 28¢ to $2.05/lb [Hagarman (1991)], cost of high amylose starch is about 27¢/lb, but cost of maize starch can be 6¢/lb).
- Lower density than other spherical fillers like glass spheres (the density of glass is about 2.5 g/cm^3, whilst the density of starch is close to 1.5 g/cm3 at

---

[1]

$$\bar{D}_w = \frac{\sum_{i=1}^{n} D_i^2}{\sum_{i=1}^{n} D_i} \qquad \bar{D}_n = \frac{\sum_{i=1}^{n} D_i}{n} \qquad \sigma_{n-1} = \sqrt{\frac{\sum_{i=1}^{n} (D_i - \bar{D}_n)}{n-1}}$$

equilibrium moisture and about 1.2 g/cm3 at 1% moisture level [Griffin (1985)]).

CELLULOSE ACETATE

Cellulose acetate was one of the blend components used in the second set of experiments. It is derived from the chemical modification of cellulose, a naturally occurring polymer. Cellulose (Figure 8a) is a polysaccharide (as starch), consisting of β-D-glucopyranosyl units. Because of strong hydrogen bonding with the hydroxyl groups, cellulose is not a thermoplastic (like starch, it's theoretical melting point is above the decomposition temperature). In order to convert cellulose to a material which can be molded, some of the hydroxyl groups need to be replaced. If all hydroxyl groups are replaced by acetate groups, this modification leads to cellulose triacetate. Partial replacement by acetate groups leads to the so called cellulose acetate (CA). The number of acetate groups per anhydroglucose unit is called degree of substitution (DS). So, the DS for cellulose triacetate is 3. A CA with DS of 2.5 is represented in Figure 8b).

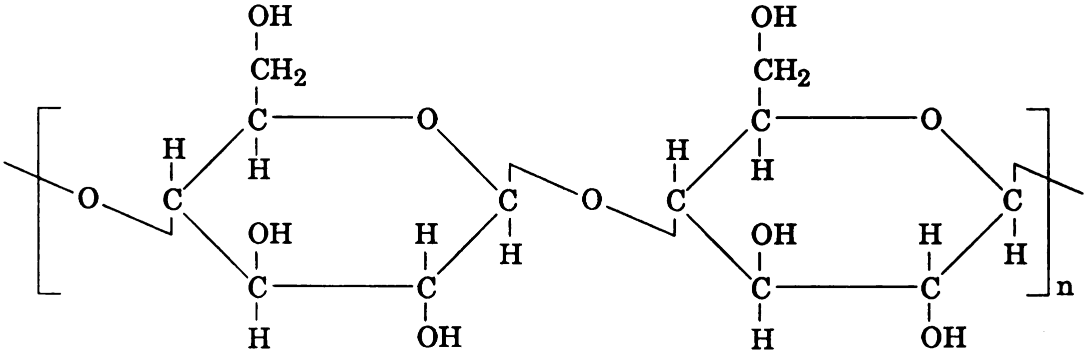

(a) Cellulose

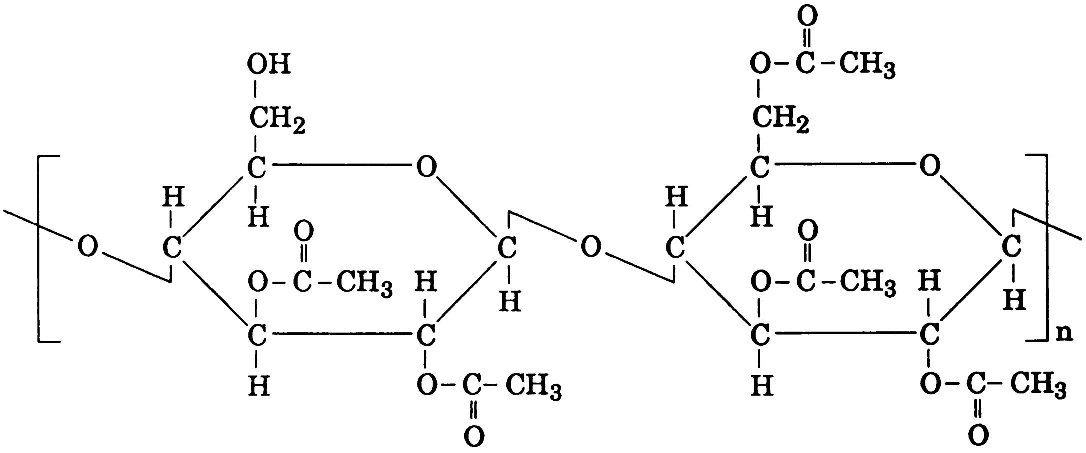

(b) Cellulose acetate (DS: 2.5)

Figure 8: Cellulose and cellulose acetate.

CA's processibility is generally poor, so, most of the times it is used with plasticizers. It has good clarity, excellent colorability, high gloss and quite high toughness and hardness. It is, however, quite expensive compared to many of the newer thermoplastics, although this might change in the future since CA comes from a renewable resource (cellulose), whilst the other thermoplastics depend on the cost of petrochemical feedstocks. Another disadvantage of CA is it's affinity for moisture [Dick (1987)]. The addition of an inexpensive, hydrophobic, synthetic thermoplastic polymer as a blend component in the CA phase, could eliminate the need for a plasticizer, reduce cost, increase stiffness and potentially increase strength and reduce moisture adsorption (depending on the morphology of the blend). It was, therefore, of interest to study blending CA with a synthetic hydrophobic polymer. It was also of interest to see how the properties are affected, and how they can be improved though compatibilization.

The CA was provided by Courtaulds. It was in the form of a white powder, consisting basically of particles around 100-400 μm (Figure 9) ($\overline{D}_w$ = 250 μm, $\overline{D}_n$ = 230 μm, and σ_{n-1} = 80 μm). Some much smaller particles however are also present. Data for CA is given in Table 2.

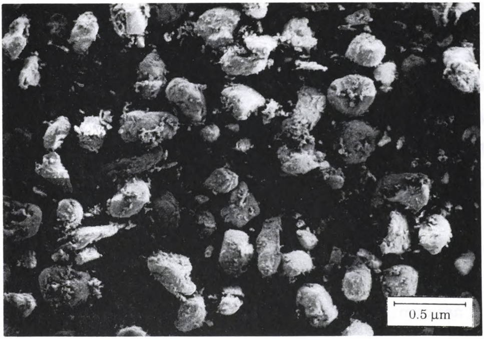

Figure 9: SEM picture of CA particles.

Table 2: Data for CA.

Degree of substitution:	2.45	
Molecular weight:		
	$\overline{M}_w$	= 140,000
	$\overline{M}_n$	= 70,000
Glass transition temperature:	T_g	= 187°C
Melting temperature:	T_m	= 232°C

Plasticized CA provided by Courtaulds (Dexel) having 33% diethyl phthalate (DEP) as a plasticizer, has also been used for some experiments.

STYRENE MALEIC ANHYDRIDE COPOLYMER

Commercially available styrene maleic anhydride copolymer (SMA) (Figure 10) was used as a matrix for the first set of experiments, and as a blend component for the second set. SMA is a thermoplastic copolymer manufactured by continuous free-radical polymerization of styrene and maleic anhydride (MA). The MA is randomly incorporated into the polystyrene (PS) backbone, and acts as a chain stiffener resulting in increasing the glass transition to approximately 114°C. This modification, has other advantages when SMA is mixed with other materials, because of the possible interaction or reaction of the MA functionality with these materials. The highly polar MA group can for example result in excellent adhesion with glass [Francis and Wambach (1988)], or it can also react with hydroxyl or amino groups. The reason for the MA modifications mentioned in chapter 2 (for compatibilization of polymer blends or improved matrix-filler adhesion) was the expectation for such an interaction of reaction. Possible reaction (or hydrogen bonding) of the anhydride functionality with the hydroxyl of amylose or CA, was also the reason SMA was selected for our experiments.

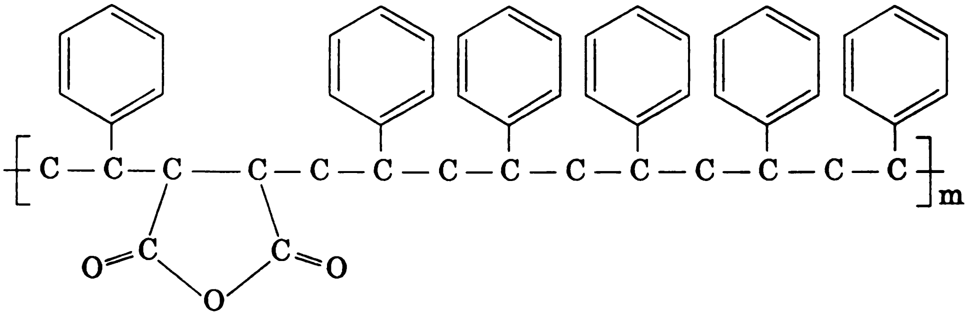

Figure 10: Styrene maleic anhydride copolymer.

The SMA's used were provided by ARCO Chemical Company. Three grades with different MA content were basically used. They will be called SMA-4, SMA-8 and SMA-14 respectively, the number corresponding to the weight % of MA. Data for these SMAs are given in Table 3. A rubber modified SMA (ARCO Chemical Company, Dylark 250) which will be called SMA-R has also been used.

Polystyrene (PS) supplied by Dow Chemical USA was used as a matrix for some of the experiments of the first set.

Table 3: Data for SMA.

	Trade name	Maleic anhydride content (%)	Molecular weight	Density (g/cm^3)	Melt flow (g/10 min)	Vicat softening point (^{o}C)
SMA-4	Dylark 132	4	Not available	1.08	"L": 1.5 "N": 1.9	112
SMA-8	Dylark 232	8	$\overline{M}_w = 200,000$ $\overline{M}_n = 100,000$	1.08	"L": 1.7 "N": 1.8	118
SMA-14	Dylark 332	14	$\overline{M}_w = 180,000$ $\overline{M}_n = 90,000$	1.10	"L": 1.9 "N": NA	130

Figure 11 represents the possible grafting reaction between CA and SMA. The free hydroxyl groups on the CA react with the anhydride functionality on the SMA backbone, to form half esters. A similar reaction can occur between the hydroxyl of amylose and the anhydride of SMA. However, in this case, only hydrogen bonding (hydroxyl-anhydride) is probably occurring.

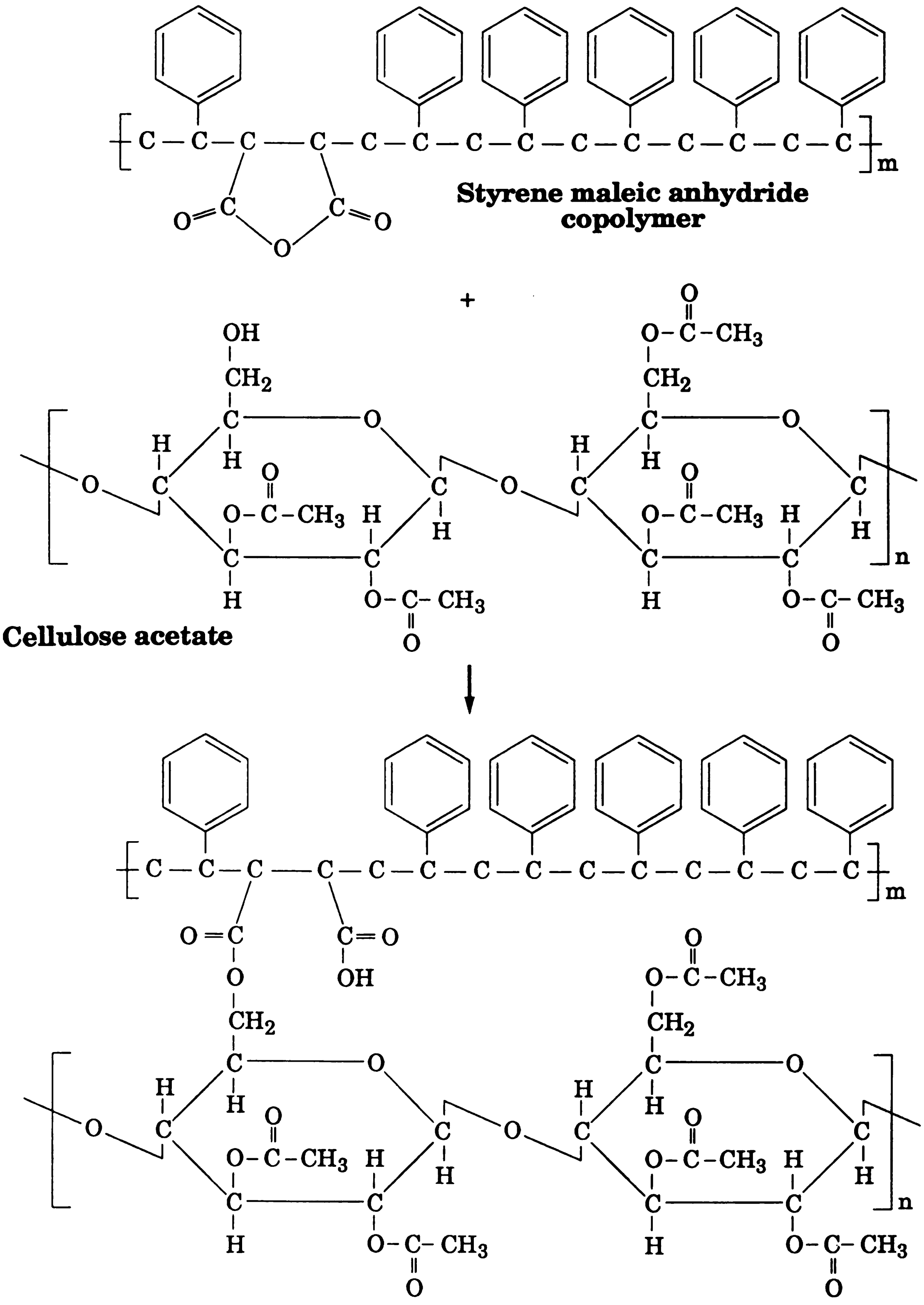
Styrene maleic anhydride copolymer
Cellulose acetate

Figure 11: Grafting reaction between the hydroxyl group of cellulose acetate and the anhydride functionality of styrene maleic anhydride copolymer.

CATALYST

A catalyst was added, when this was found necessary. Potassium chloride (KCl, Mallinckrodt) was previously found to work as a catalyst for the CA-SMA reaction [Neu (1989)]. This was not however the case for our experiments. Poly(2-vinylpyridine) (MW: 200,000, Polysciences) and Poly(4-vinylpyridine-co-styrene) (styrene content 10%, Aldrich Chemical Company) were also tried without the desired results. The only catalyst which was found to work was 4-dimethylaminopyridine (DMAP, Aldrich Chemical Company) (Figure 12). DMAP, a colorless, crystalline solid with a melting point of 114°C and a boiling point of 162°C at 50 torr, is a good catalyst for many types of reactions, and it is many times used on an industrial scale. DMAP is also available supported on an insoluble polymer with the name POLYDMAP polymer (Reilly Industries) [Goe *et al.* (1990)].

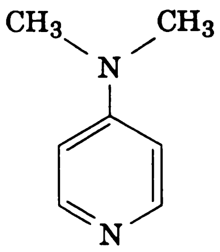

Figure 12: 4-dimethylaminopyridine.

PROCESSING AND CHARACTERIZATION

The experimental protocols followed was basically the same for both sets of experiments. It consists of two parts. The first is the preparation of the CA blends or amylose composites, and the second is the materials characterization. A schematic of the protocol followed is given in Figure 13.

BLENDS OR COMPOSITES PREPARATION

Grinding

The extruder where the materials were mixed had only one feeder. It was therefore necessary to first prepare a homogeneous dry mixture of the materials, and then pour this mixture in the feeder. As was discussed in the previous chapter, the particles of amylose and CA had dimensions 5-10 μm and 100-400 μm respectively. SMA, PS and Dexel were, however, supplied in pellet form, with pellet dimensions 2-4 mm.

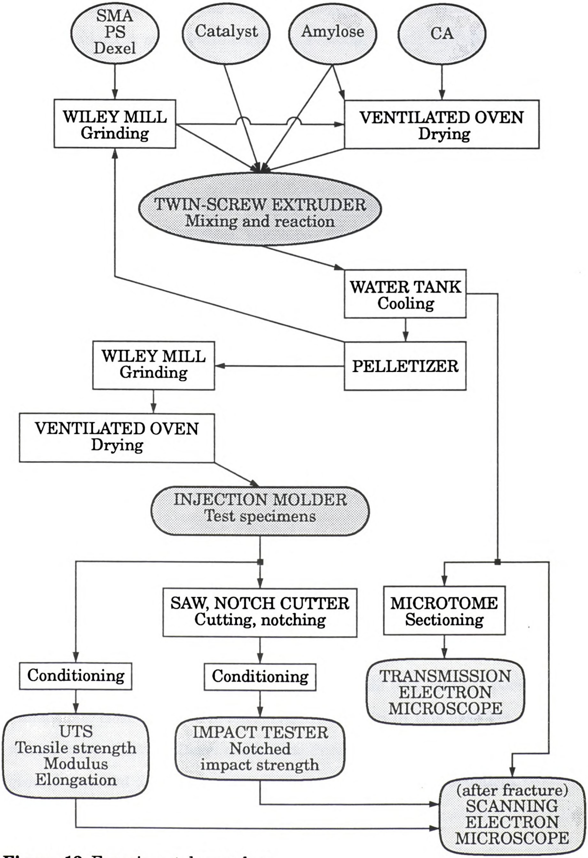
SMA
PS
Dexel
Catalyst
Amylose
CA
WILEY MILL
Grinding
VENTILATED OVEN
Drying
TWIN-SCREW EXTRUDER
Mixing and reaction
WATER TANK
Cooling
WILEY MILL
Grinding
PELLETIZER
VENTILATED OVEN
Drying
INJECTION MOLDER
Test specimens
SAW, NOTCH CUTTER
Cutting, notching
MICROTOME
Sectioning
Conditioning
Conditioning
TRANSMISSION
ELECTRON
MICROSCOPE
UTS
Tensile strength
Modulus
Elongation
IMPACT TESTER
Notched
impact strength
(after fracture)
SCANNING
ELECTRON
MICROSCOPE

Figure 13: Experimental procedure.

The problem, therefore, was how to homogeneously mix the pellets and the much smaller CA or amylose particles. Besides, even if this was possible, the pellets would advance faster than the particles in the screw feeder used, so again the mixture fed in the extruder would not be homogeneous.

For the above reasons, grinding of the materials provided in pellet form was found necessary. A Wiley mill was used for this purpose. This is a special type of mill made of stainless steel, which can effectively grind hard materials. A sieve is used to control the size of the ground material. A sieve with 0.5 mm holes was appropriate for mixing the material with CA. However, the process with this sieve was very slow, and for this reason a sieve of 1 mm was used. Most of the particles after grinding were 0.6-1 mm, but there were also some very fine particles present, because of brittle fracture. An SEM picture of SMA-8 particles after grinding is shown in Figure 14. Care should be taken during this step so that the material does not get contaminated by impurities of the mill, since such impurities might act as initiators of degradation during further processing.

In the case where Dexel was mixed with SMA, both materials were in pellet form. It was, therefore, acceptable to mix them without pre-grinding. However, when catalyst was added, homogeneous mixing of the very low amount of catalyst particles with the pellets was impossible (the catalyst particles had dimensions close to those of CA). Therefore, even in this case the materials were ground. Further, Dexel needs to be dried before extrusion, and drying the ground material was much faster and easier than drying the pellets.

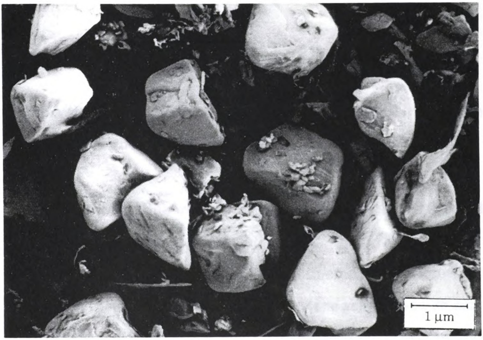

Figure 14: SMA-8 Wiley milled using a 1 mm sieve.

However, this step will not be necessary if a second feeder is available, and this would be the case if the process was carried out in an industrial scale.

Drying

For CA and ground Dexel, drying was needed before extrusion. This was conducted in a ventilated oven at 70°C for 5 hours. The thickness of the material's layer on the tray was always less than 5 cm.

As will be explained in chapter 5, amylose was not dried before extrusion. There was only one experiment where dry amylose was used. It is, however, very difficult to dry amylose using a ventilated oven, this is why for this experiment amylose was dried in a vacuum oven (~-30 in Hg) at 70°C for 12 hours (thickness of material's layer on the tray ~5 cm).

Extrusion

Extrusion was the main step of the experiments. It was where the materials were mixed, and in situ compatibilization reaction occurred.

The extruder used was a Baker-Perkins co-rotating intermeshing (closely self-wiping) twin-screw extruder. This extruder is shown in Figure 15, while Figure 16 is a representation of the screws. The diameter of each screw was 3 cm, the distance from the feeding point to the end of the screws was 38 cm and the length of each screw was 42 cm. There were two feed ports on the barrel, two barrel valves and a venting port. The materials were fed at the first feed port, and the other ports and valves where kept closed. The material was coming out of a die having two 3 mm holes. Each screw had two sets of six paddles, and a Camel back discharge screw at the end. The temperature was measured at three points on the barrel, at one point on the die, and at four points inside the barrel (melt temperature), defining zone 1, zone 2, zone 3, and the discharge. Four manually adjusted valves were controlling the flow rate of the cooling water used to cool the barrel. There was no cooling water supply for the die. Four valves turning the supply of cooling water to the barrel on and off, controlled the temperature of zones 1-3.

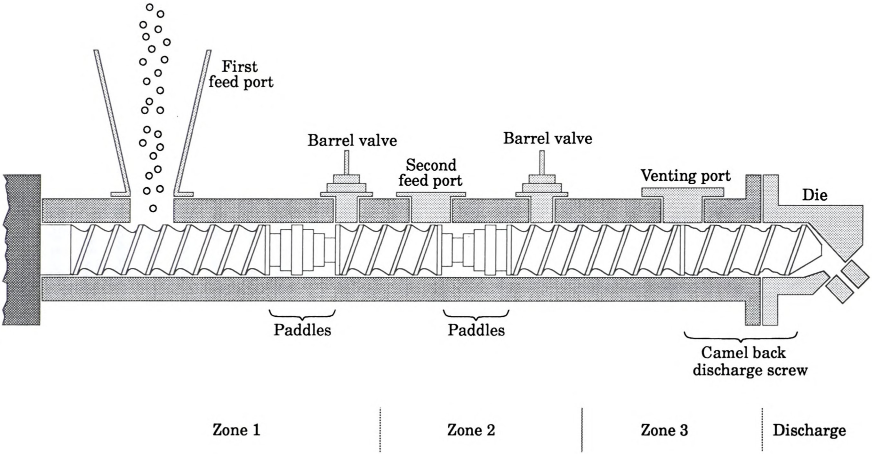
First
feed port
Barrel valve
Second
feed port
Barrel valve
Venting port
Die
Paddles
Paddles
Camel back
discharge screw
Zone 1
Zone 2
Zone 3
Discharge

Figure 15: Baker-Perkins extruder (Composite Materials and Structures Center, Michigan State University).

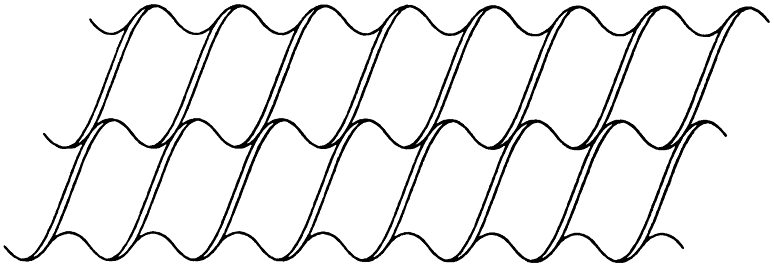

Figure 16: Co-rotating intermeshing (closely self-wiping) twin-screws.

The extruder was cleaned before and after each run. One way to clean the extruder is with a wire brush by opening the barrel (while hot). This, however, is not only difficult, but also not reliable since many points under the screws can not be reached, and impurities are not totally removed. The extruder was cleaned by running PS through it. When PS coming out of the extruder was crystal clear, it was assumed that no other material (or impurity) except PS was in the extruder. Our material was run directly after the PS run. Obviously, in this way at the beginning the extrudate was a mixture of our material and PS. This material was not collected for further testing. In order to have enough material for further processing the dry mixture fed in the extruder was 1600 g. At the point where our material started coming out of the extruder the extrudate (crystal clear PS) was becoming opaque. From this point the material was collected and weighted. When the weight of this material was 250-300 g, almost all the PS had been pushed out, and the extrudate was pure enough to be collected for further testing. Collection of the material was stopped when the load (torque) of the extruder, which was kept constant

during extrusion (maximum ±8%), started decreasing. Although there was still material left in the extruder, this material had been subjected to an extended residence time, which was not desirable. Usually this material was about 150-200 g. Therefore, from the initial 1600 g fed, about 1100-1200 g were collected. This was sufficient for the characterization work.

The temperature controllers keep the barrel temperature close to the set point (this is where the heating devices are). It is, however, the melt temperature (measured by the thermocouples in the barrel) which is more important for our experiments, and this is usually different than the barrel temperature. For this reason, the set point temperature was set in such a way as to maintain the desired melt temperature. Care was also taken to ensure that the flow rate of the cooling water was low enough to decrease the barrel temperature only 2-3 degrees below the set point. For this purpose the valves had to be only 1/24 turn open. The variation of the melt temperature was ±3°C among the different runs, and ±2-3°C for the same run. The extrusion conditions are shown in Table 4. The feed rate was manually controlled so that the load is close to 102%, which means that the extruder was run close to it's high torque limits. and, for the temperatures selected, the volumetric flow rate was as high as possible. The variation of the load was ±7% among the different runs, and ±5-8% for the same run.

Table 4: Extrusion conditions.

Temperature	Set 1				Set 2	
Desired(°C)	180		195		235*	
	Set point	Melt	Set point	Melt	Set point	Melt
Zone 1(°C)	150	~125	165	~136	180	~146
Zone 2 (°C)	159	~180	174	~195	210	~232
Zone 3 (°C)	195	~181	210	~196	250	~235
Discharge (°C)	180	~184	195	~198	235	~236
Screw speed:		200 rpm (revolutions per minute)				
Discharge pressure:		1-5 atm (1-2 atm in most of the cases)				
Load (torque):		~102%				
* Dexel was extruded at 200°C						

A water tank was used to cool the materials directly after extrusion, so that they can be continuously pelletized. It should, however, be noted that although water cooling facilitates the process by allowing continuous pelletization, it might result in water absorption by the material. This is why the material was dried before re-extrusion or injection.

In the cases where the material was to be passed through the extruder again, it was ground after pelletization, and dried (in a ventilated oven, at 70°C, for 5 hours. The thickness of the material's layer on the tray was always less than 5 cm). Grinding was necessary, in order to reduce the size of some big pieces, because it increases the torque of the extruder higher than the instrument specifications. Grinding also facilitated drying. Grinding was also necessary if the material was to be mixed with catalyst. The Wiley mill and a sieve of 2 mm was used, except when the material was mixed with catalyst, where a sieve of 1 mm was used.

MATERIALS CHARACTERIZATION

Preparation for injection molding

The materials had to be pelletized so that they can be molded to a specimen shape. Die swelling for the material was coming out of the die was observed. This increases the diameter of the extrudate significantly (sometimes up to 2 cm). If the pelletization was continuous, the pelletizer was pulling the extrudate. This resulted in a diameter thin enough to be pelletized. In cases where a continuous process was not possible (for example when the flow rate of the extrudate was not high enough to match the minimum speed of the pelletizer), the extrudates were pulled manually, so that they are thin enough to be fed later in the pelletizer.

After pelletization, and before injection, the materials were ground (Wiley milled) with a sieve of 2 mm and dried (same conditions as before re-extrusion). Grinding reduced the size of big pieces which could cause problems during injection, and helped dry the material better. As will be explained in chapter 5, the grinding process does not affect the properties of the material.

Injection molding

A New Britain (model 75) injection molder was used for molding the materials

into ASTM D638 type I specimens. The injection molding conditions are shown in Table 5 (zone 1 is the one closer to the nozzle).

Table 5: Injection molding conditions.

Temperature	Set 1		Set 2
Nozzle (°C)	200	210*	240
Zone 1 (°C)	200	210*	240
Zone 2 (°C)	180	190*	215
Stroke length (in):	1 3/8		
Holding time (s)	8		
Cooling time (s)	35		
* When SMA-14 was the matrix			

A release agent was sprayed on the mold before every injection session, or every two runs (different run means different sample). Before and after each run, PS was used to clean the injection molder. Each sample was about 1050-1150 g, and each injection consumed approximately 20 g (the density of the materials run was not much different). This means that about 50-55 specimens were collected every time. The first specimens were obviously a mixture of PS and our material. As the injection proceeded, more PS free specimens were obtained. The specimens obtained close to the end of the run were the ones used for testing. The amount of material which was left in the injection molder at the point when the feeder was empty was enough for about 8 specimens. In order to get this material out, PS was fed. The cooling time was high enough to allow solidification and some shrinkage of the material. This allowed the injected part to be pushed out of the mold. However, the cooling into ASTM D638 type I specimens. The injection molding conditions are shown in Table 5 (zone 1 is the one closer to the nozzle).

Table 5: Injection molding conditions.

Temperature	Set 1		Set 2
Nozzle (°C)	200	210*	240
Zone 1 (°C)	200	210*	240
Zone 2 (°C)	180	190*	215
Stroke length (in):	1 3/8		
Holding time (s)	8		
Cooling time (s)	35		
* When SMA-14 was the matrix			

A release agent was sprayed on the mold before every injection session, or every two runs (different run means different sample). Before and after each run, PS was used to clean the injection molder. Each sample was about 1050-1150 g, and each injection consumed approximately 20 g (the density of the materials run was not much different). This means that about 50-55 specimens were collected every time. The first specimens were obviously a mixture of PS and our material. As the injection proceeded, more PS free specimens were obtained. The specimens obtained close to the end of the run were the ones used for testing. The amount of material which was left in the injection molder at the point when the feeder was empty was enough for about 8 specimens. In order to get this material out, PS was fed. The cooling time was high enough to allow solidification and some shrinkage of the material. This allowed the injected part to be pushed out of the mold. However, the cooling time should not be very high, because the part close to the nozzle should be kept soft enough to allow separation of the injected part from the rest of the material. In addition, lower cooling time means less residence time of the rest of the material in the injection molder, and this reduces degradation (if any).

Compression molding

Compression molding was also evaluated for specimen preparation. An ASTM D638 type V specimen mold was used for this purpose. Both compression and injection molding have advantages and disadvantages. The advantage of injection molding is that it is a continuous process which produces many homogeneous specimens quickly. Lot of material is required to purge the injection molder from the material previously run. Also, there is an orientation in the direction of injection which might make the properties measured to be different than the transverse properties.

Compression molding does not generate such an orientation, and does not require much material, but it is a much slower (batch) process. The major disadvantage is the general lack of homogeneity of the specimens produced and alteration of the blend morphology. This is specially true for polymer blends. Degradation can also result from this annealing of the sample. In the case of CA-SMA blends, compression molding temperatures higher than the T_g of CA generally resulted in degradation of the material. Also, since SMA was melting faster, the gap between the pellets was basically filled by SMA (specially for compression molding temperatures lower than CA's T_g) and the relative transparency of this phase was making the lack of homogeneity quite obvious. The above reasons made us select injection molding as the specimen preparation method of choice.

Tensile and Izod impact tests

All specimens where conditioned prior to test for at least 40 h. All mechanical tests where conducted at room temperature.

Tensile tests for strength, elongation and Young's modulus were conducted with constant strain rates in a UTS testing machine (ASTM D638). An extensometer was used for measuring the modulus. The testing speed was 0.2 %/min for the modulus measurement and 2 %/min for breaking the specimen. At least five specimens were tested from each sample.

The injection molded specimens were also used for Izod impact test. The arrows in Figure 17 indicate the points where the specimens were cut (using a saw) for preparing a specimen with length 2.4 in, width 0.5 in and thickness 0.125 in. A TMI notch cutter and impact tester were used for notching and testing the specimens according to ASTM D256A. Care was taken so that the notch (the most sensitive part of the specimen) is as free of defects as possible. At least 10 specimens were tested from each sample.

Using a notch cutter, instead of injecting the material into a mold already having a notch, is generally preferred. This is because the flow lines of such an injection might result in a different morphology around the notch compared to the rest of the specimen.

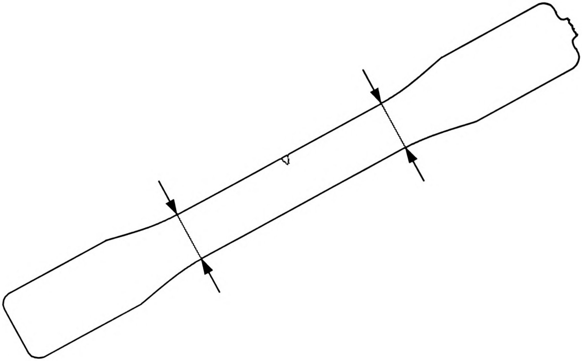

Figure 17: ASTM D638 type I specimen (actual size). The points where it was cut and notched for ASTM D256A (Izod) impact test are also indicated.

Transmission electron microscopy (TEM)

TEM was one of the main tools used for studying blend morphology. It was also the most difficult step, mainly because of the sectioning required before looking at the samples under the microscope. For successful sectioning what is basically required is practice and patience. Some tips, however, are given below.

First each sample was cut (using a small saw) to dimensions approximately 4x6x10 mm, and it was polished using a file, so that it is stable when clamped on the chock (sample holder). If the sample was not large enough to be cut to such dimensions (for example for extracted samples - see chapter 6), it was embedded in epoxy resin and then the resin was polymerized at 65°C for 2 days. A silicon rubber embedding mold giving blocks approximately 3x5x10 was used for this purpose, and the procedure was the generally used procedure for embedding biological specimens.

One of the 4x6 sides of the block was then trimmed to a trapezoid using a razor blade (which means that the sectioning orientation must be decided before cutting the sample). The razor blade was always new and cleaned with ethanol before trimming. Both the shape and the dimensions of the trapezoid are important. The dimensions (and shape) found to be more efficient for the samples sectioned are shown in Figure 18a. Figure 18 also shows the trimming process. A bigger trapezoid was first prepared (from 18b to 18c). Sometimes it was found necessary to cut horizontally to top of this truncated pyramid, in order to prepare a fresh surface (specially if this surface was the result of polishing). Then, this trapezoid was trimmed to a smaller one. It is better that this step is completed at once with four precise and stable cuts. Most probably only practice can help at this point. The height of the resulting truncated pyramid was usually about 0.2 mm (and it was generally sharper than the bigger one). It is better that for the last cutting steps a new razor blade is used. A razor blade having nicks, might leave metal particles on the sample, which might later cause chips on the diamond knife used for sectioning. After the trapezoid was prepared, usually the bottom of the block was cut, to reduce its length and make it approximately 2 mm longer than the sample holder. The longer the block, the more the vibrations during sectioning.

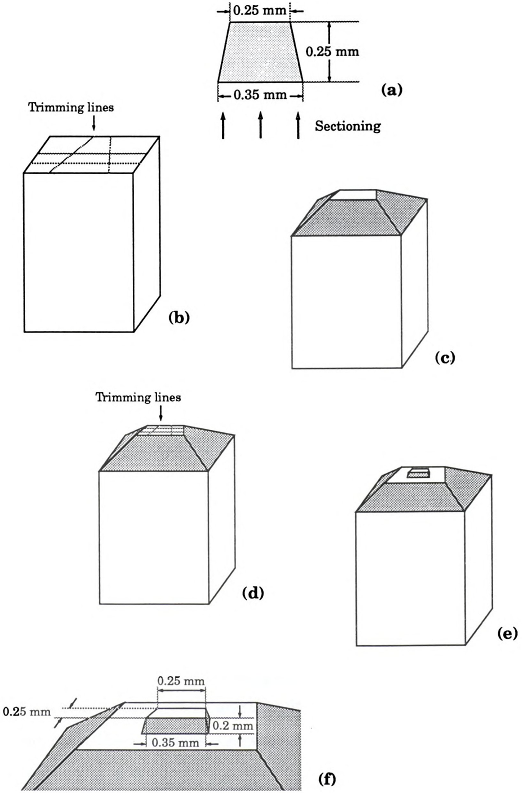
0.25 mm
0.25 mm
0.35 mm
(a)
Sectioning
Trimming lines
(b)
(c)
Trimming lines
(d)
(e)
0.25 mm
0.25 mm
0.2 mm
0.35 mm
(f)

Figure 18: Block trimming (not on scale).

Some of the sectioning was conducted using a glass knife, and others using a 3 mm MICRO STAR diamond knife (from Micro Engineering). A good diamond knife certainly helps reducing the artifacts generated by a glass knife, like compression, chattering and knife marks (see chapter 6). A mistake, however, could easily result in a chip on the extremely sharp (~50 Å) and brittle edge of the diamond knife, which would generate knife marks during sectioning. For someone with no sectioning experience it is, therefore, strongly recommended to practice with a glass knife at least for 10 times before using a diamond knife.

All sectioning was conducted at room temperature. An angle of 4^0 and a moderate speed were used. Both the knife and the sample were cleaned using pressurized air before sectioning. The water level in the boat is important for successful sectioning. It should be right below the point where a black reflection starts appearing on the water near the edge of the knife. It is strongly recommended to always use the same part on the diamond knife until it becomes dull, and not to jump back and forth. It is also recommended to use a dull part of the knife (if any) for preparing the surface, and then move to a sharper part for getting the sections which will be examined.

The thickness of the sections can be estimated by their color. Sections 60-90 nm are silver, sections 90-150 nm are gold, and as the thickness is increasing the color becomes purple, green and blue. Variations to the color of the sample is mainly caused by vibrations. Any activities or conditions which could cause vibration during sectioning (even talking in front of the knife) should be avoided. Many times curling of the sections was observed. This was mainly happening when the section was quite thick. Reduction of the thickness was, therefore, required in these cases. Xylene was not found to stretch the sections of the CA-SMA blends.

Gold sections were found to give the best contrast under the transmission electron microscope (TEM) (for silver section the contrast was sometimes not enough). Gold sections were therefore placed in the middle of the boat, and were collected by placing a grid on the top of them (the sections were adhering to the grid). The diamond knife was cleaned (rinsed with water, ethanol and water, and dried with pressurized air) directly after sectioning, before removing the water from the boat (since the sections of our material could easily adhere on the dry diamond).

The sections were then examined under a JEOL 100CX TEM. 100 kV were used. Objective apertures were also inserted in most of the cases for improving contrast. No carbon coating of the section was found necessary. Care was, however, taken when converging the beam, since a very condensed beam was destroying the sample. Also, no staining was found necessary, since quite high contrast between the CA and SMA phases was resulting after exposing the samples under the electron beam for a short period of time (usually for 10-20 seconds). This contrast can be attributed to mass thickness contrast developed due to loss of material from the CA phase (which was appearing lighter) under the electron beam, whereas the SMA phase (darker) didn't seem like being significantly affected [Thomas and Talmon (1978)].

Scanning electron microscopy (SEM)

SEM was also found very useful for examining the composites or blends morphology, and specially the adhesion between the phases. A JEOL 35CF scanning electron microscope (SEM) was used. Small pieces of the samples (usually cut with a small saw from the one side, and polished) were first mounted on a stub. Carbon paint was applied all around the samples, in order to improve conductivity. Then the samples were sputter coated with gold for 3 minutes (a gold layer of ~21Å was applied). 10 kV were used for most of the cases (15 kV resulted in charging problems). Objective aperture 2, condenser lens 600, working distance 15 or 20 and no gamma were the other conditions used.

Other tests

The extent of the reaction between the CA-SMA phases was quantified using a extraction technique. Small pieces of the samples were Soxhlet extracted with toluene for 48 h. Toluene is a good solvent for SMA and a non-solvent for CA. The residue from the extraction was dried for two days at room temperature, vacuum dried at 80°C for 20 h, and then analyzed using a Perkin-Elmer CHN analyzer and Fourier transform infrared (FTIR). The moisture content was also measured and was used for correcting the elemental analysis results. Since SMA is soluble in toluene, appearance of SMA in the residue after extraction suggests that this SMA is covalently linked to CA. The SMA content could be identified by FTIR (if higher than the detection limits of the method), and quantified (using elemental analysis) from the C content of the residue (comparison with the C content of CA and SMA). A number could, therefore, be calculated for the extent of the reaction. The problem is that good separation (extraction) is required, and in the case of immiscible polymer blends, good separation depends on the morphology of the sample. This will be explained in more details in chapter 6. Gel permeation chromatography was also conducted for some samples.

Chapter 5

AMYLOSE COMPOSITES

Amylose and SMA-8 where found to react to a limited extent in solution in the absence of a catalyst [Argyropoulos *et al.* (1991)]. When catalyst was added both the grafting rate and the grafting degree were greatly increased. Among the factors affecting the reaction, water was found to play an important role. Addition of water resulted in an increase of the reaction rate. It is possible that water functions as a co-catalyst in the esterification process. Because of the potential enhancement of the reaction rate by water, it was decided not to dry the amylose granules before mixing them with the synthetic polymers in the extruder. All the results reported below correspond, therefore, to amylose having an initial equilibrium moisture of approximately 12% (unless otherwise specified). It is, however, by no means suggested that the reaction mechanism in solution is the same as that occurring in the melt state.

MORPHOLOGY

In order to study the role of MA, amylose/PS composites were also prepared. Figures 19 and 20 show a fracture surface of an amylose/PS 15/85 extrudate (all compositions are by weight). It is seen that there is no adhesion between the amylose particles and PS and that the propagation of the crack front was around the amylose granules. This was the case for all amylose/PS samples examined, both after extrusion (Figures 19 and 20) and after injection molding (Figure 21). There was also no significant change to the dimensions or the shape of the particles.

Starch particles have a reasonably long lifetime for temperatures below 265°C [Griffin (1985)]. Thermogravimetric analysis proved that below that temperature the starch we used (amylose) is stable. A sharp pyrolysis started at about 280°C. The T_g is certainly above that temperature. By an extrapolation of T_g data of plasticized amylose, the T_g of pure amylose was estimated to be approximately 330°C [Nakamura and Tobolsky (1967)].

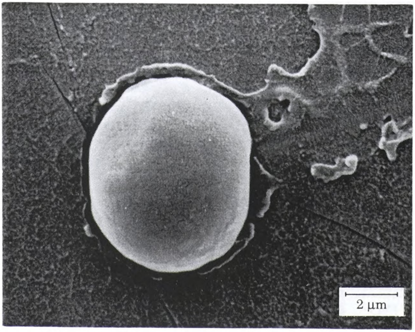

Figure 19: SEM picture of amylose/PS 15/85 after extrusion. No matrix/filler adhesion.

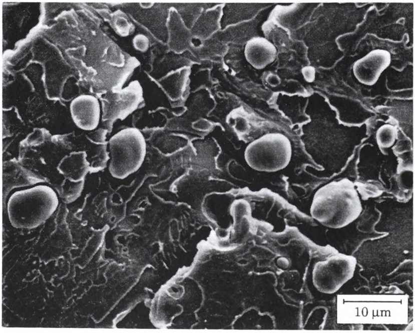

Figure 20: SEM picture of amylose/PS 15/85 after extrusion. No matrix/filler adhesion.

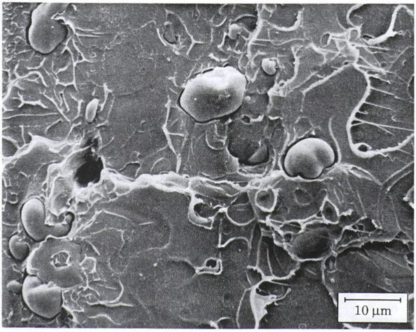

Figure 21: SEM picture of amylose/PS 15/85 after injection (Izod impact fracture surface). No matrix/filler adhesion.

Figure 22 shows a particle after extrusion with SMA-8. In contrast with PS it can be seen that there is excellent adhesion between the amylose granule and the matrix. A typical electron micrograph of the amylose/SMA-8 15/85 extrudates obtained is shown in Figure 23, where only the top of the particles can be seen. This is an interesting phenomenon. PS and SMA deform by crazing. The above observation implies that in the case of composites with good adhesion, any crazes formed that transformed to a crack were near the poles of the particles. A similar behavior was observed for PS filled with glass beads [Dekkers and Heikens (1983a)].

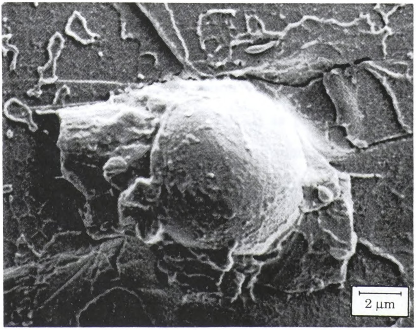

Figure 22: SEM picture of amylose/SMA-8 15/85 after extrusion. Good interfacial adhesion.

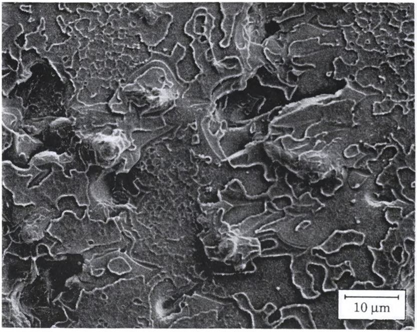

Figure 23: SEM picture of amylose/SMA-8 15/85 after extrusion. Good interfacial adhesion.

It was easier to see the particles when 30% or 45% amylose was used (Figures 24 and 25 respectively), since in this case the crazes had to travel around more particles. Similar morphology was observed for the case of SMA-4 (Figure 26) and SMA-14 (Figure 27), and also when vacuum dried amylose was used (approximately 2% moisture) (Figure 28). It is possible that the adhesion between SMA and amylose is due to a grafting reaction between the hydroxyl and anhydride groups. A different type of interaction (e.g. hydrogen bonding), however, should not be excluded.

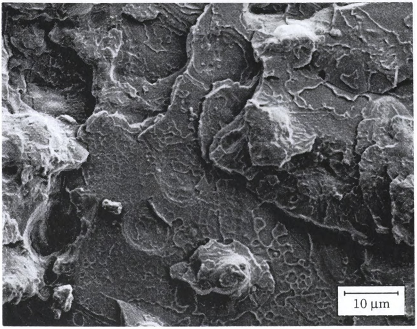

Figure 24: SEM picture of amylose/SMA-8 30/70 after extrusion. Good interfacial adhesion.

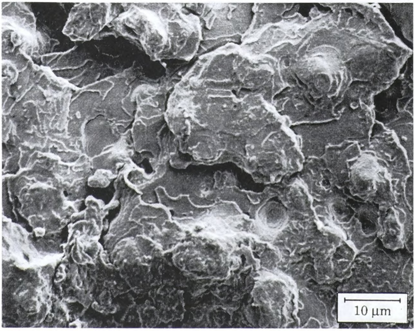

Figure 25: SEM picture of amylose/SMA-8 45/55 after extrusion. Good interfacial adhesion.

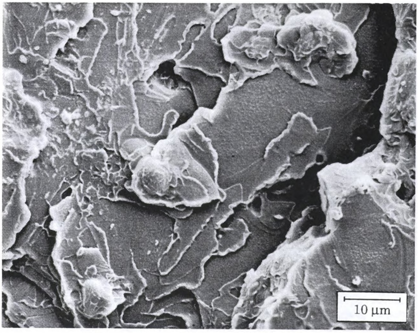

Figure 26: SEM picture of amylose/SMA-4 15/85 after extrusion. Good interfacial adhesion.

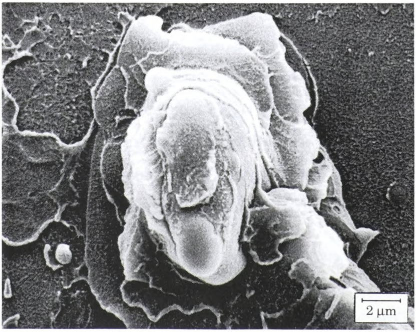

Figure 27: SEM picture of amylose/SMA-14 15/85 after extrusion. Good interfacial adhesion.

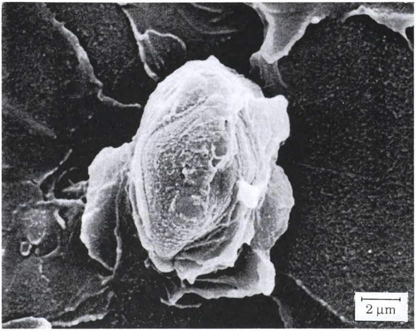

Figure 28: SEM picture of amylose/SMA-8 15/85 after extrusion (amylose was vacuum oven dried before it was mixed with SMA-8). Good interfacial adhesion.

Another interesting point is that the amylose granules didn't break, which means that they are stronger than SMA. There were very few examples (as in Figure 29) where maybe the relative position of the particles together with good adhesion resulted in a broken amylose granule. A central void contained in the granule is also evident in Figure 29. Because of this void which is typical for all maize starch granules having equilibrium moisture or less, maize starch behaves as a strong hollow-sphere filler [Griffin (1985)].

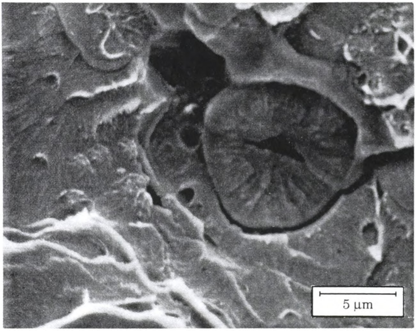

Figure 29: SEM picture of amylose/SMA-8 15/85 after extrusion. One of the few amylose granules which broke.

A TEM examination of the composites was also tried. It was, however, almost impossible to section the amylose phase (although a diamond knife was used). TEM pictures of amylose/SMA-8 composites are shown in Figure 30. Basically holes are appearing in the place where amylose was, and amylose is appearing as dark areas near the edge of the holes. It can, however, be noticed that there are no obvious changes to the general shape and size of the particles. Figure 31 is a high magnification TEM picture where one part of the amylose remained as a section. The reason for this was the very small size of the amylose phase (either a small particle, or a particle sectioned near the pole). The interesting point is that although there are some holes appearing, these holes are not formed at the interface, but inside the amylose part, which means that there is good adhesion between the two phases.

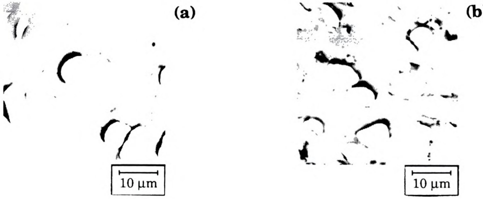

Figure 30: TEM picture of amylose/SMA-8 after extrusion. For (a) the composition is 15/85 and for (b) is 45/55.

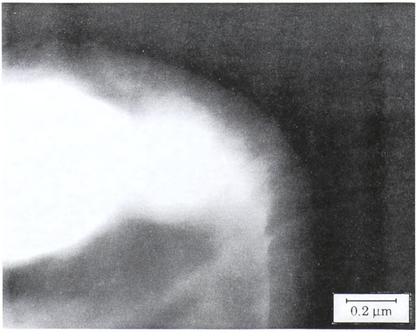

Figure 31: TEM picture of amylose/SMA-8 15/85 after extrusion. The lighter part is amylose, and the darker part is SMA-8.

The effect of water on the morphology of the amylose/SMA blends should also be mentioned. Figure 32 shows a fracture surface of an amylose/SMA-8 36/64 compression molded specimen, where the amylose contained initially 33% moisture (the granules were mixed with water before extrusion). The arrows indicate the amylose regions. Amylose is not in granular form any more and breaks when the specimen is fractured. The water functioned as a plasticizer and destroyed the physical integrity of the amylose grain. A fracture surface of a amylose/SMA-8 20/80 compression molded specimen soaked in water for 31 days is shown in Figure 33. The water absorbed by the amylose also softens the particles and makes them unable to resist the crack propagation effectively.

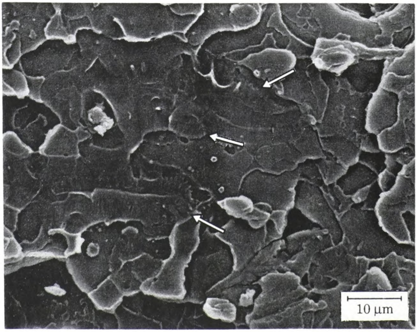

Figure 32: SEM picture of an amylose/SMA-8 36/64 compression molded specimen (fracture in tension). Amylose had before extrusion 33% moisture.

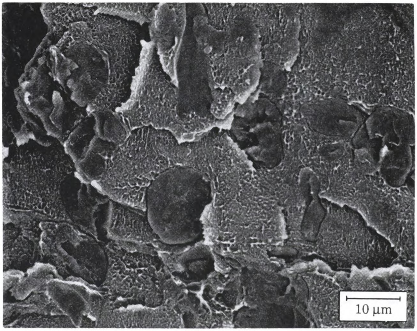

Figure 33: SEM picture of an amylose/SMA-8 20/80 compression molded specimen, soaked in water for 31 days (fracture in tension).

MECHANICAL PROPERTIES

Table 6 shows the mechanical properties of the amylose composites. Typical stress-strain curves for most of the compositions, are shown in Figures 34 and 35. Brittle failure was observed for all composites. A slight change of the modulus indicating crazing is seen only for the material where PS is the matrix.

Table 6: Mechanical properties of the amylose composites.

Synthetic polymer	Weight % amylose	% amylose moisture	Feed rate (%) (% load)	Extrusion temperature (°C)	Tensile strength at break (psi) ASTM D638	Elongation at break (%) ASTM D638	Tensile modulus (10^6psi) ASTM D638	Izod impact strength (ft lb/in of notch) (1/8 in thick specimen) ASTM D256A
SMA-4	0				7300±90	2.9±0.1	0.433±0.011	0.24±0.03
SMA-8	0				7320±170	2.8±0.2	0.433±0.029	0.22±0.02
SMA-14	0				7020±130	2.6±0.1	0.433±0.011	0.19±0.03
PS	0				7240±130	3.0±0.4	0.444±0.015	0.35±0.06
SMA-4	15	~12	4 (105)	180	6320±90	2.1±0.1	0.472±0.009	0.18±0.04
SMA-4	30	~12	5 (104)	195	5710±70	1.7±0.1	0.514±0.008	0.20±0.03
SMA-8	15	~2	5 (111)	180	6490±30	2.4±0.1	0.460±0.006	0.20±0.03
SMA-8	15	~12	4 (107)	180	6120±120	1.9±0.1	0.484±0.011	0.20±0.03
SMA-8	15	~12	*		4160±510	1.6±0.2	0.446±0.011	0.20±0.01
SMA-8	30	~12	4 (102)	195	5310±150	1.6±0.1	0.517±0.015	0.22±0.03
SMA-14	15	~12	5 (107)	195	5890±100	1.9±0.1	0.494±0.015	0.18±0.02
PS	15	~12	4 (93)	180	6170±80	2.1±0.1	0.471±0.009	0.25±0.03

*** Amylose and SMA 232 were mixed in the injection molder only (they were not pre-extruded).**

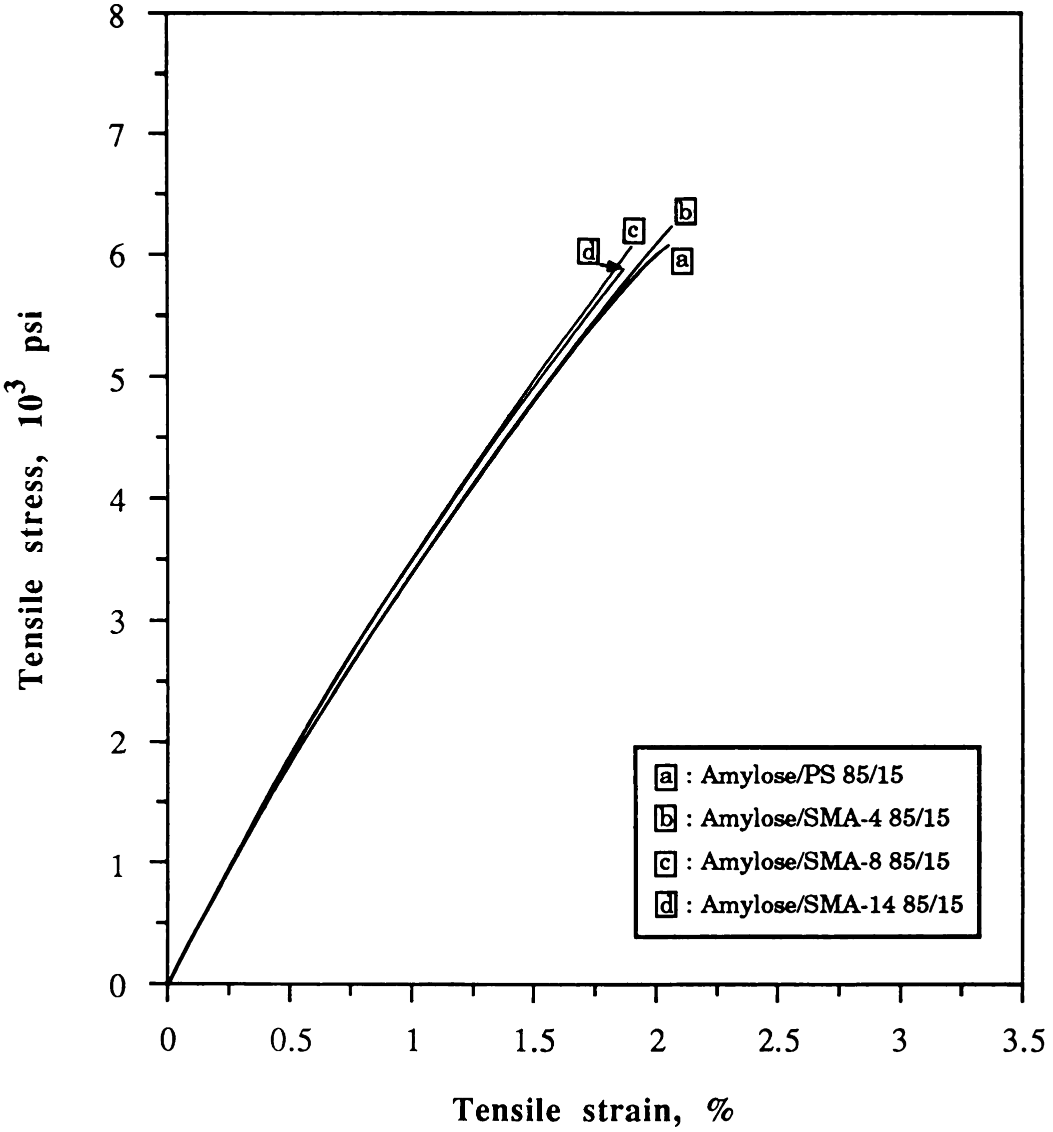

Figure 34: Stress-strain curves of amylose composites.

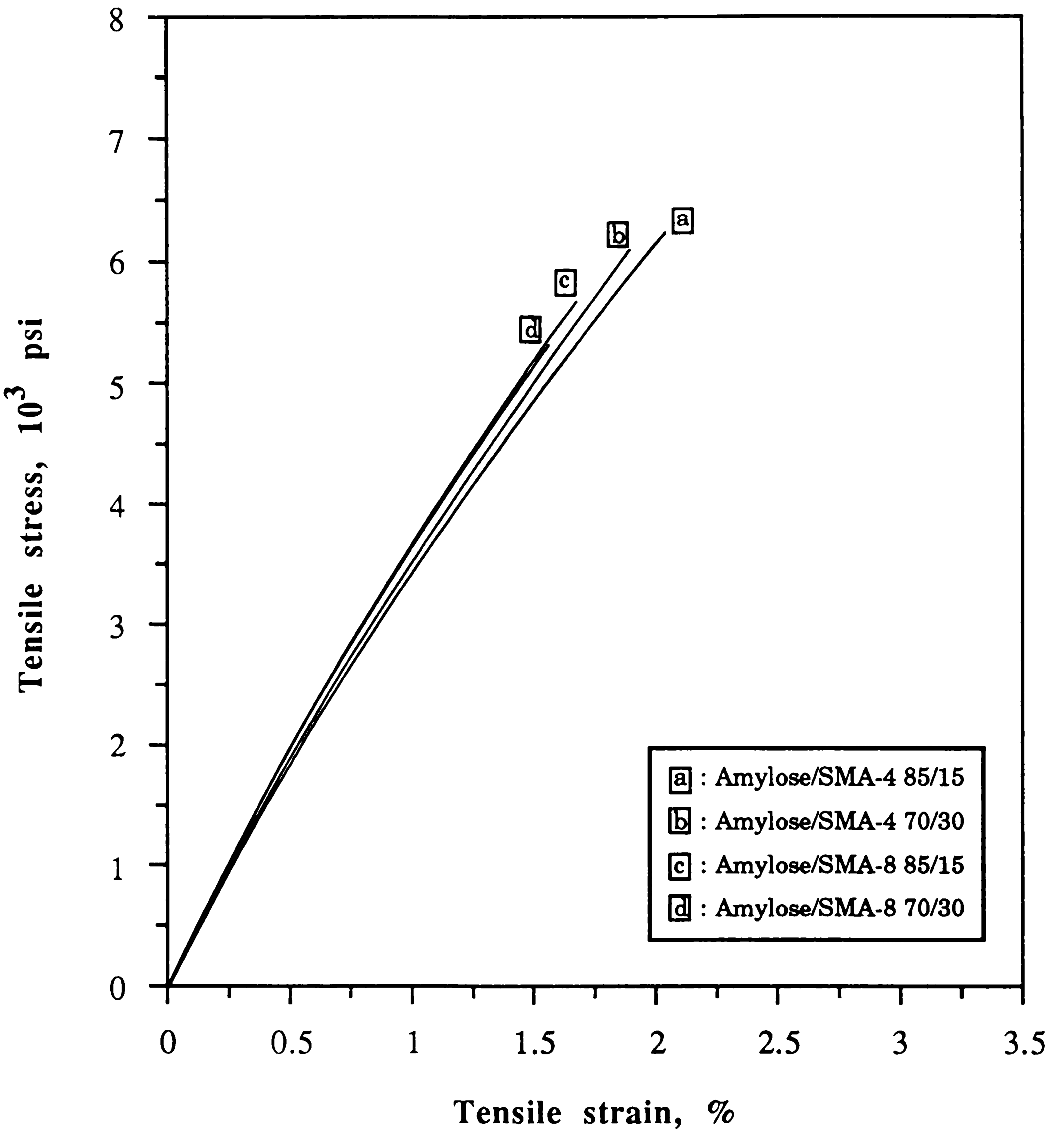

Figure 35: Stress-strain curves of amylose composites.

In Figure 36 the relative Young's modulus (modulus of the composite/modulus of the matrix) is plotted as a function of the MA level (Figure 36a) and the amylose content (Figure 36b). It is obvious that the modulus increases with increasing amylose content. This is always the case when high modulus particles are added to a low-modulus polymeric matrix [Young (1986)].

An equation for predicting the modulus of filled systems is that of Ishai and Cohen (for uniform boundary displacement) [Ishai and Cohen (1967)]:

$$\frac{E_c}{E_o} = 1 + \frac{v_f}{\frac{m}{m-1} - v_f^{1/3}} \qquad m = \frac{E_p}{E_o} \tag{15}$$

where E_c, E_o and E_p are the composite, matrix and filler moduli, and v_f is the volume fraction.

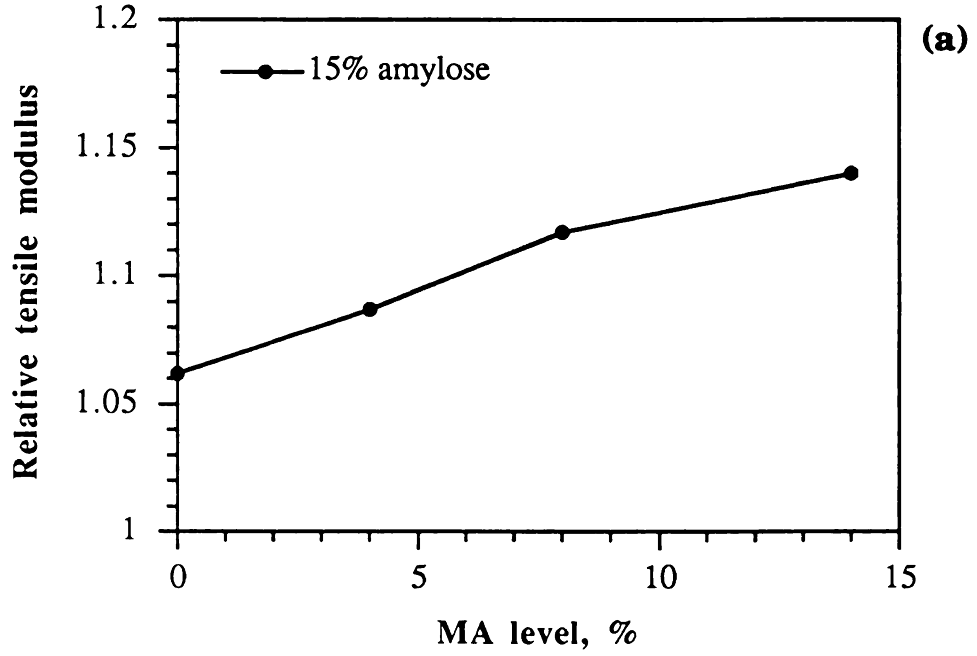

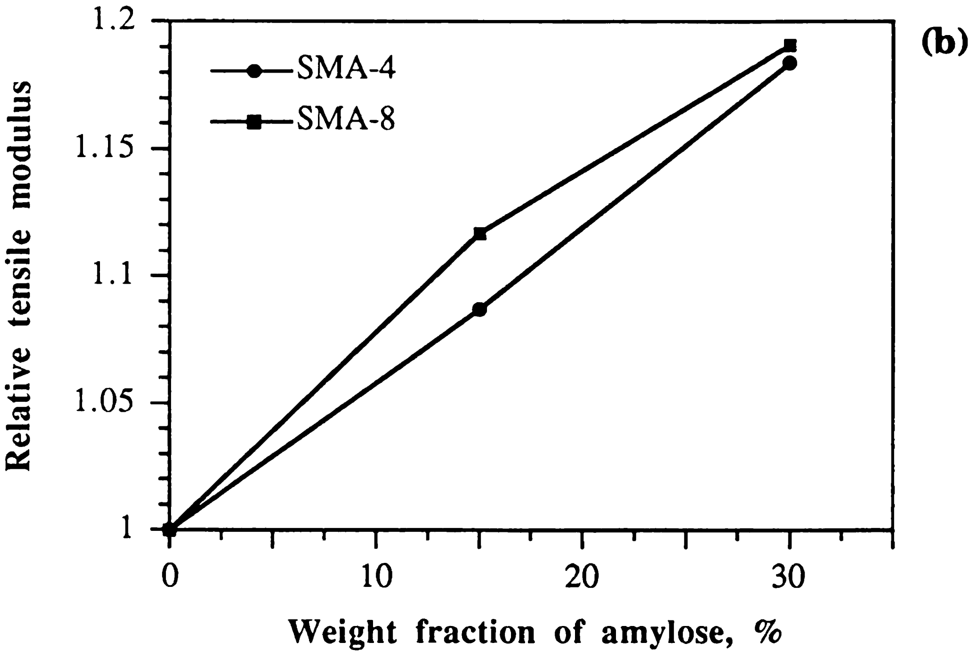

Figure 36: Relative Young's modulus (composite/matrix) as a function of the MA level (a) and the amylose content (b).

A number can be calculated for the modulus of the amylose particles, so that the above equation (for uniform boundary displacement) best fits the above data. This number is 6.6 GPa when SMA-4 is the matrix and 8.1 GPa when SMA-8 is the matrix. The difference between the two numbers suggests that such calculations can only give an estimate of the magnitude of the amylose modulus (Young's modulus for SMA-8 is 3.0 GPa and for glass is 70 GPa).

According to Figure 36a better adhesion (provided by a higher MA content) also helps to increase the modulus. This is not the case for glass-bead-filled polymers [Dekkers and Heikens (1983b)], where the modulus is hardly affected by the degree of interfacial adhesion. The reason for this might be due to the difference between the moduli of glass and amylose. The modulus of glass is 20 times higher than the modulus of PS, and that may be the reason as to why the particle/matrix adhesion has a negligible effect. It seems that this effect can not be neglected in the case of amylose which has a modulus much closer to that of the matrix.

Figure 37 presents the tensile strengths of the amylose filled composites. It can be seen that the tensile strength of the composite is always lower than the strength of the matrix, decreases with increase in weight fraction of the filler and appears to be unaffected by the level of adhesion. These results are generally in agreement with the literature. In the case of particulate-filled brittle thermosets [Sahu and Broutman (1972), Hojo *et al.* (1974), Leidner and Woodhams (1974)], when there is no particle/matrix adhesion there is a decrease of the ultimate strength with increase of the particle content. In the case of good adhesion a retention of the matrix strength is observed, while moderate adhesion data fall between the upper and lower bounds. There is also a decrease in strength as the average size of the particles increases. In the case of particulate-filled brittle thermoplastics [Dekkers and Heikens (1983b), Lavengood *et al.* (1973)] (deforming by crazing), the composite's strength decreases with the filler content, even with excellent adhesion. This suggests that adhesion can not effectively control craze formation and growth.

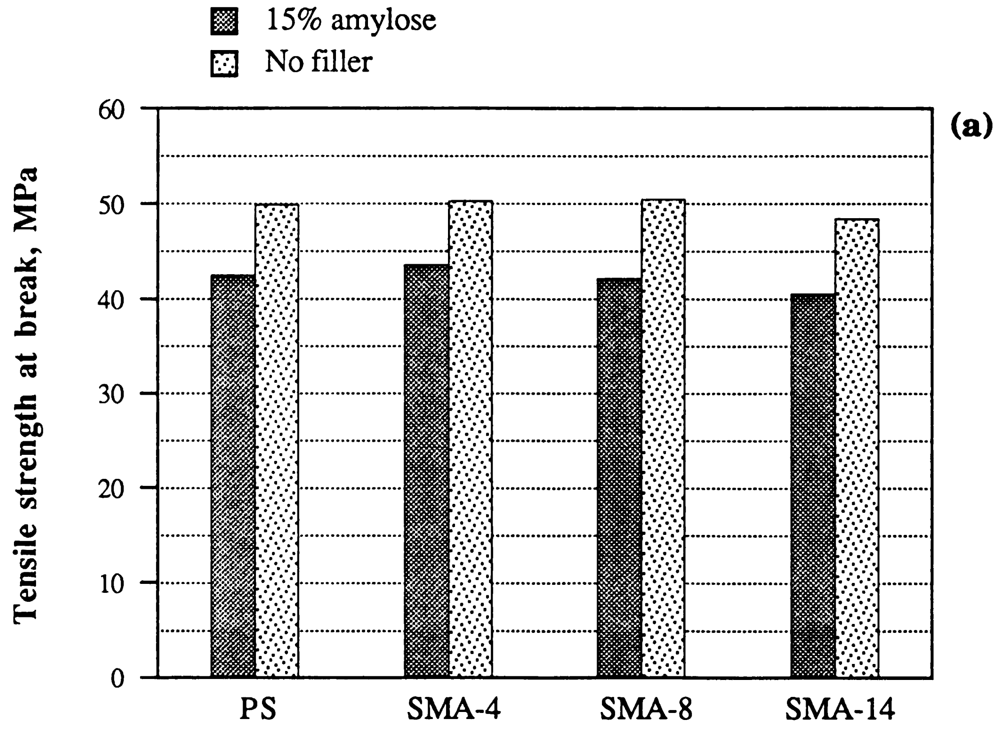

Figure 37: Tensile strength of the composites containing 15% amylose and of their corresponding matrixes (a), and relative tensile strength (composite/ matrix) as a function of the MA level (b) and the amylose content (c).

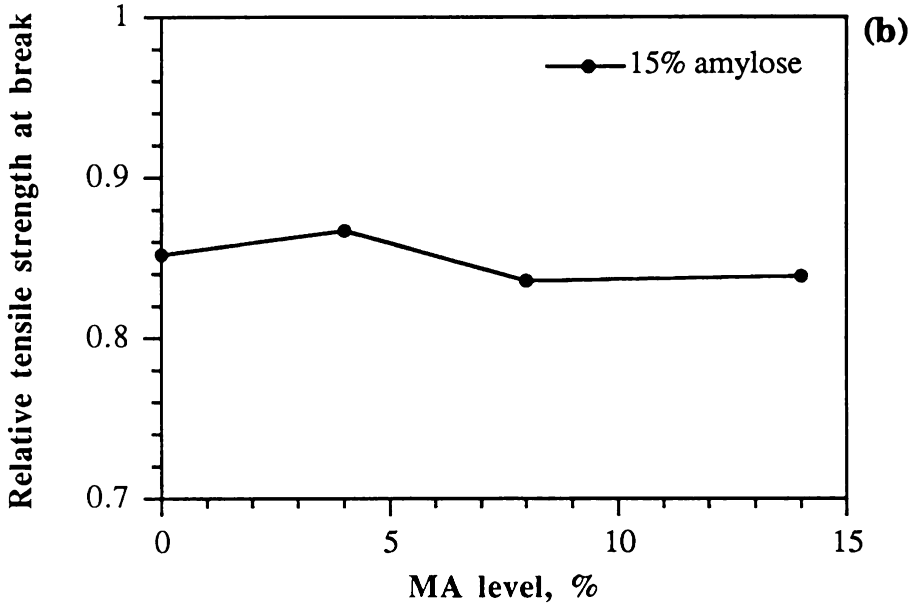

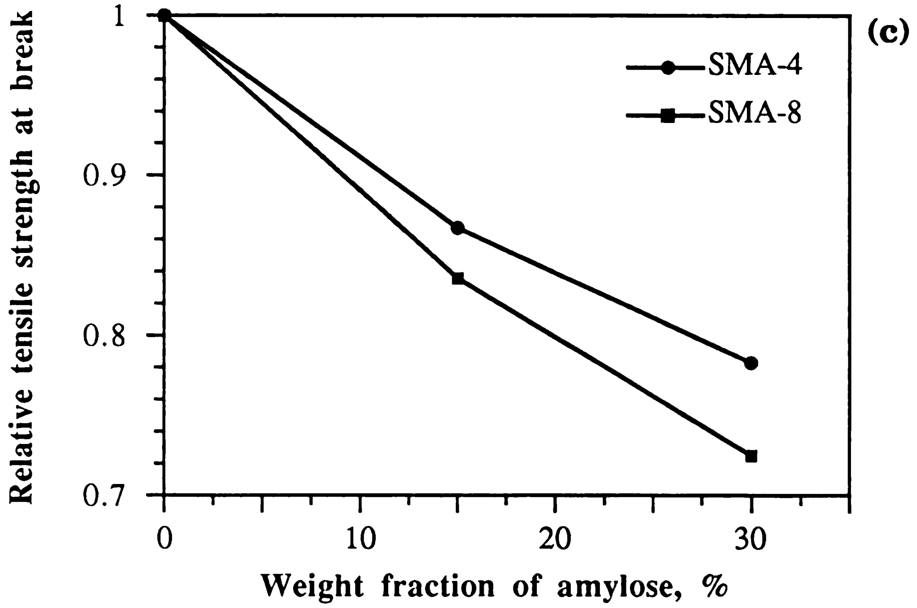

Figure 37: (cont'd).

The relative Izod impact energies as a function of the MA level and the filler content are shown in Figure 38. For particulate-filled brittle polymers, the impact strengths are normally less than those of the pure matrix, and strong particle/matrix adhesion gives the highest impact strengths [Young (1986)]. In agreement with literature, better adhesion between amylose and SMA resulted in improvement of the impact strength, although the difference between the values is not significant when compared to the standard deviations. It should, however, be noted that for excellent adhesion (SMA-14) or good adhesion and high amylose content (amylose/SMA-8 30/70) the impact strength is almost equal or even higher than that of the base resin. A general retention of the impact strength can therefore be claimed.

The main advantage of particulate-filled polymers is their higher toughness compared to the matrix, expressed as an increase of the fracture energy [Broutman and Sahu (1971), Spanoudakis and Young (1984)] (although conflicting results have been reported as to whether good or poor adhesion results in the toughest material [Phillips and Harris (1977)]). The increase of the fracture energy is not reflected to the impact energy, which according to Broutman and Sahu [Broutman and Sahu (1971)] decreases with increasing filler content. The reason for this is that impact tests are rather high strain rate flexural tests and can not be considered as measuring the actual toughness of the material [Phillips and Harris (1977)]. The retention of the impact strength observed for some of the amylose-filled samples can, therefore, be considered as a suggestion that the toughness of these materials is higher than that of the base resin. Significant toughening should not, however, be expected.

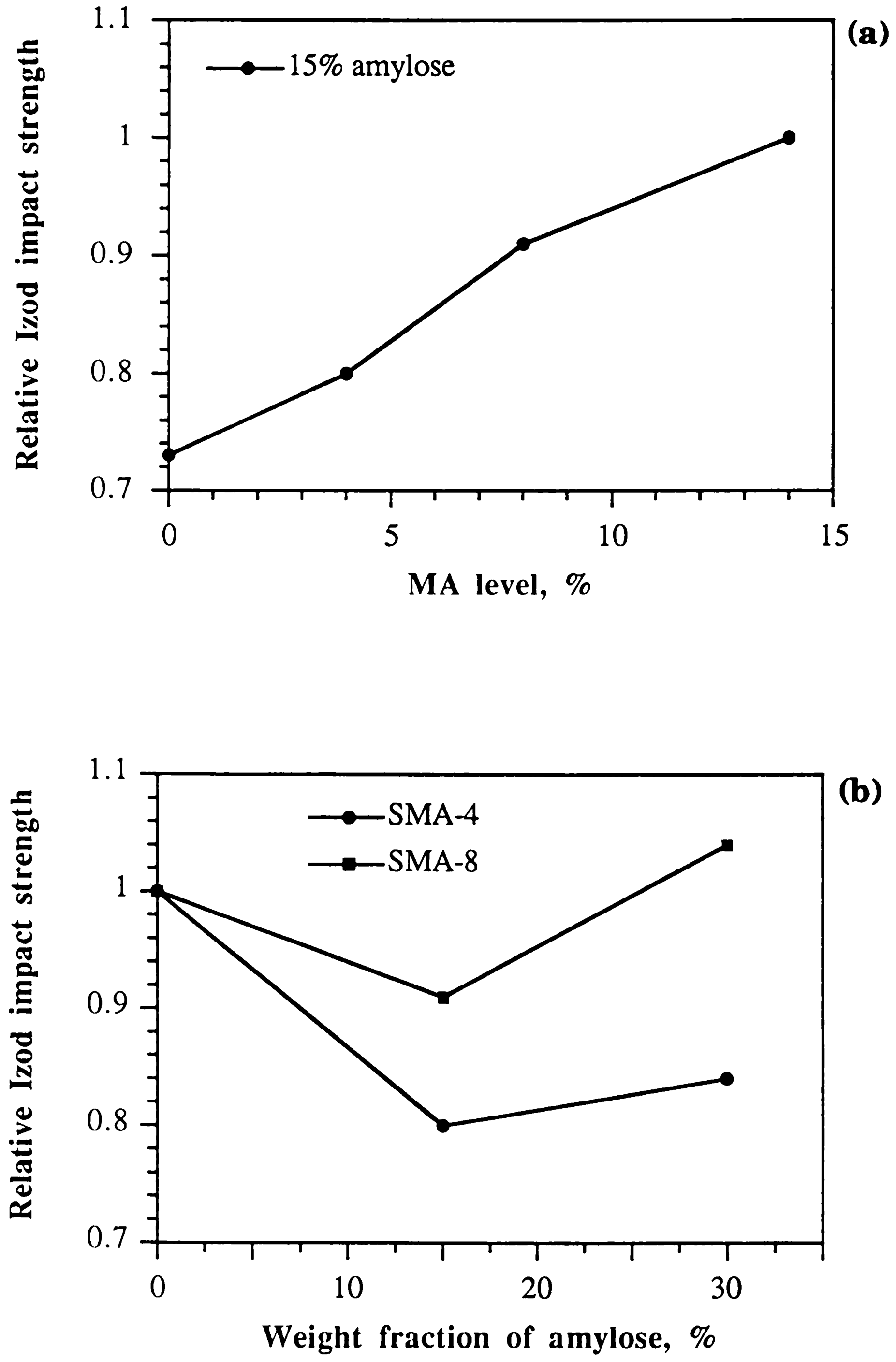

Figure 38: Relative Izod impact strength (composite/matrix) as a function of the MA level (a) and the amylose content (b).

Good distribution of the amylose particles in the matrix is essential for optimum properties. Shortening of the mixing time reduced tensile strength. The minimum value was obtained when amylose was mixed with the matrix in the injection molder only (without pre-extrusion). Inadequate mixing results in incorporation of particles which become dangerous flaws. Better distribution is favored by particle /matrix adhesion.

All the above data concerning the mechanical properties of the composites are based on testing of injection molded specimens. Grinding of the samples before injection, doesn't seem to be affecting the mechanical properties. For amylose/SMA-8 15/85 composites, the difference between the average mechanical properties of specimens molded from ground and non ground materials was 0.5%, 0.6%, 1.0% and 2.9% for tensile strength, elongation, modulus and Izod impact strength respectively.

When amylose/SMA-8 15/85 (injection molded) specimens were prepared using dry amylose granules instead of those containing the normal 12% moisture, the tensile strength was 6% higher (but still lower than that of the matrix). This suggests that the properties of the particle affect the tensile strength, and not the adhesion. Further investigation is needed.

Chapter 6

CELLULOSE ACETATE BLENDS

MORPHOLOGY

CA/SMA blends - No catalyst

Figure 39 is a fracture surface (all fractures were at room temperature) of a CA/SMA-8 70/30 blend (all the compositions are by weight). It is obvious that there are two phases (the materials are certainly not miscible), and that there is no adhesion between the two phases (incompatible blend). The continuous phase is CA and SMA-8 is the dispersed phase (in droplet form). The dimensions of these droplets are in the order of a few microns. As was expected (since both materials were in melt condition), the mixing in the extruder was dispersive (dispersive is the mixing which reduces the size of particles and optimizes their distribution). In contrast, the mixing in the case of amylose/ SMA composites was distributive (increase of the randomness of the spatial distribution, without reduction of the size) [Cheremisinoff (1987)].

The morphology observed in the CA/SMA system is quite common in the cases where there is high interfacial tension between the two components. The smooth surface of SMA-8 and the absolute lack of adhesion is also visible in the higher magnification electron micrograph of Figure 40.

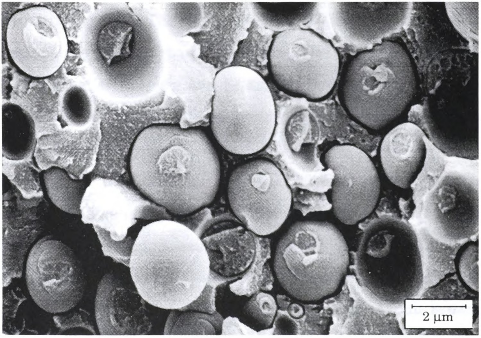

Figure 39: SEM picture of CA/SMA-8 70/30 after extrusion (fracture perpendicular to the flow direction).

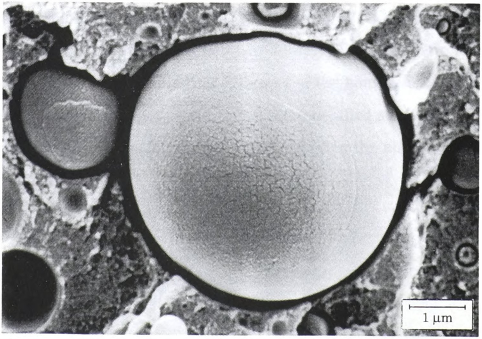

Figure 40: SEM picture of CA/SMA-8 70/30 after extrusion (fracture perpendicular to the flow direction).

The morphology of the CA/SMA-8 70/30 blend is also clearly visible in the TEM picture (Figure 41). The darker regions are the SMA-8 phase and the lighter regions are the CA phase. There are some bigger and some smaller droplets. The smaller droplets can be satellite droplets formed during the breakup (see Figure 3). It can also be noticed that the SMA-8 phase appears as an ellipse, although in the SEM picture it is more spherical. This is basically an artifact of the sectioning procedure (compression). These samples were sectioned using a glass knife. There are also some knife marks appearing, certifying that the longer axis of the ellipse is normal to the direction of the knife. If a diamond knife was used, the knife marks would most probably be eliminated, and the compression reduced. There is also some separation of the phases called debonding (generation of holes at the interface), because of the lack of interfacial adhesion.

TEM pictures in Figures 42 and 43 show what happens when the above blend is passed through the extruder one or two more times. It can be noticed, that the morphology of the blend has not considerably changed. There is a better dispersion of the SMA-8 phase (improvement of the homogeneity of the droplet dimensions), but it is not significant. A more detailed study and discussion of the droplet dimensions for various runs (including the above), is presented later in this chapter.

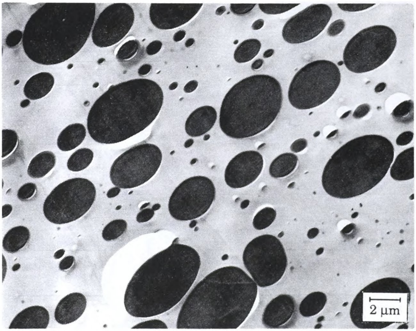

Figure 41: TEM picture of CA/SMA-8 70/30 after extrusion (sectioning perpendicular to the flow direction).

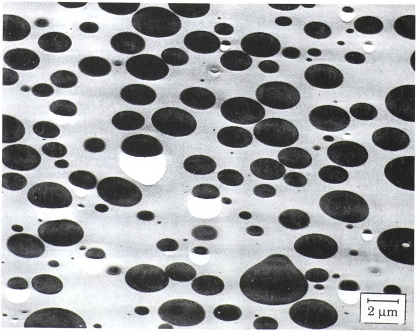

Figure 42: TEM picture of CA/SMA-8 70/30 after two extrusion passes (sectioning perpendicular to the flow direction).

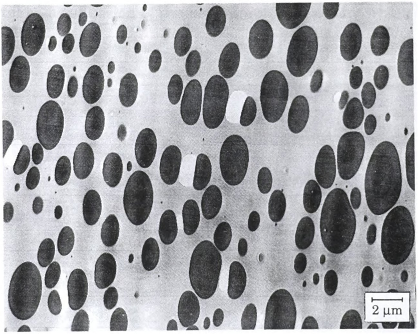

Figure 43: TEM picture of CA/SMA-8 70/30 after three extrusion passes (sectioning perpendicular to the flow direction).

All the above micrographs were perpendicular to the flow direction. A TEM picture of a sample sectioned parallel to the flow direction, is shown in Figure 44. Some knife marks indicate the direction of sectioning (east-northeast to west-southwest or the reverse). Some of the SMA-8 droplets are in spherical form, but there are also some bigger droplets, elongated parallel to the extrusion direction. This would not be visible if the picture was taken perpendicular to the flow direction. There are also some droplets, right before or right after breakup (dumbbell shaped droplets or droplets with an elongated part). So, after the first extrusion, the distribution can progress to a morphology closer to equilibrium.

Figure 39 shows that there are some appendages sticking out many SMA droplets. This is due to fracture of the narrow part of a dumbbell or of an elongated part of the droplets (similar to those shown in Figure 44), and should not be mistaken as adhesion of the SMA droplets to the matrix.

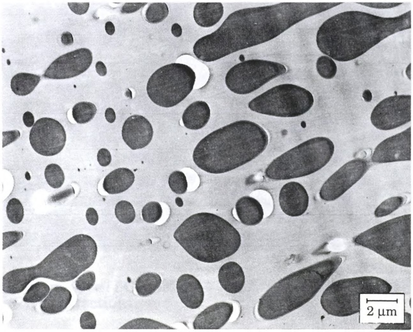

Figure 44: TEM picture of CA/SMA-8 70/30 after extrusion (sectioning parallel to the flow direction).

The morphology of the CA/SMA-14 70/30 blend (the SMA phase contains 14% MA) is shown in Figures 45 and 46. There is again no adhesion between the phases (incompatible blend), and the SMA-14 phase is in droplet form with dimensions close to those of SMA-8. This time, however, the use of a diamond knife for sectioning, reduced compression and eliminated debonding.

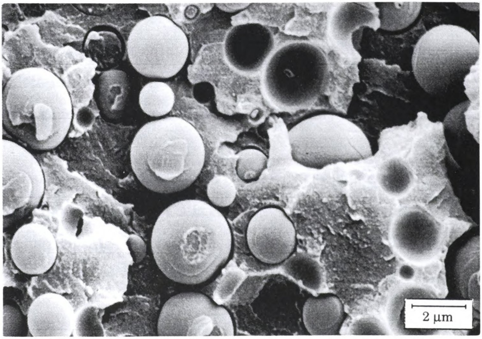

Figure 45: SEM picture of CA/SMA-14 70/30 after extrusion (fracture perpendicular to the flow direction).

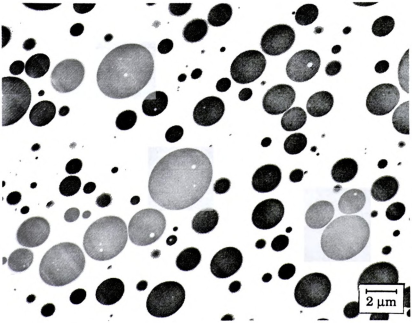

Figure 46: TEM picture of CA/SMA-14 70/30 after extrusion (sectioning perpendicular to the flow direction).

Figure 47 is an SEM pictures of a fracture surface of a CA/SMA-8 70/30 injection molded specimen after tensile test. The injection process (elongational flow), together with lack of interfacial adhesion, resulted in transformation of the droplets into fibers. This fibrillation is more obvious in Figure 48, where the injection molded specimen is examined parallel to the flow direction.

Figure 49 shows a CA/SMA-8 30/70 blend (reverse blend composition). SMA-8 is the continuous phase and CA is the dispersed phase, and there is no interfacial adhesion. In this case, however, the dispersed phase (CA) is not in droplet form, but is fibrillar.

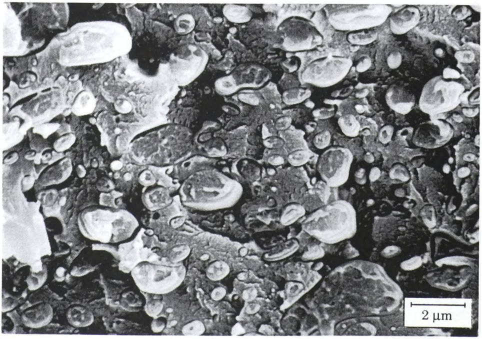

Figure 47: SEM picture of CA/SMA-8 70/30 injection molded specimen (fracture in tension, surface perpendicular to the flow direction).

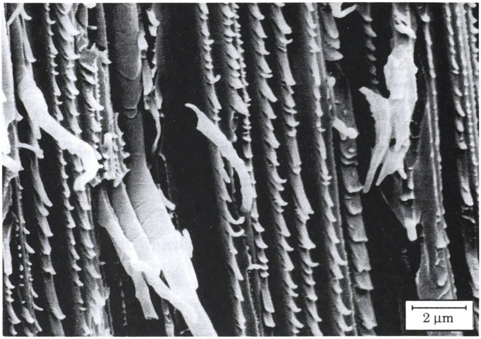

Figure 48: SEM picture of CA/SMA-8 70/30 injection molded specimen (fracture parallel to the flow direction).

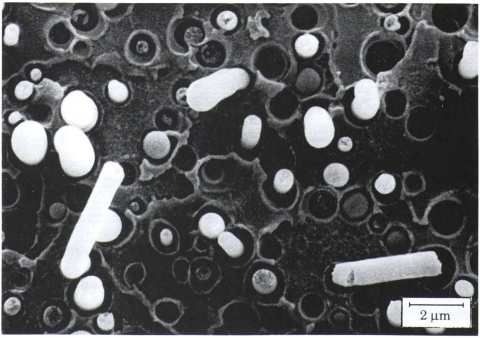

Figure 49: SEM picture of CA/SMA-8 30/70 after extrusion (fracture perpendicular to the flow direction).

The reason for this is the viscosity difference between the two phases. At the extrusion temperature used, CA is more viscous than SMA-8. In the case of polymer systems (in uniform shear flow), breakup of the dispersed phase occurs as shown in Figure 3 usually when the viscosity ratio *k* (chapter 2, equation 11) is between 0.14 and 0.65 [Han (1981)]. When, *k* is less than 0.14 or more than 3.8, usually no breakup occurs, but just deformation from a spherical to an ellipsoid form. When, however *k* is between 0.7 and 2.2, deformation generally occurs in a way similar to that shown in Figure 40. There is basically a fibril formed, which may break.

Figure 50: Droplet deformation in uniform shear flow for viscosity ratio between 0.7 and 2.2.

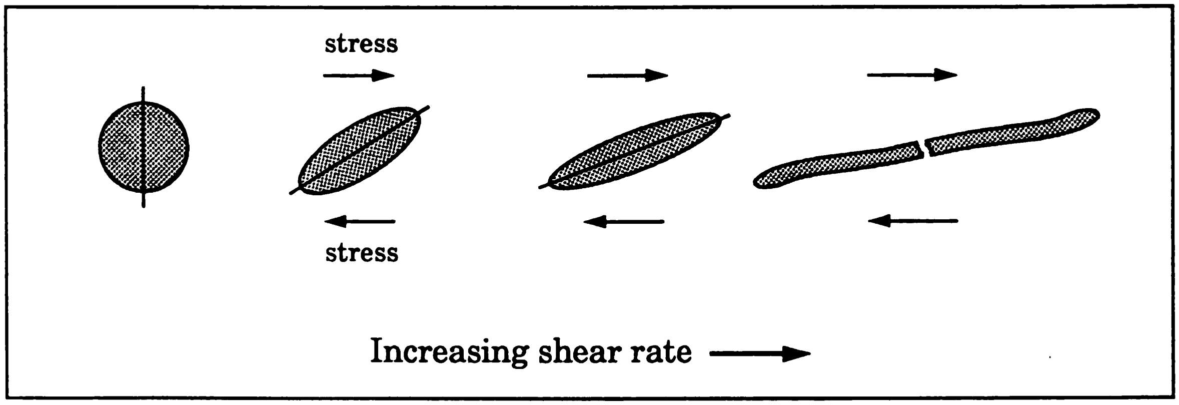

Application of the above theory to our system, suggests that in the case where SMA-8 is the dispersed phase, the viscosity ratio (dispersed phase versus continuous phase) should be from 0.14 to 0.65, and in the case where CA is the dispersed phase, it should be from 0.7 to 2.2. This means that (for having both of the above true) for the temperature used:

$$0.45 < \frac{\eta_{SMA-8}}{\eta_{CA}} < 0.65 \tag{16}$$

Addition of potential catalysts

As was mentioned in chapter 3, KCl is one of the potential catalysts which was tried before DMAP. Figure 51 shows the morphology of the blend when 1% of KCl is added to the CA/SMA-8 30/70 mixture (1 part of KCl with 100 parts of CA/SMA-8). The morphology is similar to that of Figure 49, and there is no adhesion between the phases. This indicates that the addition of KCl does not promote adhesion.

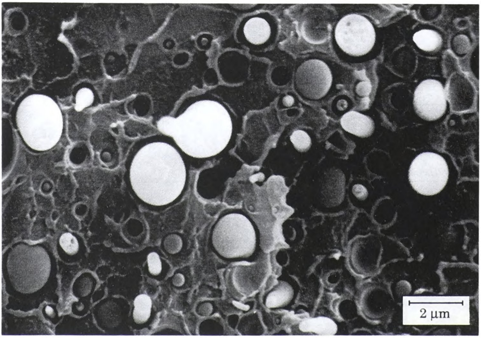

Figure 51: SEM picture of CA/SMA-8/KCl 30/70/1 after extrusion (fracture perpendicular to the flow direction).

A similar lack of adhesion is seen in Figure 52, where 1% of KCl is extruded with a 50/50 mixture of CA and SMA-8. In this case, SMA-8 is still the continuous phase, although there is 50% CA (and co-continuity would be possible). The reason for this, is that the lower viscosity of SMA-8 (as was mentioned above) shifts the morphology from co-continuity to continuous phase of SMA-8 (see also Figure 2).

No adhesion was observed in the case of a 30/70 CA/SMA-8 blend, even when 2% KCl was used and the residence time was increased (screw speed was 15 rpm) (Figure 53). Also, the lower shear rate (because of the lower screw speed) resulted in worse dispersion of the SMA-8 phase (bigger droplets or other formations).

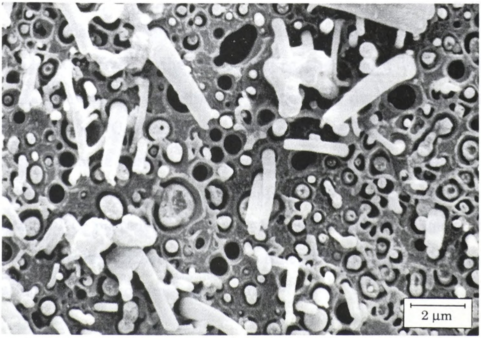

Figure 52: SEM picture of CA/SMA-8/KCl 50/50/1 after extrusion (fracture perpendicular to the flow direction).

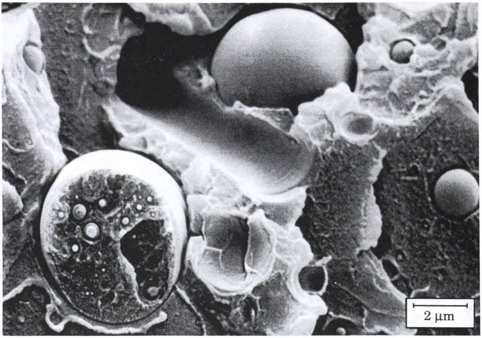

Figure 53: SEM picture of CA/SMA-8/KCl 30/70/2 after extrusion (screw speed 15 rpm, fracture perpendicular to the flow direction).

The dispersion of the catalyst in the system is important. In the case of a solution reaction where all components including the catalyst are soluble, this is not a problem. However, in the case of melt reactions, good dispersion is possible only if the material is melting or evaporating during processing. KCl's melting point is 770°C. There is, therefore, only distributive mixing of the catalyst particles in the system, which means that reaction between the components of the blend can occur only at the interface of the catalyst and the blend. One of these KCl particles is shown in Figure 54. The morphology near the KCl particle/blend interface is similar to that of the rest of the blend, indicating that no reaction is occurring.

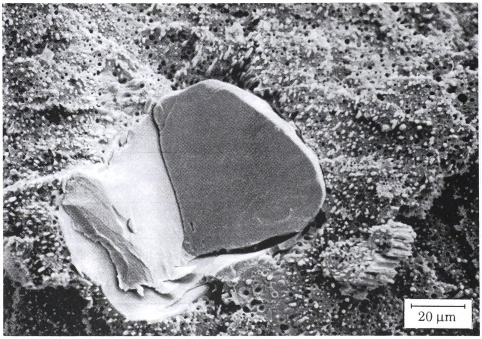

Figure 54: SEM picture of a KCl particle in a CA/SMA-8/KCl 50/50/1 system after extrusion (fracture perpendicular to the flow direction).

For the blends of Dexel and SMA-8 (Figures 55 and 56), poly(4-vinylpyridine-co-styrene) and poly(2-vinylpyridine) were used as potential catalyst respectively. No adhesion was observed (many smooth surfaces). The interesting point is that there was co-continuity although the Dexel content was 70%. This indicates, again, that at this temperature SMA-8 is less viscous than Dexel.

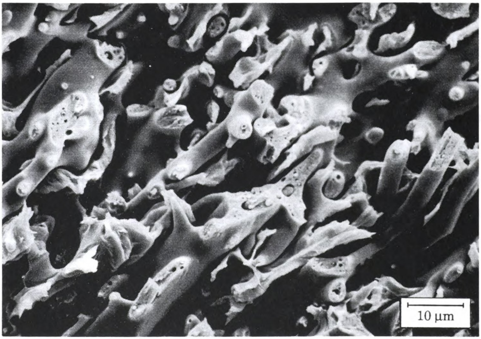

Figure 55: SEM picture of Dexel/SMA-8/poly(4-vinylpyridine-co-styrene) 70/30/0.5 after extrusion (fracture between parallel and perpendicular to the flow direction).

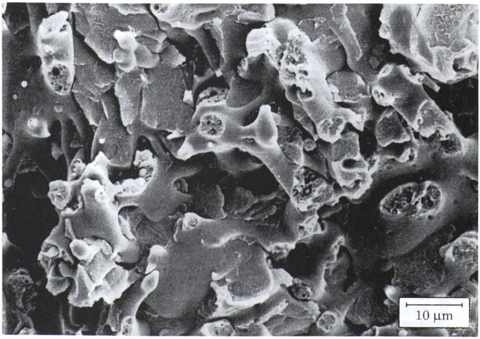

Figure 56: SEM picture of Dexel/SMA-8/poly(2-vinylpyridine) 70/30/2 after extrusion (fracture perpendicular to the flow direction).

Morphology after reaction

DMAP was the only material which was found to work as a catalyst for our system. When 0.1% DMAP was added to a CA/SMA-8 70/30 blend which had already been passed through the extruder twice (see Figure 42), the morphology of Figure 57 was obtained. In this system, there is a much better dispersion of the SMA-8 phase (reduction of the droplet size), as compared to the CA/ SMA-8 70/30 blend after three extrusion passes (Figure 43), and there is no debonding during sectioning.

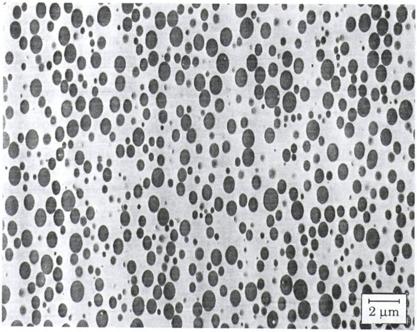

Figure 57: TEM picture of CA/SMA-8/DMAP 70/30/0.1 after three extrusion passes, the catalyst added before the third extrusion (sectioning perpendicular to the flow direction).

The criterion for droplet breakup of a Newtonian drop in a Newtonian matrix in uniform and steady shear field is given by equation 12 (chapter 2). For the more complex mixing during reactive extrusion of polymers, a similar equation based on experimental data has been proposed [Wu (1987)]:

$$\frac{G\eta_m a}{\gamma} \geq 4k^{\pm 0.84} \tag{17}$$

where G is the shear rate, η_m the matrix viscosity, a the droplet diameter, γ the interfacial tension, and k the viscosity ratio (the dispersed phase viscosity η_d versus the matrix viscosity η_m). The plus sign is for $k > 1$ and the minus sign for $k < 1$. The left side of the equation is again the Weber number, i.e. the ratio of viscous forces ($G\eta_m$) to interfacial forces (γ/a).

The difference between the systems of Figures 43 and 47 is only the addition of catalyst. G was the same (same screw speed), and if we assume that the addition of the catalyst didn't change the viscosities of the two phases, then according to the above equation the reduction of the droplet diameter, was only due the reduction of the interfacial tension. This reduction of the interfacial tension was obviously due to a reaction between the two phases resulting from the addition of catalyst. Therefore, this time the addition of the catalyst was successful.

Figure 58 is an SEM picture of a fracture surface of the above system. Some small spherical particles can be noticed which are exhibiting adhesion with the matrix. For the majority of the particles, however, the crack didn't propagate around the particles, but went through and broke them. The droplets,

therefore, appear on the micrograph as circles being almost at the same plane with the matrix. This phenomenon is certainly the result of good adhesion between the two phases. The adhesion is due to a reaction catalyzed by DMAP, and formation of CA-SMA graft copolymer (the hydroxyl groups on the CA react with the anhydride groups on the SMA to form a half ester). This morphology is more visible at the higher magnification picture of Figure 59. On the left of this picture there is a particle where the crack propagated around it, but there is obvious adhesion with the matrix. On the right there is a circle which corresponds to a particle which broke (the crack went through). Figure 60 is another picture of a particle showing similar adhesion. This picture is interesting because it is close the magnification limits of the SEM (the picture was taken at a magnification of 60,000).

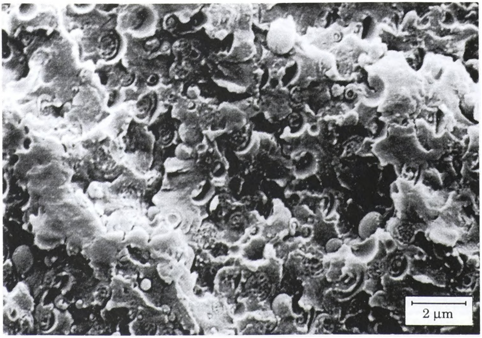

Figure 58: SEM picture of CA/SMA-8/DMAP 70/30/0.1 after three extrusion passes, the catalyst added before the third extrusion (fracture perpendicular to the flow direction).

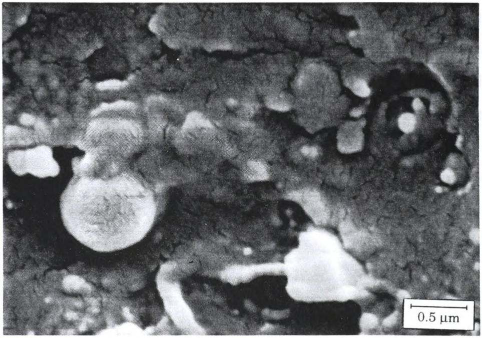

Figure 59: SEM picture of CA/SMA-8/DMAP 70/30/0.1 after three extrusion passes, the catalyst added before the third extrusion (fracture perpendicular to the flow direction).

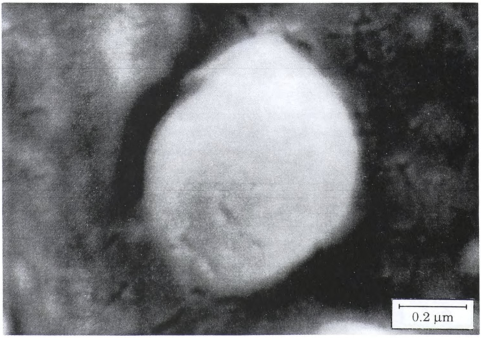

Figure 60: SEM picture of CA/SMA-8/DMAP 70/30/0.1 after three extrusion passes, the catalyst added before the third extrusion (fracture perpendicular to the flow direction).

Figures 61 and 62 are micrographs of the same system after extraction of the fractured surface with toluene. Toluene is a solvent for SMA-8 and a non solvent for CA. It extracted the SMA-8 phase from the surface and made the morphology more clear. The difference between the two pictures is that the first one is fractured perpendicular to the flow direction, and the second is fractured parallel to the flow direction. The dispersed phase, therefore, is very close to being spherical (since it appears almost circular in both directions). It was appearing as an ellipse in Figure 37 because of compression during sectioning with a glass knife.

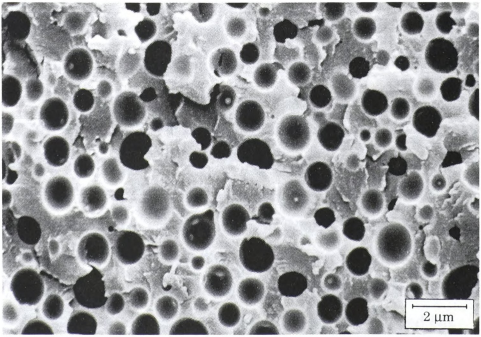

Figure 61: SEM picture of extracted CA/SMA-8/DMAP 70/30/0.1 after three extrusion passes, the catalyst added before the third extrusion (fracture perpendicular to the flow direction).

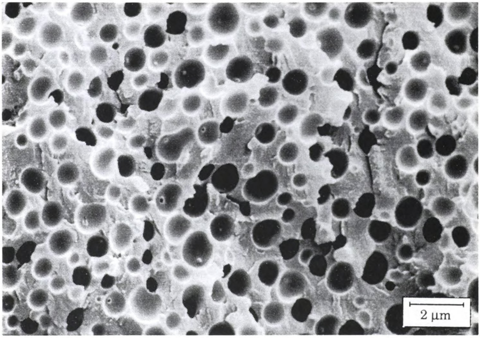

Figure 62: SEM picture of extracted CA/SMA-8/DMAP 70/30/0.1 after three extrusion passes, the catalyst added before the third extrusion (fracture parallel to the flow direction).

A similar morphology is observed when even less amount of catalyst (0.05%) is added after only the first extrusion of a CA/SMA-8 70/30 blend (Figure 63). The size of the dispersed phase is almost the same as compared to that of CA/SMA-8/DMAP 70/30/0.1 after three extrusion passes, where the catalyst was added before the third extrusion (Figure 57) (there is, however, less compression and no knife marks because of the use of a diamond knife). The SEM picture of Figure 64 is also similar to that of Figure 58. The morphology didn't significantly change when the alloy of Figures 63 and 64 (CA/SMA-8/DMAP 70/30/0.05 after two extrusion passes, where the catalyst was added before the second extrusion) was extruded one more time (Figures 65 and 66).

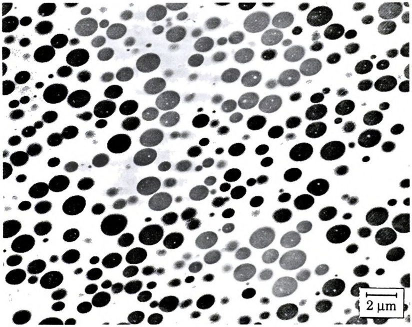

Figure 63: TEM picture of CA/SMA-8/DMAP 70/30/0.05 after two extrusion passes, the catalyst added before the second extrusion (sectioning perpendicular to the flow direction).

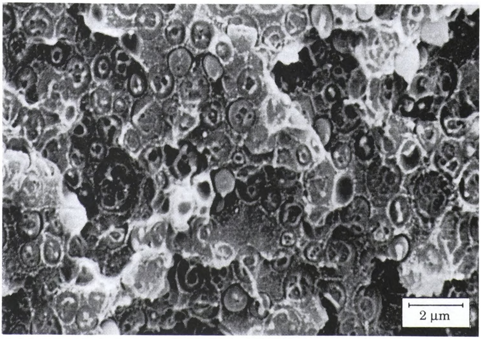

Figure 64: SEM picture of CA/SMA-8/DMAP 70/30/0.05 after two extrusion passes, the catalyst added before the second extrusion (fracture perpendicular to the flow direction).

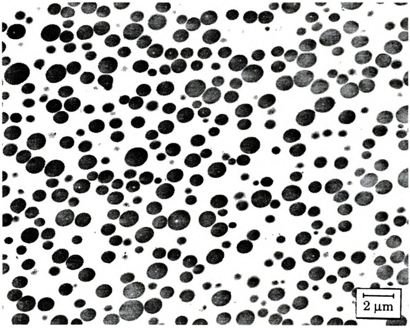

Figure 65: TEM picture of CA/SMA-8/DMAP 70/30/0.05 after three extrusion passes, the catalyst added before the second extrusion (sectioning perpendicular to the flow direction).

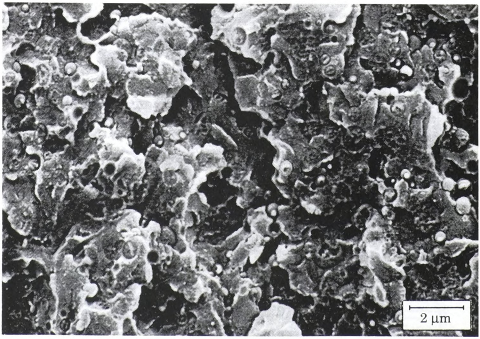

Figure 66: SEM picture of CA/SMA-8/DMAP 70/30/0.05 after three extrusion passes, the catalyst added before the second extrusion (sectioning perpendicular to the flow direction).

When 0.1% catalyst was added before the first extrusion, the morphology observed was that of Figure 67. There was actually co-continuity of the two phases, a morphology totally different from that of Figure 41 (CA/SMA-8 70/30). This difference certainly implies that a reaction took place. Figures 68 and 69 are SEM pictures of this system. It is not very easy to distinguish the two phases. On the TEM picture, however, it can be noticed that there are small SMA-8 droplets encapsulated in the CA phase (the opposite is not observed to any great extent, because of the higher viscosity of CA). These droplets can also be noticed in one of the two phases of Figures 68 and 69, which means that this phase is CA. No separation can be observed at the interphase, which indicates that a reaction took place. It should be noted that in the case of CA adhesion can not be the result of other interactions (like hydrogen bonding) since no adhesion is observed when catalyst is not added.

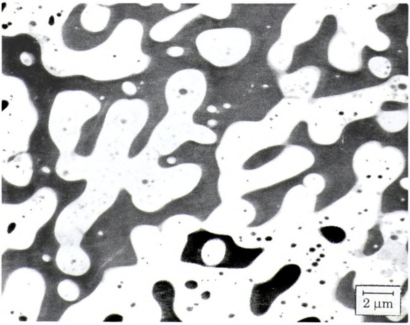

Figure 67: TEM picture of CA/SMA-8/DMAP 70/30/0.1 after extrusion (sectioning perpendicular to the flow direction).

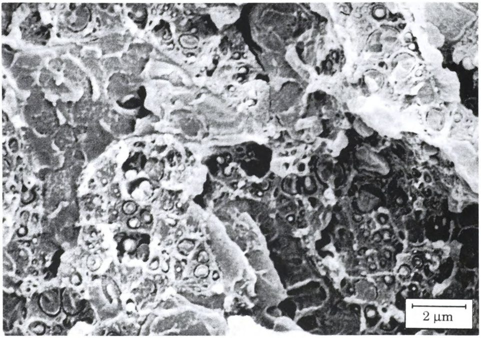

Figure 68: SEM picture of CA/SMA-8/DMAP 70/30/0.1 after extrusion (fracture perpendicular to the flow direction).

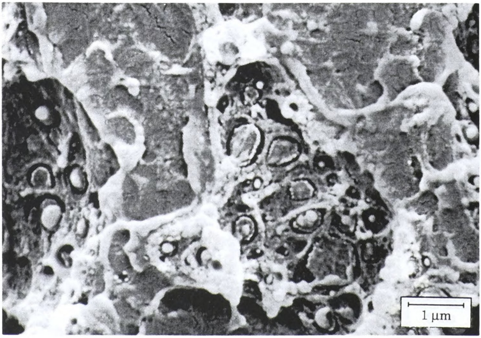

Figure 69: SEM picture of CA/SMA-8/DMAP 70/30/0.1 after extrusion (fracture perpendicular to the flow direction).

The morphology of this system is more obvious in Figures 70 and 71, where after fracture, the SMA-8 phase has been extracted with toluene. There is co-continuity oriented in the direction of flow.

This co-continuity, however, is something which was not expected. According to Figure 2 (chapter 2), the volume ratio and the viscosity ratio are the parameters determining which phase will be continuous or if there will be co-continuity. The reaction and adhesion is expected to reduce the size of the dispersed phase (what was observed earlier). It is not expected to result in co-continuity. An explanation for the above morphology is that this morphology is not in equilibrium. This will be shown later.

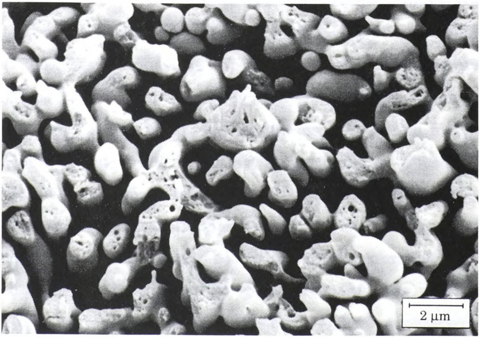

Figure 70: SEM picture of CA/SMA-8/DMAP 70/30/0.1 after extrusion and extraction (fracture perpendicular to the flow direction).

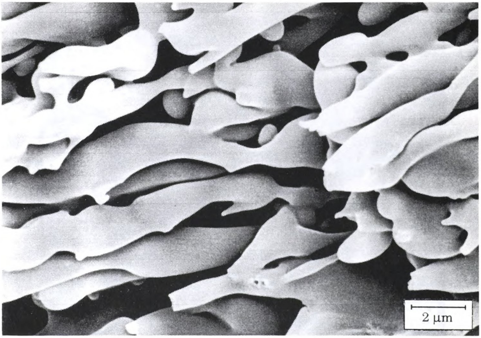

Figure 71: SEM picture of CA/SMA-8/DMAP 70/30/0.1 after extrusion and extraction (fracture parallel to the flow direction).

Figure 72 is a TEM picture of CA/SMA-8/DMAP 70/30/0.05 after extrusion. It can be observed that in this case CA is the continuous phase. SMA-8,however, which is the dispersed phase, is not in droplet form, and there are points showing that at the moment of solidification the SMA-8 phase was breaking up. This means that it is not still equilibrium. When this material was extruded one more time, the morphology shown in Figure 73 resulted. It can be noticed that many small droplets were formed. Still the morphology is not in equilibrium, but it is certainly closer to equilibrium than the one of Figure 72. A similar phenomenon should be expected if the material of Figure 67 is extruded one more time. Figure 74 shows the morphology which resulted when 0.01% of catalyst was used. In this case droplets are observed smaller than those of Figures 41, 42 and 43, which means that even with this small amount of catalyst, a reaction took place.

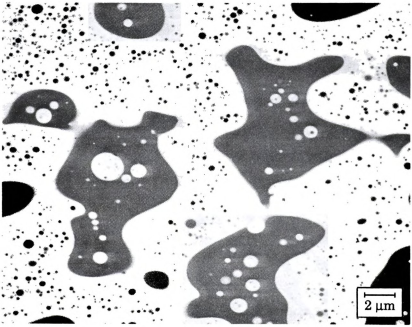

Figure 72: TEM picture of CA/SMA-8/DMAP 70/30/0.05 after extrusion (sectioning perpendicular to the flow direction).

Figures 73 and 74 indicate that in equilibrium, SMA-8 is in droplet form, and that the more the catalyst used (the more the reaction and adhesion), the longer it takes for the morphology to reach equilibrium. An explanation for this, can be the following:

Both mixing and reaction are taking place in the extruder. The reaction, however, affects the mixing. When more catalyst is added, the reaction starts early in the extruder and results in a network morphology similar to that of Figure 67. Then the stress applied by the extruder is basically absorbed as deforming this network, instead of breaking up some existing droplets. When, however, less catalyst is added, there is some droplet formation (similar to that observed when no catalyst is added) and then there is breakup of those droplets.

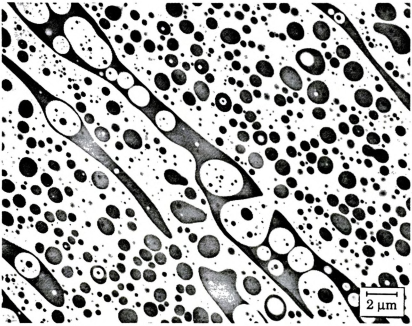

Figure 73: TEM picture of CA/SMA-8/DMAP 70/30/0.05 after two extrusion passes, the catalyst added before the first extrusion (sectioning perpendicular to the flow direction).

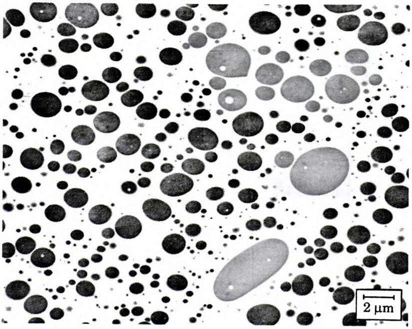

Figure 74: TEM picture of CA/SMA-8/DMAP 70/30/0.01 after extrusion (sectioning perpendicular to the flow direction).

Figures 75, 76 and 77 are SEM pictures of the samples of Figures 72, 73 and 74 respectively. Not significant gap can be observed between the phases, and many small SMA-8 droplets which broke can be noticed. The fact that the crack went through, indicates not only that there is good adhesion between the phases, but also that the CA phase is stronger than the SMA-8 phase. If the opposite was true, a phenomenon similar to that observed with the amylose particles (see chapter 5) would occur.

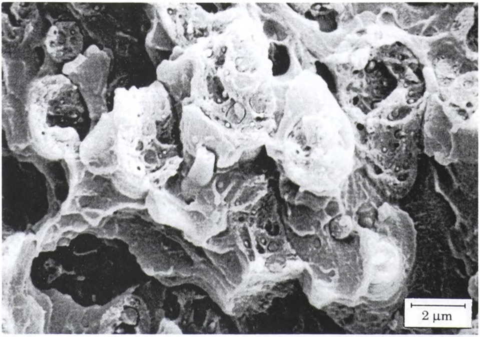

Figure 75: SEM picture of CA/SMA-8/DMAP 70/30/0.05 after extrusion (fracture perpendicular to the flow direction).

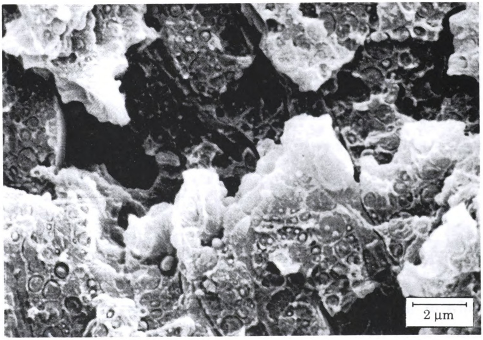

Figure 76: SEM picture of CA/SMA-8/DMAP 70/30/0.05 after two extrusion passes, the catalyst added before the first extrusion (fracture perpendicular to the flow direction).

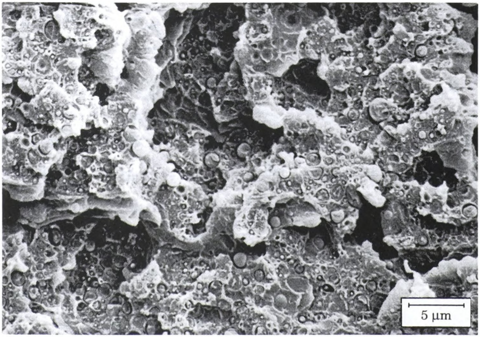

Figure 77: SEM picture of CA/SMA-8/DMAP 70/30/0.01 after extrusion (fracture perpendicular to the flow direction).

One important point about the reaction should be added. Good dispersion of the catalyst is obviously important, specially when the amount of catalyst added is as low as 0.01%. When the catalyst added, however, remains a solid during extrusion and is just dispersed in the blend, even if the catalyst is working, the reaction will be limited. DMAP has a melting and boiling point lower than the extrusion temperature. This means that in the extruder it is melting and then evaporating, which certainly helps the reaction.

Another point is that the more the reaction the more the degradation of the CA phase. This was observed as a brown color for the samples with 0.1 or 0.05% catalyst (when no catalyst is added the color is close to white). Very light change of the color was, however, observed for all the samples where 0.01% of catalyst was added. This color became only slightly darker after the injection of the material.

Figures 78 and 79 are SEM pictures of an injection molded specimen of CA/SMA-8/DMAP 70/30/0.05 after tensile test. It can be noticed that there is an orientation in the direction of injection, and that there are some points of no adhesion. During injection, there is elongational flow which results in this orientation, but also there is some mixing which results in the creation of new interfaces of the two components. There is, however, not enough time for a reaction to occur at these points, and probably not enough catalyst since some of the catalyst might have evaporated during extrusion.

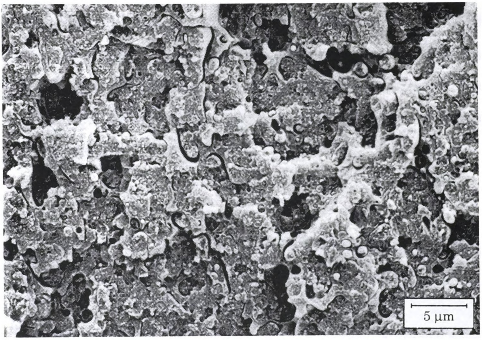

Figure 78: SEM picture of CA/SMA-8/DMAP 70/30/0.05 after injection (fracture in tension, surface perpendicular to the flow direction).

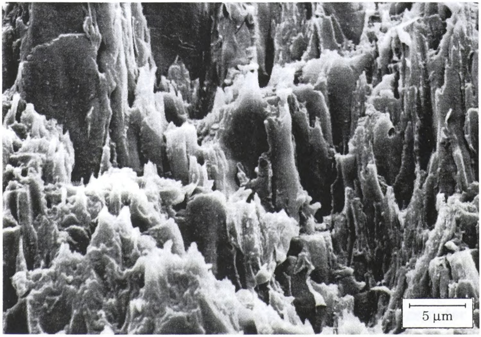

Figure 79: SEM picture of CA/SMA-8/DMAP 70/30/0.05 after injection (fracture in tension, surface parallel to the flow direction).

Figure 80 is an SEM picture of a CA/SMA-8/DMAP 70/30/0.01 injection molded specimen after tensile test, which also shows some lack of adhesion. Also there are some big SMA parts, which probably occurred by incorporation of smaller particles. So, although elongation helps in better longitudinal properties, the lack of adhesion and the appearance of bigger parts of the dispersed phase does not help.

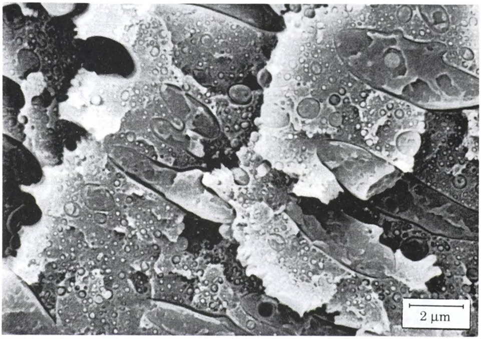

Figure 80: SEM picture of CA/SMA-8/DMAP 70/30/0.01 after injection (fracture in tension, surface perpendicular to the flow direction).

Figure 81 is a TEM picture of CA/SMA-14/DMAP 70/30/0.01 extrudate. It can be noticed that the higher MA content (lower value for γ) resulted in better dispersion compared to Figure 74. This was also the finest dispersion observed. According to equation 17 (this chapter), another parameter affecting the droplet diameter is the viscosity ratio k. The left side of equation 17 has a minimum when k is equal to 1. This means that at this viscosity ratio and if the other parameters are the same, the minimum dispersed phase size can be observed. According to Table 3 (chapter 3), at 230°C (condition "L") which is very close to the extrusion temperatures, the viscosity of SMA-14 is lower than the viscosity of SMA-8. Therefore, since the viscosity of CA is higher than the viscosity of SMA-8, *k* for SMA-8 is closer to 1 compared to *k* for SMA-14. This means that in the case of SMA-14 the viscosity ratio does not help the reduction of the dispersed phase size. The grafting reaction, therefore, contributed even more than what can be observed from the droplet diameter. Figure 82 is an SEM picture of the above sample, showing the very fine dispersion of the SMA-14 phase.

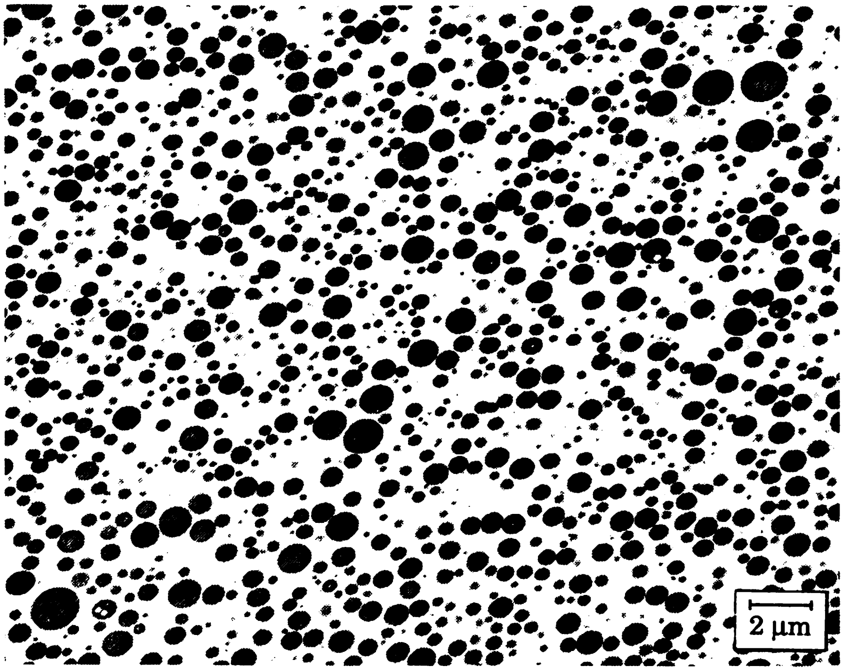

Figure 81: TEM picture of CA/SMA-14/DMAP 70/30/0.01 after extrusion (sectioning perpendicular to the flow direction).

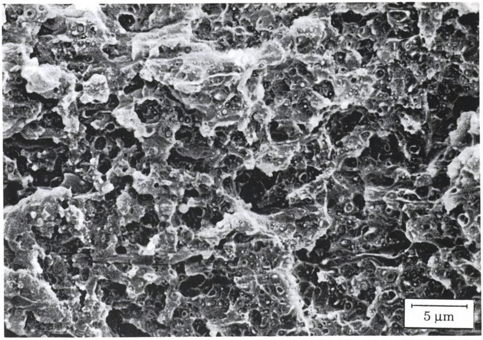

Figure 82: SEM picture of CA/SMA-14/DMAP 70/30/0.01 after extrusion (fracture perpendicular to the flow direction).

Figure 83 shows the morphology of a CA/SMA-R/DMAP 70/30/0.01 extrudate. The black parts in the darker SMA phase are the rubber. The softness of the rubber makes sectioning difficult, and this is why holes are appearing near the black parts. It can be noticed that the presence of the rubber didn't allow complete breakup of the SMA-R phase into droplets (in contrast to the blends of SMA-8 and SMA-14 with the same amount of catalyst). Good interfacial adhesion is shown in the SEM picture of Figure 84.

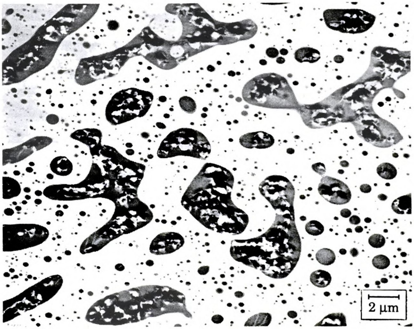

Figure 83: TEM picture of CA/SMA-R/DMAP 70/30/0.01 after extrusion (sectioning perpendicular to the flow direction).

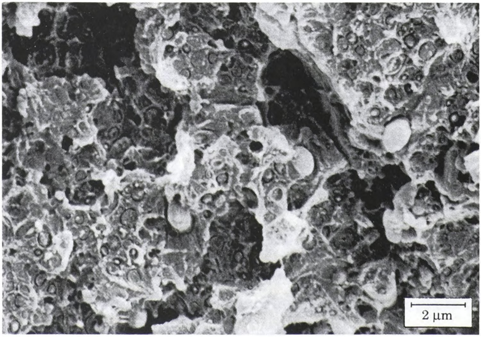

Figure 84: SEM picture of CA/SMA-R/DMAP 70/30/0.01 after extrusion (fracture perpendicular to the flow direction).

As was mentioned in chapter 4, a method based on extraction was used to quantify the extent of the reaction. Good separation, however, was required. Figure 85 shows TEM pictures of blends extruded, pelletized, extracted with toluene, embedded in epoxy and sectioned. For those pictures, the darker areas are SMA-8, the lighter areas are CA, the intermediate darkness areas are the epoxy, and some white areas are holes. The goal of these experiments was to check if the above method can be used for quantifying the extent of the reaction, and if a layer of SMA can be observed around the CA phase, indicating a reaction. The extrudate of CA/SMA-8/KCl 30/70/2 (screw speed 15 rpm, Figure 53) was extracted with toluene as a control representing no adhesion (Figure 85a). It was selected because SMA-8 was the continuous phase. If CA was the continuous phase, extraction of the dispersed SMA-8 phase would not be possible. No dark layer is obvious at the interface. There is, however, some SMA-8 which was not extracted because it was surrounded by CA. This SMA-8 fraction is not extractable but is not grafted onto CA. Elemental analysis and FTIR (the techniques used to establish grafting) would, therefore, have led to wrong conclusion about grafting.

Figures 85bcd are extrudates of CA/SMA-8/DMAP 70/30/0.1. For Figure 85b, the sample was sectioned near the surface of the extracted particle, where circulation of the solvent was easy (also because of the continuity of the SMA-8 phase). For Figures 85cd, sectioning was close to the middle of the particle. It is obvious that in the middle of the particle where circulation of the solvent was more difficult, more SMA-8 was left unextracted. This is even more obvious in Figure 85d where CA starts becoming the continuous phase (the latter does not allow penetration of the epoxy resin, this is why the holes are appearing). The amount of material extracted, is, therefore, highly dependent on the morphology of the sample, and it is obvious that for the above extraction, elemental analysis and FTIR would result in wrong conclusions. As was shown earlier in this chapter, there was a reaction for the sample of Figures 85bcd. A interfacial layer of SMA-8 can, however, hardly be claimed for Figure 85b, where there was good extraction. This can be an indication that even for this sample, the extent of the reaction is very low (maybe less than 1%). Such a low extent, can, however, be considered enough if it gives the desired adhesion and morphology change. More reaction also results in more degradation, which means that there is an optimum to obtain good mechanical properties.

Gel permeation chromatography was also used to find out the extent of degradation when a brown sample color was observed. The samples with 0.05% catalyst were examined. No significant decrease of the MW was observed, compared to the CA/SMA-8 70/30 blend.

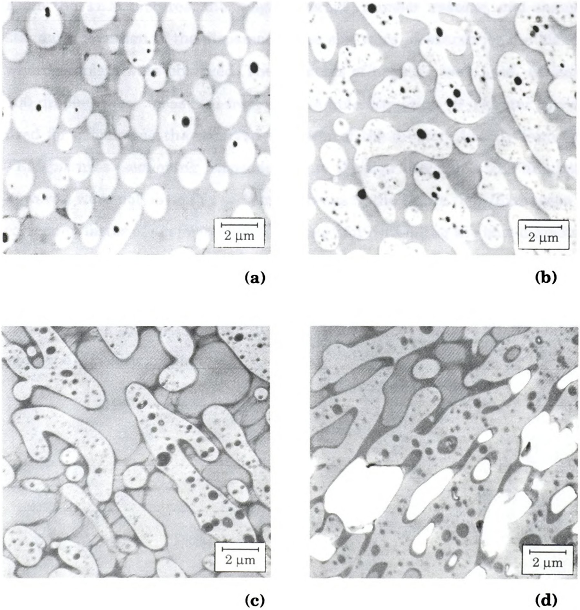
2 µm
2 µm
(a)
(b)
2 µm
2 µm
(c)
(d)

Figure 85: TEM pictures of (a): CA/SMA/KCl 30/70/2 (screw speed 15 rpm), (b), (c) and (d): CA/SMA-8/DMAP 70/30/0.1, after extrusion, pelletization, extraction and epoxy embedding.

Dispersed phase size

From the TEM pictures, the weight average, number average, and sample standard deviation of the dispersed phase size were measured for the blends where droplets were observed. The formulas of page 27 were used. At least 100 droplets were measured from each sample. Equation 14 (chapter 3) was used for calculating the observed diameter of the droplet, directly from the TEM pictures (sectioning perpendicular to the flow direction). The droplets, however, were not obviously sectioned always in the centre. For this reason a correction factor of $4/\pi$ [Wu (1985)] was used for estimating the true diameter from the observed diameter.

Table 7 shows the results of these calculations, whilst Figures 86, 87 and 88 show the size distributions.

Table 7: Size of the dispersed phase (SMA) in CA/SMA blends.

Weight % CA	Second component	Weight % of the second component	Weight % catalyst	Number of extrusion passes	Weight average diameter (µm)	Number average diameter (µm)	Sample standard deviation (µm)	Size distribution (figure #)	TEM picture (figure #)
70	SMA-8	30	0	1	2.88	1.46	1.45	86a	41
70	SMA-8	30	0	2	2.36	1.75	1.04	86b	42
70	SMA-8	30	0	3	2.32	1.81	0.97	86c	43
70	SMA-8	30	0.01	1	1.70	1.01	0.84	87a	74
70	SMA-8	30	0.05	2[I]	1.21	1.05	0.41	87b	63
70	SMA-8	30	0.05	3[II]	1.13	1.03	0.32	87c	65
70	SMA-8	30	0.1	3[III]	1.02	0.85	0.38	88a	57
70	SMA-14	30	0	1	2.18	1.54	1.00	88b	46
70	SMA-14	30	0.01	1	0.72	0.60	0.27	88c	81

[I]: The catalyst was added before the second extrusion.
[II]: The catalyst was added before the second extrusion.
[III]: The catalyst was added before the third extrusion.

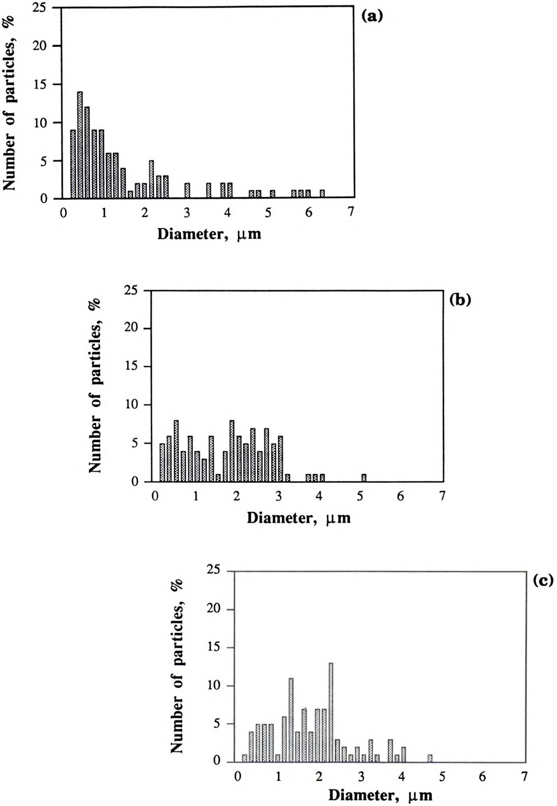

Figure 86: Size distributions for the dispersed phase (SMA) of CA/SMA blends (refer to Table 7).

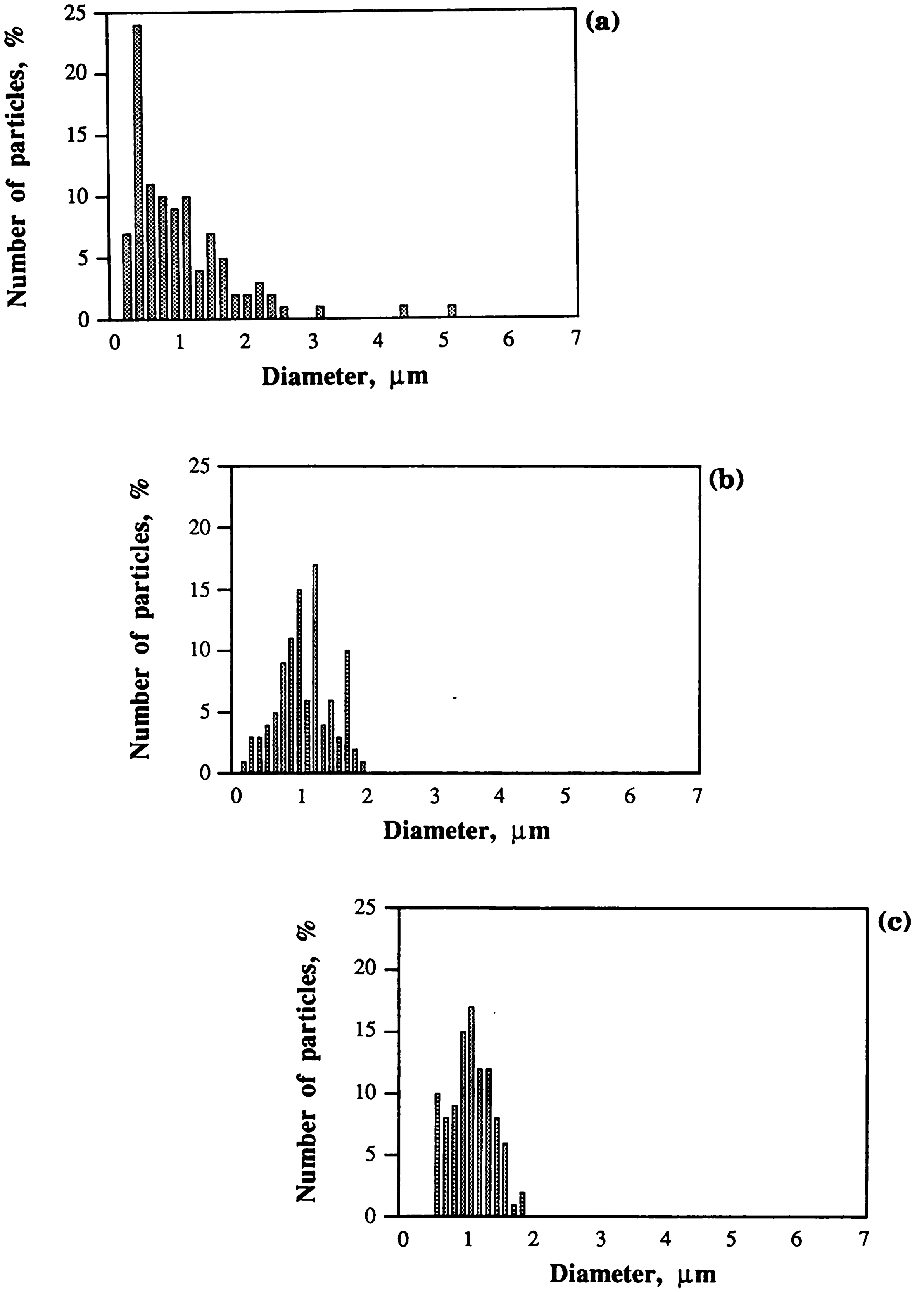

Figure 87: Size distributions for the dispersed phase (SMA) of CA/SMA blends (refer to Table 7).

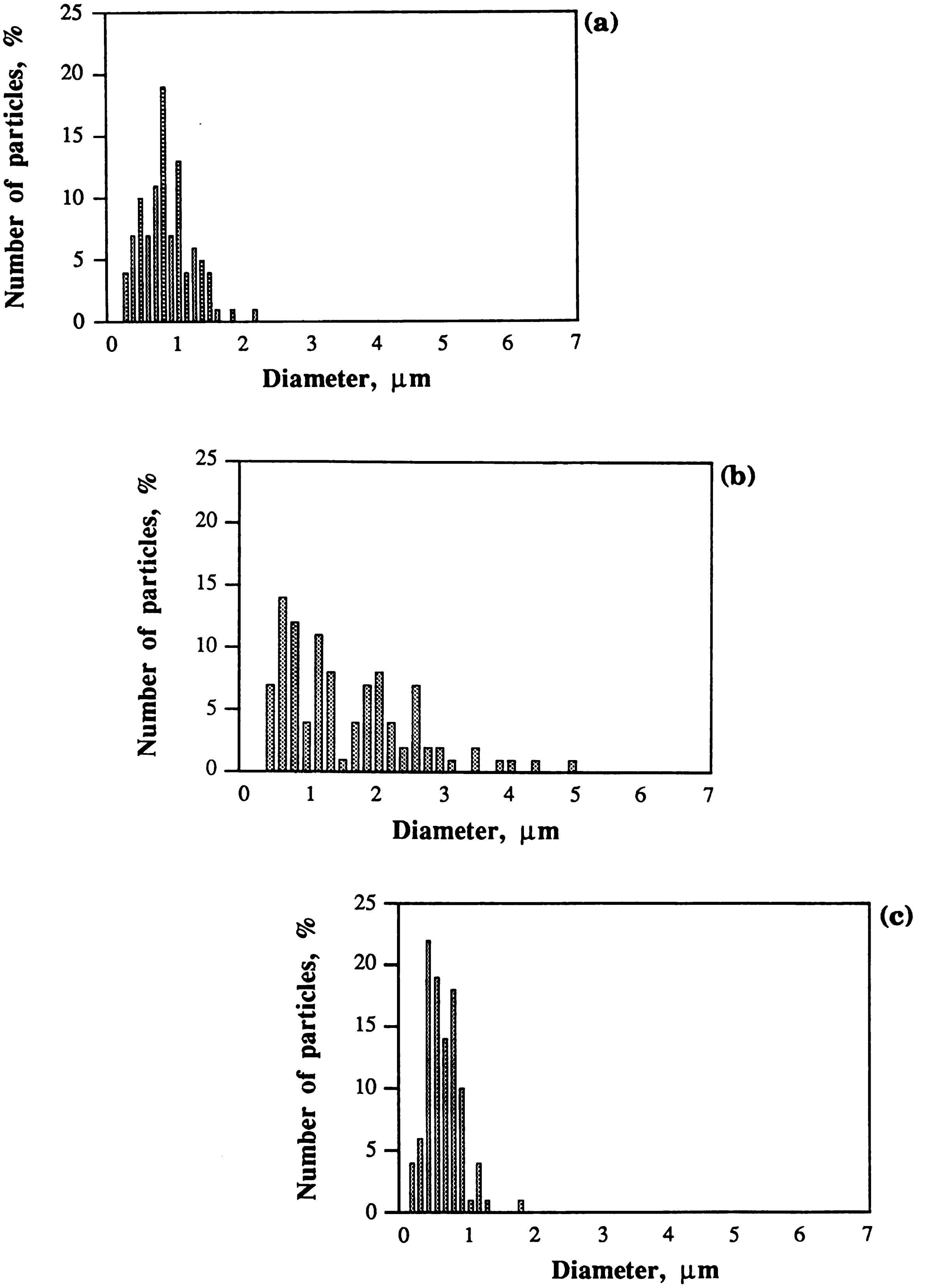

Figure 88: Size distributions for the dispersed phase (SMA) of CA/SMA blends (refer to Table 7).

For the first three samples (blends of CA/SMA-8 70/30 extruded one, two and three times), the more the extrusion passes, the smaller the standard deviation and the weight average diameter (which is expected). There is not much difference between the second and third run, which means that the third is close to equilibrium. The number average diameter however is increasing, and this is because some small droplets (maybe satellite droplets) observed basically for the first run are eliminated (probably incorporated with others during the second and third extrusion pass). Also, for the first sample some droplets are elongated in the direction of flow, but they appear smaller when the sample is sectioned perpendicular to the flow direction.

When catalyst was added, reduction of the diameters and the standard deviation was always observed. As was noticed earlier, the finest dispersion (0.72 μm) is observed for the CA/SMA-14/DMAP 70/30/0.01 blend, due to the presence of 14% MA in the SMA phase. For SMA-8 the smallest diameter (1.02 μm weight average) was observed when 0.1% of catalyst was added.

MECHANICAL PROPERTIES

The effect of reaction, adhesion and morphology change on the mechanical properties of the CA blends will be discussed in this part. Table 8 shows the tensile strength, elongation, modulus and Izod impact strength of these blends. Typical stress-strain curves for most of the materials are shown in Figures 89, 90 and 91.

Table 8: Mechanical properties of the CA blends.

Weight % CA	Second component	Weight % of the second component	Weight % catalyst	Tensile strength at break (psi) ASTM D638	Elongation at break (%) ASTM D638	Tensile modulus (10^6 psi) ASTM D638	Izod impact strength (ft lb/in of notch) (1/8 in thick specimen) ASTM D256A
0	SMA-8	100	0	7320±170	2.8±0.2	0.433±0.029	0.22±0.02
0	SMA-14	100	0	7020±130	2.6±0.1	0.433±0.011	0.19±0.03
0	SMA-R	100	0	4290±60†	7.5±1.3	0.305±0.003	2.61±0.04
70	SMA-8	30	0	3500±300	1.1±0.1	0.527±0.011	0.31±0.07
70	SMA-8	30	0.01	10980±210	5.7±0.5	0.514±0.008	1.89±0.22
70	SMA-8	30	0.05	8890±340	4.0±0.3	0.518±0.007	1.00±0.20
70	SMA-8	30	0.05*	8140±420	3.0±0.3	0.493±0.015	0.54±0.05
70	SMA-8	30	0.05**	3980±120	1.3±0.1	0.506±0.025	0.20±0.02
70	SMA-8	30	0.05***	3030±160	0.9±0.1	0.473±0.016	0.20±0.03
70	SMA-14	30	0	3370±260	1.0±0.1	0.487±0.012	0.23±0.05
70	SMA-14	30	0.01	9460±420	3.8±0.3	0.475±0.012	0.71±0.34
70	SMA-R	30	0.01	9530±160	5.2±0.4	0.469±0.012	1.06±0.11
67‡	DEP	33	0	6230±60†	10.3±0.7	0.381±0.011	2.00±0.60

†: Tensile strength at yield.
*: After two extrusion passes, with the catalyst added before the first extrusion.
**: After two extrusion passes, with the catalyst added before the second extrusion.
***: After three extrusion passes, with the catalyst added before the second extrusion.
‡: Dexel (CA with 33% plasticizer - not extruded).

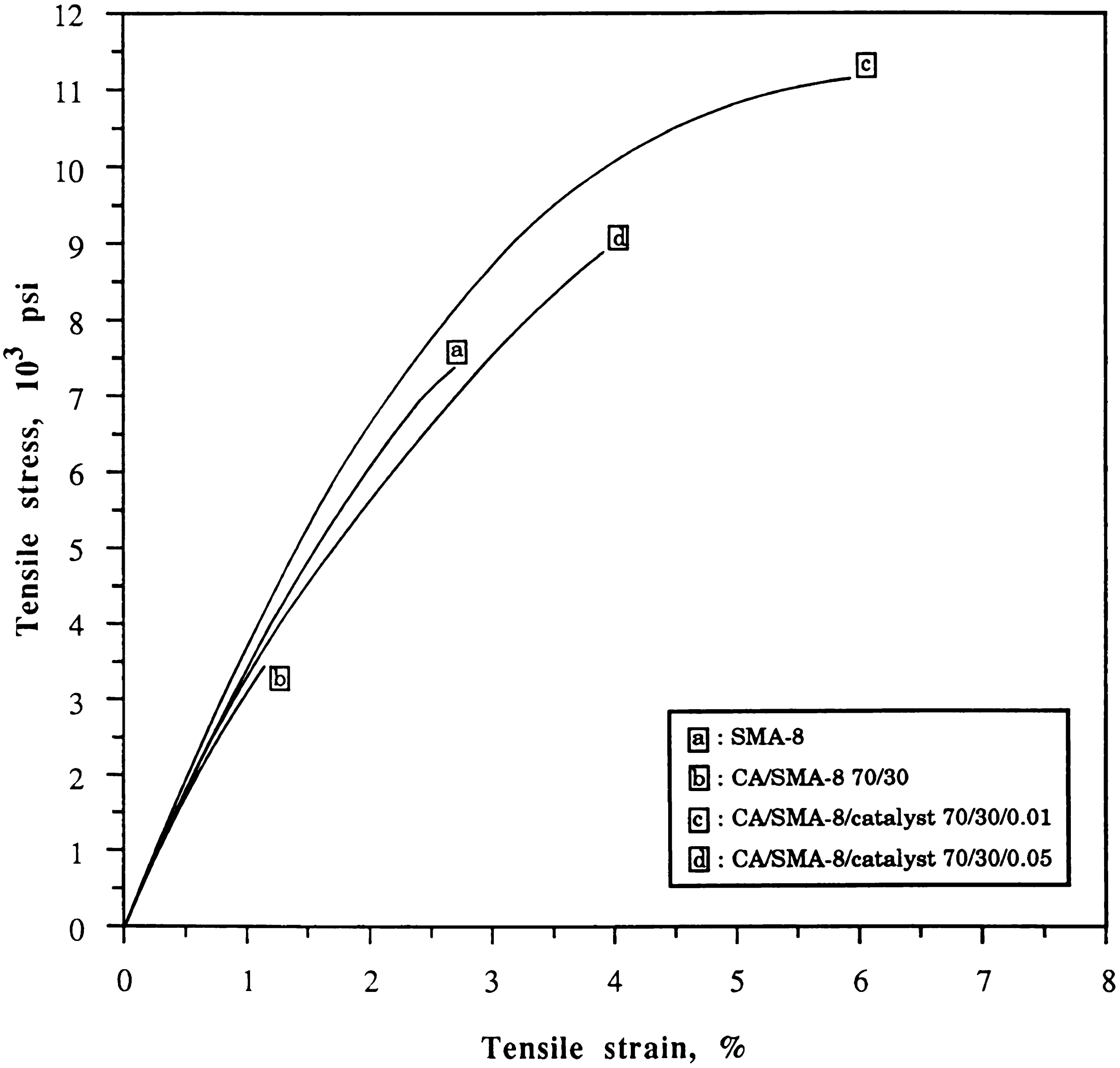

Figure 89: Stress-strain curves for CA blends.

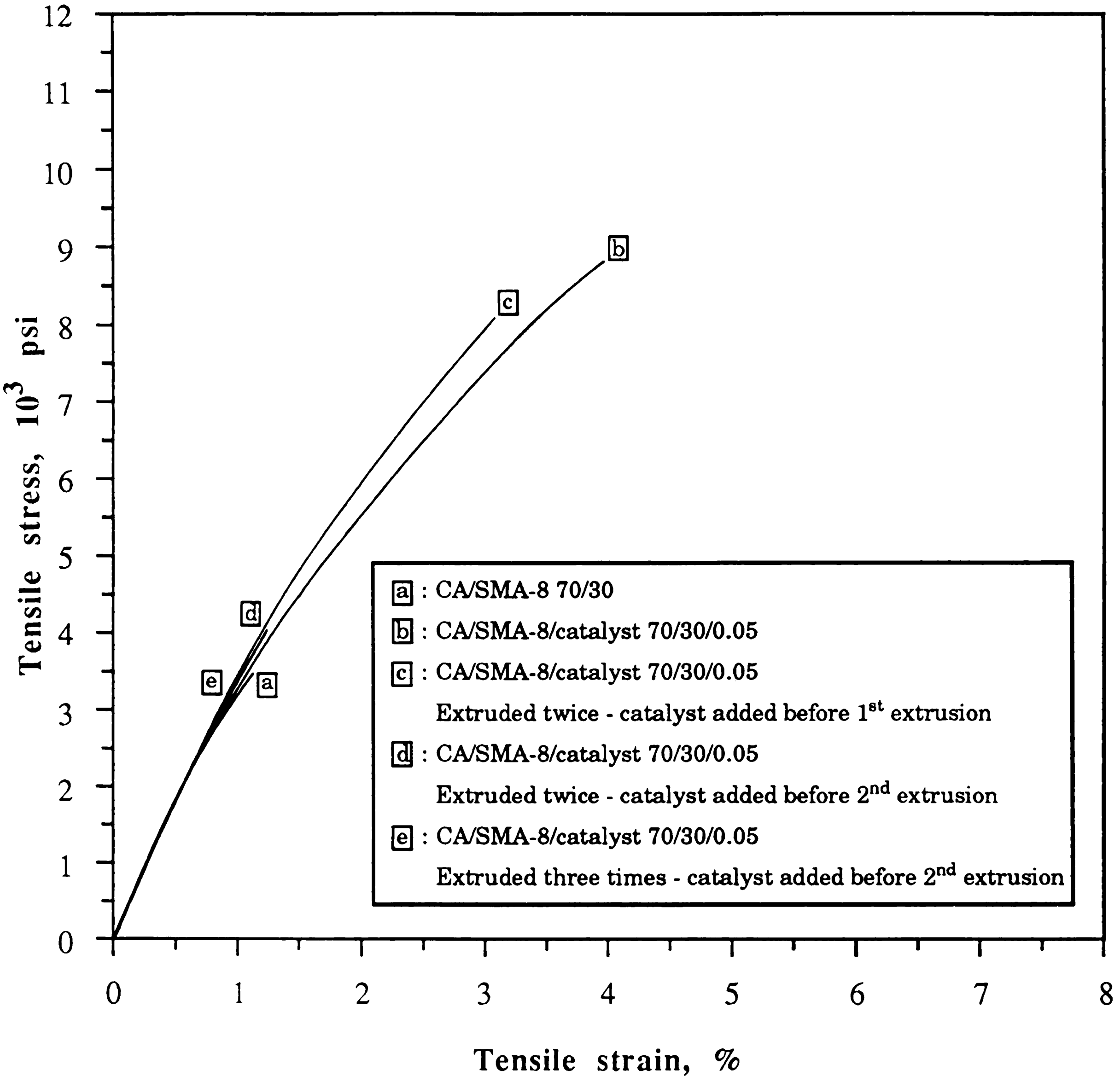

Figure 90: Stress-strain curves for CA blends.

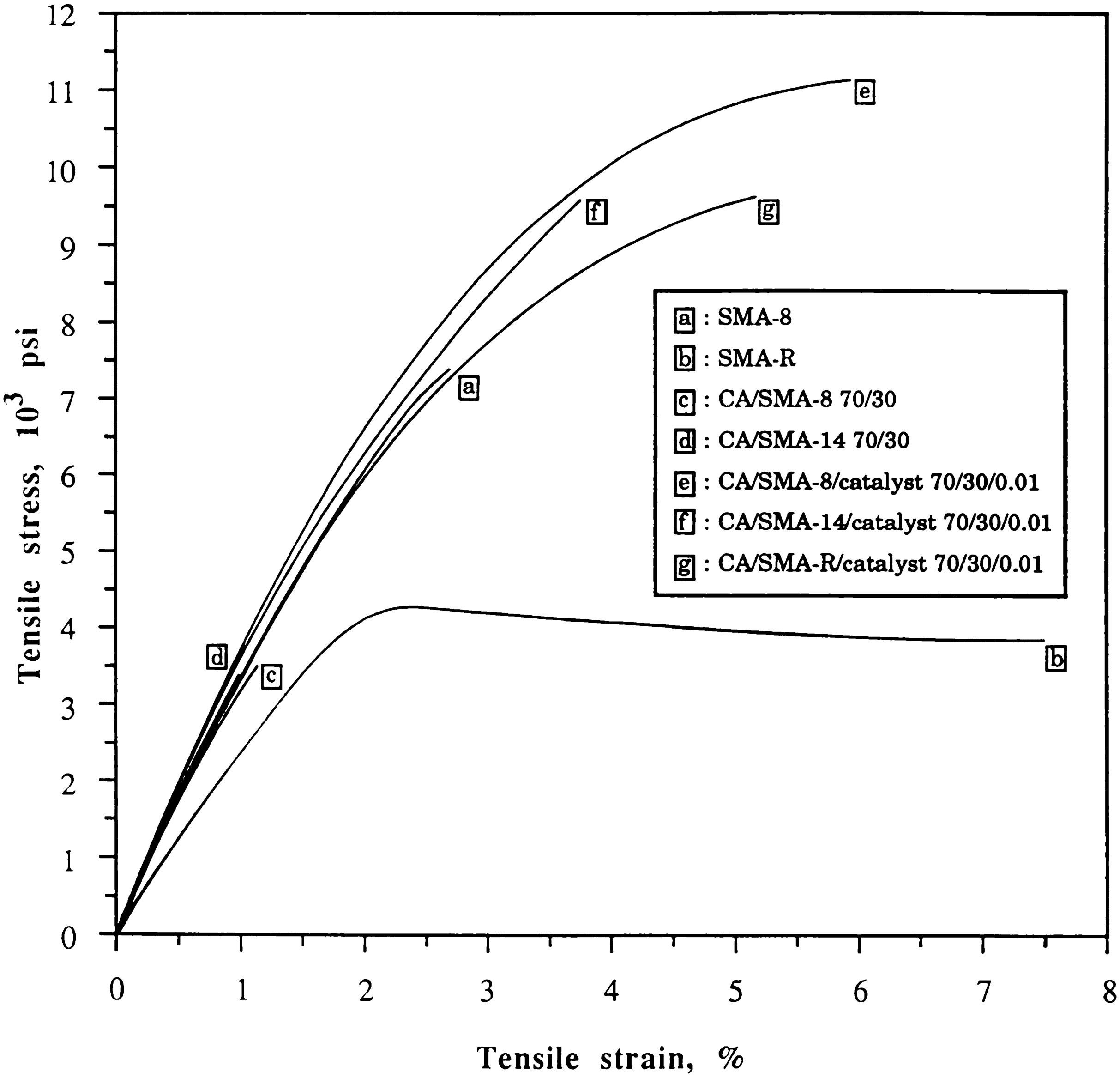

Figure 91: Stress-strain curves for CA blends.

The tensile strengths are compared in Figure 92. In Figure 92a, the tensile strength of Dexel (commercial grade CA having 33% plasticizer) is also included, so that it can be compared with the strength of the materials having approximately the same amount of SMA instead of the plasticizer.

The tensile strength of Dexel is lower than the strength of SMA-8. When CA was blended with SMA-8, the strength was much lower than that of SMA-8 and that of plasticized CA, because of the incompatibility of the two components of the blend (poor interfacial adhesion). When, however, catalyst was added, there was great improvement of the tensile strength, which in the case of 0.01% catalyst was close to 11,000 psi. The role of the grafting reaction in compatibilizing the blend was, therefore, very important. The high strength of the compatibilized material is attributed to the strength of the CA phase. This strength can not be observed if plasticizer is added, and can not be observed if SMA-8 is only blended with CA (because of incompatibility). The compatibilization of the blend (through a grafting reaction), so that the high strength of CA can be maintained, was one of the main goals of this work. It can also be noticed that higher tensile strength is observed for 0.01% catalyst content, compared to 0.05%. The reason for this can be due to the finer dispersion of the first case (Figure 74 compared to Figure 72), but also the degradation observed when 0.05% of catalyst was used.

Figure 92b shows the effect of different processing history on the tensile strength. Alloy B is alloy A extruded one more time. Although a finer dispersion was observed for alloy B (Figure 73 compared to Figure 72), the tensile strength was lower. This most probably was an effect of degradation (although the degradation was not much higher, possibly because some amount of catalyst evaporated during the first extrusion). A retention, however, of the high tensile strength (compared to the blend), can be claimed. Alloy C was prepared by extruding the CA/SMA-8 70/30 blend one more time with 0.05% catalyst. In this case, although better dispersion was observed, the tensile strength is only slightly higher than that of the blend. Increased degradation (maybe because of the continuity of the CA phase before the addition of catalyst) was most probably the reason for the low tensile strength. The tensile strength was even lower for alloy D (alloy C extruded one more time).

In Figure 92c the tensile strengths of blends having different SMAs are compared. There was an increase in strength for all materials where catalyst was added (even when the dispersed phase was SMA-R, which has lower strength than the other SMAs). Although SMA-14 gave the finest dispersion (Figure 81), the highest strength was observed with SMA-8. It is possible that there is an optimum size of the dispersed phase which gives the best strength. The above results suggest that the dispersed phase size of Figure 74 is closer to this optimum.

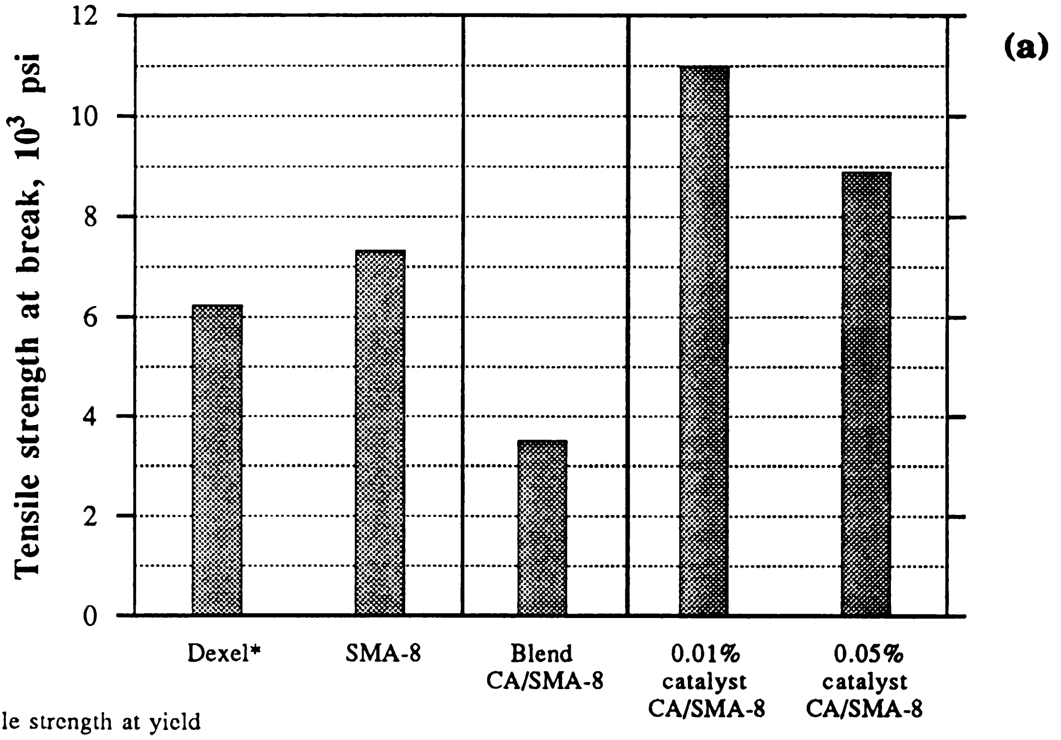

*: Tensile strength at yield

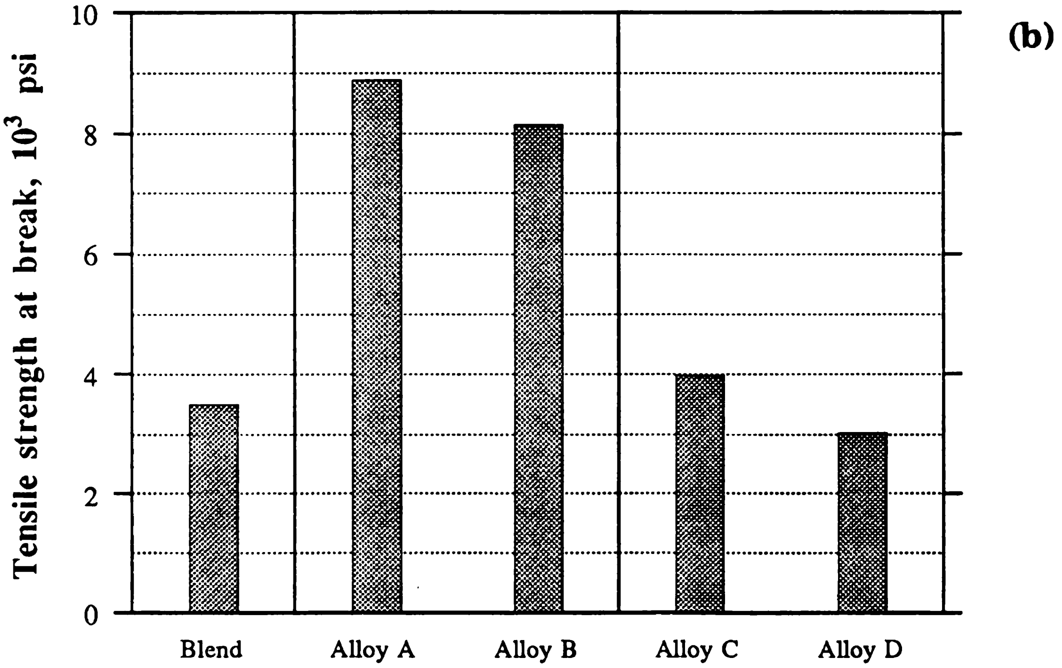

Blend: CA/SMA-8.

Alloy A: 0.05% catalyst CA/SMA-8.

Alloy B: 0.05% catalyst CA/SMA-8, extruded twice, the catalyst added before the 1st extrusion.

Alloy C: 0.05% catalyst CA/SMA-8, extruded twice, the catalyst added before the 2nd extrusion.

Alloy D: 0.05% catalyst CA/SMA-8, extruded three times, the catalyst added before the 2nd extrusion.

Figure 92: Tensile strength comparisons for the CA/SMA blends.

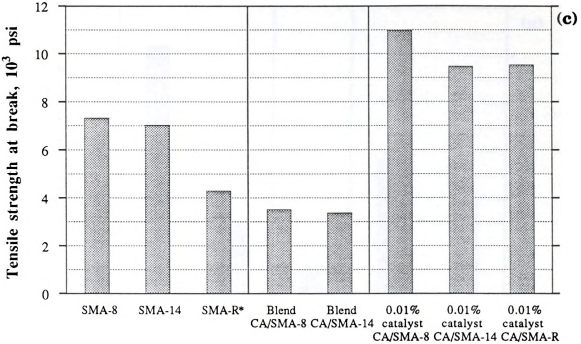

*: Tensile strength at yield

Figure 92: (cont'd).

In Figure 93, the elongations at break are compared. According to Figures 89, 90 and 91, brittle fracture was observed for all CA/SMA combinations (no yield point). For this reason the elongation results were in general similar to those of the tensile strength. Much higher elongation was observed when catalyst was added. The elongation of the compatibilized blends was lower than that of Dexel and SMA-R, but this was something expected because of the effect of the plasticizer and the rubber respectively. The presence of the rubber in the CA/SMA-R compatibilized blend also resulted in a relatively higher elongation (closer to that of CA/SMA-8 with 0.01% catalyst).

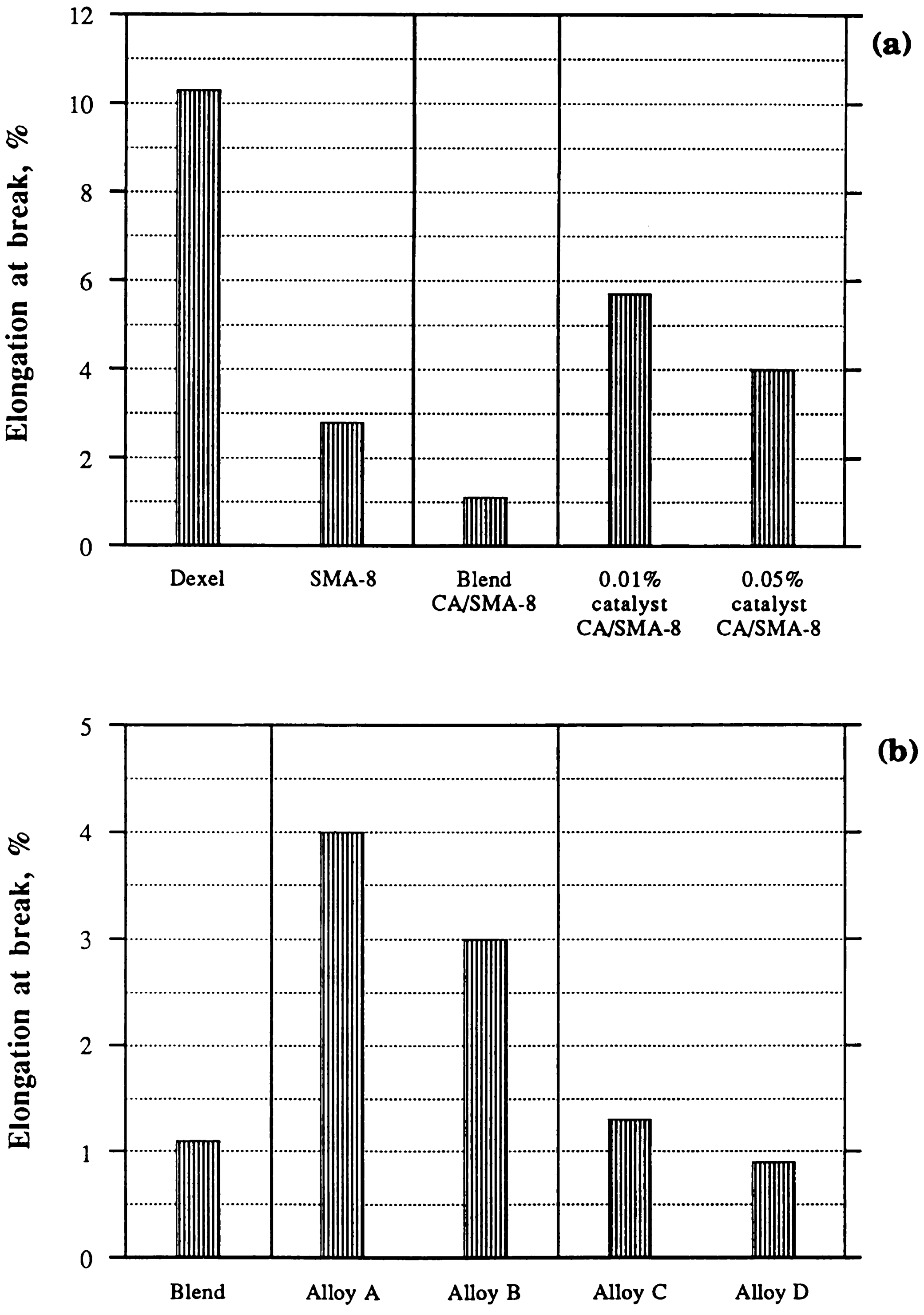

Blend: CA/SMA-8.

Alloy A: 0.05% catalyst CA/SMA-8.

Alloy B: 0.05% catalyst CA/SMA-8, extruded twice, the catalyst added before the 1st extrusion.

Alloy C: 0.05% catalyst CA/SMA-8, extruded twice, the catalyst added before the 2nd extrusion.

Alloy D: 0.05% catalyst CA/SMA-8, extruded three times, the catalyst added before the 2nd extrusion.

Figure 93: Elongation comparisons for the CA/SMA blends.

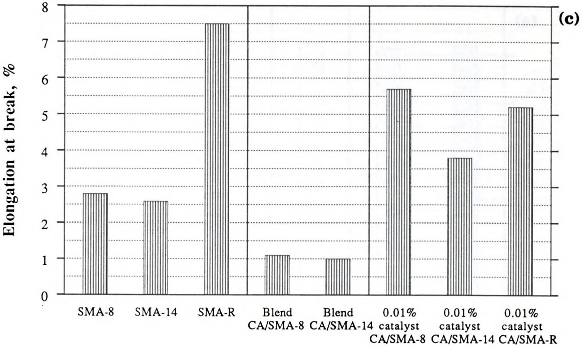

Figure 93: (cont'd).

Figure 94 compares the tensile modulus (Young's modulus) results. It can be noticed that, because of the stiffness of the CA phase, the modulus of the blends is higher than the modulus of Dexel and the modulus of the different SMAs. There is not, however, much difference between the moduli of the compatibilized and non compatibilized blends, which means that the adhesion or morphology change does not affect the modulus (as long as CA is the continuous phase). The use of SMA-R, instead of SMA-8 or SMA-14 which have higher modulus, could not be observed as a difference to the modulus of the compatibilized blend.

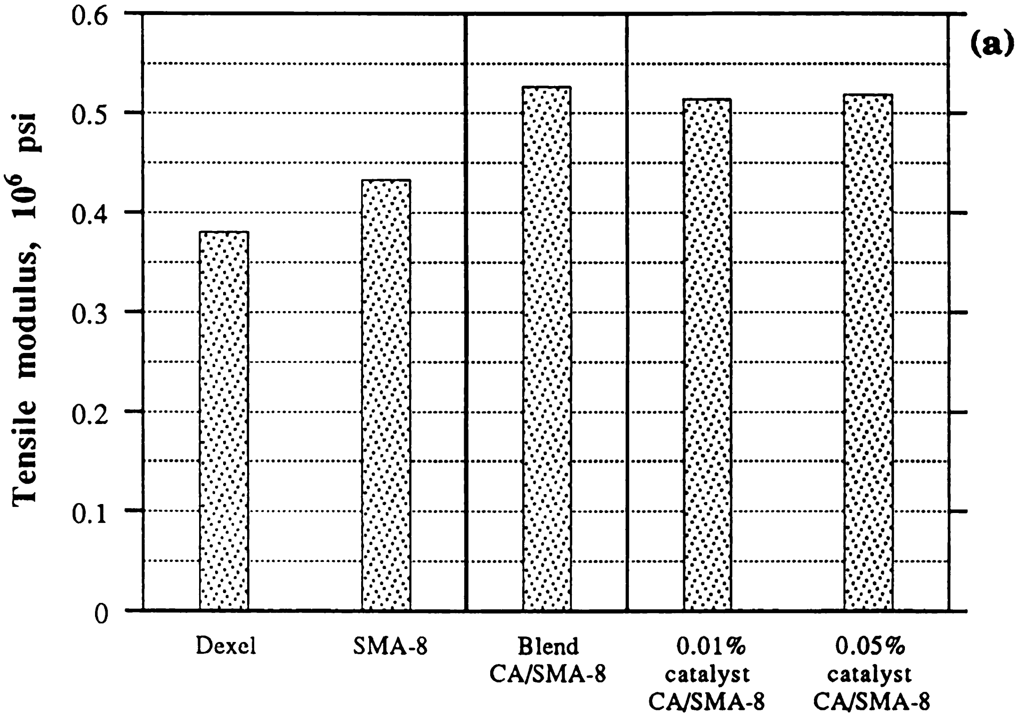

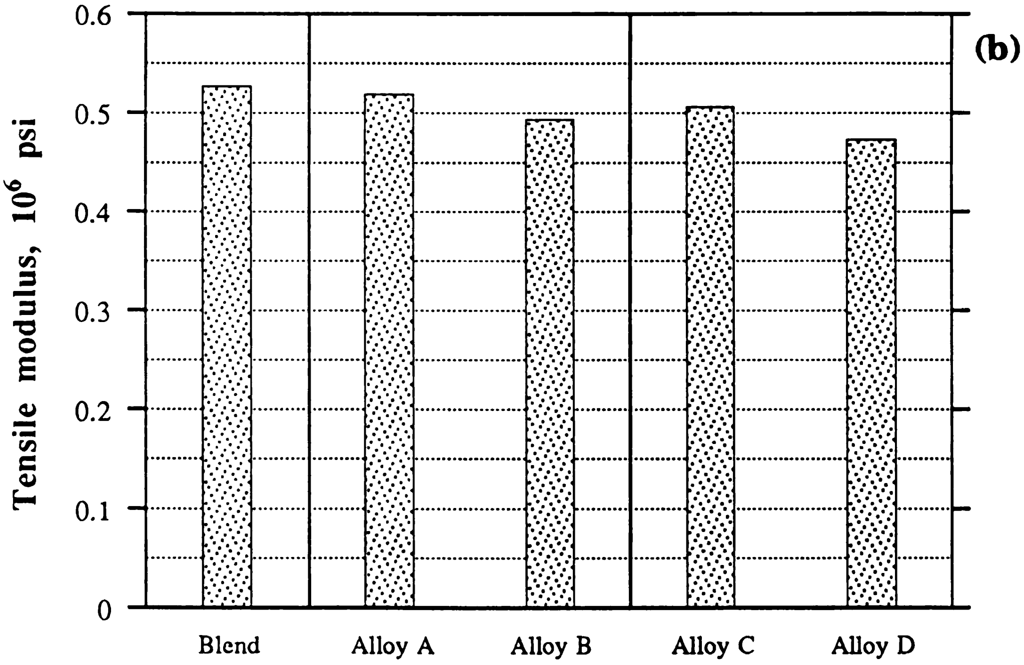

Blend: CA/SMA-8.

Alloy A: 0.05% catalyst CA/SMA-8.

Alloy B: 0.05% catalyst CA/SMA-8, extruded twice, the catalyst added before the 1st extrusion.

Alloy C: 0.05% catalyst CA/SMA-8, extruded twice, the catalyst added before the 2nd extrusion.

Alloy D: 0.05% catalyst CA/SMA-8, extruded three times, the catalyst added before the 2nd extrusion.

Figure 94: Tensile modulus comparisons for the CA/SMA blends.

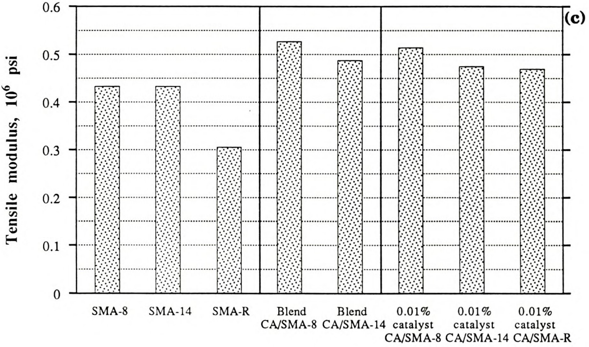

Figure 94: (cont'd).

In Figure 95, the Izod impact strengths of the materials are compared. In general, the relations are similar to those of the elongation. There is usually an optimum for the dispersed phase size which gives the highest impact strength. The results suggest that the dispersion being close to the optimum is that of the CA/SMA-8 blend with 0.01% catalyst, since this is the sample with the highest impact strength. It can also be noticed (Figure 95a) that the impact strength of this sample is close to the impact strength of Dexel. A crack pinning mechanism was observed for most of the compatibilized blends, and this is where the relatively high impact strength should be attributed.

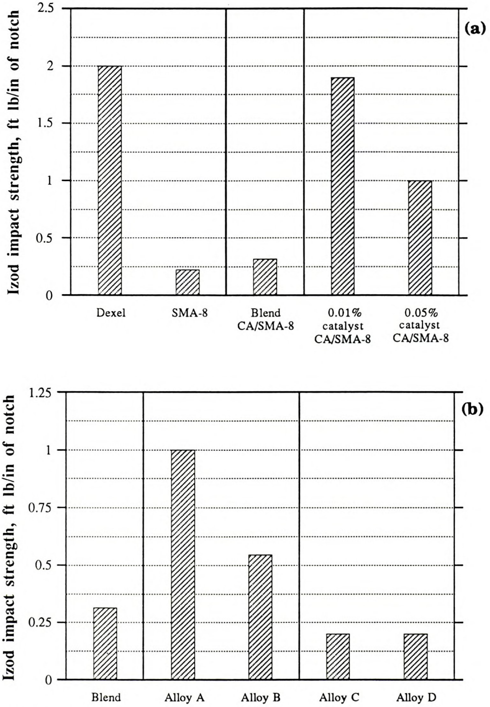

Blend: CA/SMA-8.

Alloy A: 0.05% catalyst CA/SMA-8.

Alloy B: 0.05% catalyst CA/SMA-8, extruded twice, the catalyst added before the 1st extrusion.

Alloy C: 0.05% catalyst CA/SMA-8, extruded twice, the catalyst added before the 2nd extrusion.

Alloy D: 0.05% catalyst CA/SMA-8, extruded three times, the catalyst added before the 2nd extrusion.

Figure 95: Izod impact strength comparisons for the CA/SMA blends.

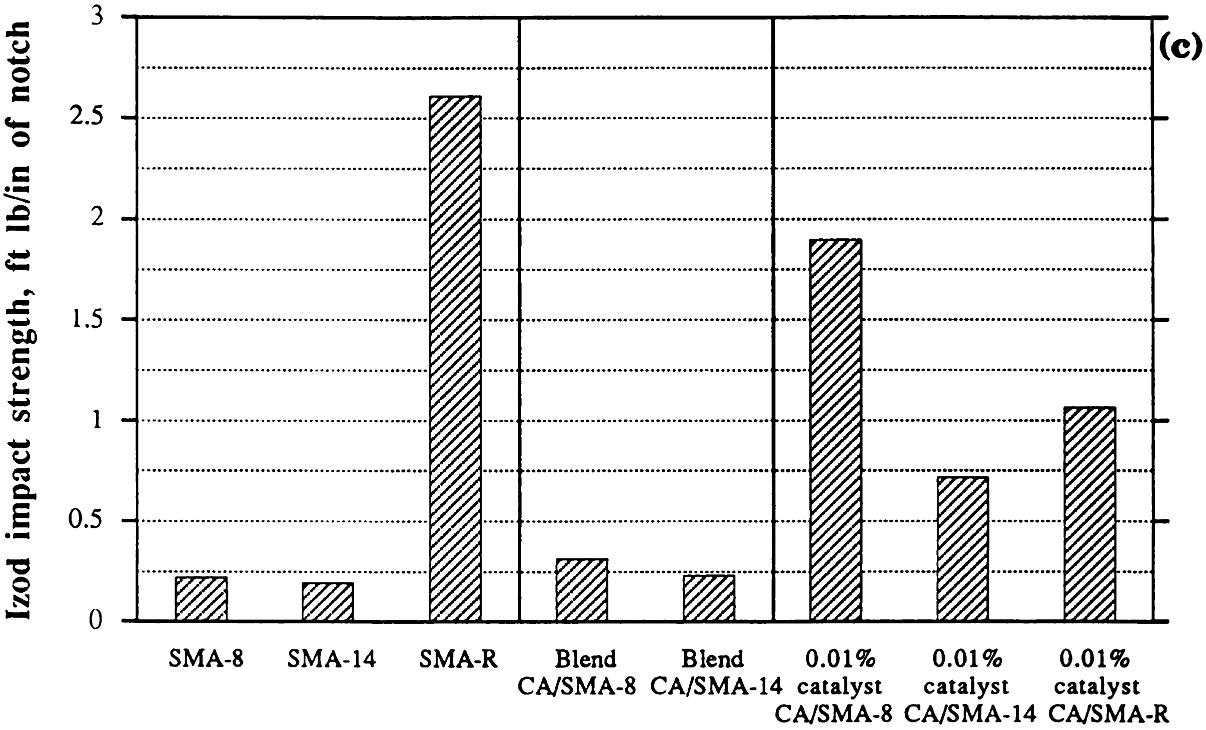

Figure 95: (cont'd).

In Table 9 of the appendix, the tensile and Izod impact strengths of most of the commercially available unfilled-unreinforced materials are given. From the materials developed during this work, the one having the best mechanical properties is the CA/SMA-8/DMAP 70/30/0.01 blend, with a tensile strength of 10,980 psi and impact strength of 1.89 ft lb/in of notch. Very few of the materials of Table 9 have such good properties. Tensile strengths close to this value are basically observed in the area of composites. The impact strength observed for this composition can also be considered high for a material having such a high tensile strength.

CONCLUSIONS AND RECOMMENDATIONS

Amylose composites

Twin-screw extrusion is an efficient method for distributing amylose granules in a thermoplastic matrix. The granules were not affected by the high-shear conditions of the mixing procedure (no significant changes to the size and shape of the granules were observed). According to SEM pictures, co-extrusion of amylose with SMA resulted in the desired matrix-filler adhesion. This was not the case when PS was used instead of SMA, which suggests that the reason for the adhesion was the MA functionality. This adhesion can be attributed to a reaction between the MA of SMA and the hydroxyl group of amylose. However, non covalent hydrogen bonded interactions between the hydroxyl groups of amylose and the anhydride groups of SMA is also possible. There were very few examples (and only with good adhesion) were the amylose granules broke when fracturing the resulting composites, which means that they are generally stronger than the matrix. They can, therefore, be considered a rigid particulate filler. The effect of water on the morphology of the materials was also observed. Water was found to destroy the granule structure and weaken the amylose phase.

Chapter 7

CONCLUSIONS AND RECOMMENDATIONS

Amylose composites

Twin-screw extrusion is an efficient method for distributing amylose granules in a thermoplastic matrix. The granules were not affected by the high-shear conditions of the mixing procedure (no significant changes to the size and shape of the granules were observed). According to SEM pictures, co-extrusion of amylose with SMA resulted in the desired matrix-filler adhesion. This was not the case when PS was used instead of SMA, which suggests that the reason for the adhesion was the MA functionality. This adhesion can be attributed to a reaction between the MA of SMA and the hydroxyl group of amylose. However, non covalent hydrogen bonded interactions between the hydroxyl groups of amylose and the anhydride groups of SMA is also possible. There were very few examples (and only with good adhesion) were the amylose granules broke when fracturing the resulting composites, which means that they are generally stronger than the matrix. They can, therefore, be considered a rigid particulate filler. The effect of water on the morphology of the materials was also observed. Water was found to destroy the granule structure and weaken the amylose phase.

No dramatic changes of the properties were observed. Compared to the base resin, the amylose composites were stiffer. This was expected because of the higher modulus of the granules. The modulus of amylose was estimated as being two to three times higher than the modulus of the matrix. An acceptable reduction of the tensile strength was also observed and a general retention of the impact strength (when the composites were compared to the base resin). The mechanical properties of composites with the same amylose content but with different MA level in the matrix (different level of adhesion) were also compared. The adhesion did not affect the tensile strength, but helped to increase the modulus (maybe because of the relatively small difference between the moduli of the matrix and the filler).

In general a retention of the properties can be claimed when the composites are compared to the base resin. These properties are only slightly affected by better matrix-filler adhesion. The reduction of the cost and the use of renewable resources are, however, advantages, which will probably be considered even more important in the near future.

Cellulose acetate blends

The case of CA was quite different compared to that of amylose. No interfacial adhesion was observed when CA was blended with SMA, a classical example of an incompatible blend. Many differences where, however, observed when a suitable catalyst was added, which suggests that a grafting reaction took place during the mixing of the materials in the extruder. This reaction occurred between the anhydride functionality of SMA and the hydroxyl group of CA, resulting in a half ester.

Lower interfacial tension, better adhesion, and different blend morphology were the results of reaction. Comparison of the equilibrium morphologies of the blends, showed that reduction of the dispersed phase size (SMA) was the main morphological characteristic of the reactive extrusion processing step. The finest dispersion (0.7 μm weight average) was observed with SMA-14, due to the higher MA content which resulted in more grafting reaction and lower interfacial tension. Better dispersion than the above should be expected for higher MA content, higher shear rate or different viscosities. It should, however, be noted that finer dispersion does not necessarily mean better properties. The amount of catalyst was found to affect the processing time needed for approaching the equilibrium morphology. Equilibrium was approached earlier when lower amount of catalyst was added.

There was generally a significant improvement of the mechanical properties by the addition of catalyst. Only the modulus was not affected by the reaction. The tensile strength, elongation and Izod impact strength were much higher for the compatibilized blends compared to the non-compatibilized ones. The best tensile strength was observed for the CA/SMA-8/DMAP 70/30/0.01 blend (~ 11,000 psi). Relatively high Izod impact strength was also observed for this material (1.89 ft lb/in of notch), basically due to a crack pinning mechanism.

Such high tensile strengths (~ 11,000 psi) are basically observed in the area of composites. Good impact strength was also observed, and these properties were achieved with no fiber reinforcement. The addition of 30% SMA improved the processibility (elimination of plasticizer), and lowered costs.

The high tensile strength of the compatibilized materials is due to the

strength of the continuous CA phase. This strength can not be obtained if a plasticizer is used. If CA is blended with SMA without the addition of a catalyst, the enhanced tensile strength observed can not be obtained because of the incompatibility of the blend (no interfacial adhesion). Reactive compatibilization of the CA/SMA blends was developed in situ, when mixing the two materials in a continuous and high speed process.

ADDENDIX

APPENDIX

Table 9: Tensile and Izod impact strength of unfilled-unreinforced commercially available plastics (from *Modern Plastics Encyclopedia '92*, McGraw-Hill, 1991).

	Tensile strength at break (10^3 psi)	Izod impact strength (ft lb/in of notch) (1/8 in thick specim.)
Acrylonitrile-butadiene-styrene (ABS)	2.5-8.0	1.4-12
High impact	4.4-6.3	6.0-9.3
ABS/PVC	4.3-6.6*	6.0-10.5
ABS/PC	5.8-9.3	4.1-12.0
Acetal	9.5-12.0*	1.2-2.3
Impact modified	7.5-9.4	2.7-17
Copolymer	8.8-10.4*	0.8-1.5
Impact modified	3.0-8.0*	1.7-2.8
Acrylic	8.0-11.5	0.2-0.4
Impact modified	5.0-9.0	0.4-2.5
Polymethyl methacrylate (PMMA)	7.0-10.5	0.2-0.4
Methyl methacrylate (MMA)-styrene copolymer	8.1-10.1	0.3-0.4
Acrylonitrile	9.0	2.5-6.5
Allyl diglycol carbonate	5.0-6.0	0.2-0.4
Cellulosic		
Ethyl cellulose (EC)	2.0-8.0	0.4
Cellulose acetate (CA)	1.9-9.0	1.0-8.5
Cellulose acetate-butyrate (CAB)	2.6-6.9	1.0-10.9
Cellulose acetate-propionate (CAP)	2.0-7.8	0.5-No break
Cellulose nitrate	7.0-8.0	5-7
Epoxy	4.0-13.0	0.2-1.0
Flexibilized	2.0-10.0	2.3-5.0
Ethylene vinyl alcohol (EVOH)	5.4-13.7	1.0-1.7

*: Tensile yield strength (it is higher than the tensile strength at break for this material, or it is the only available).

Table 9: (cont'd).

	Tensile strength at break (10^3 psi)	Izod impact strength (ft lb/in of notch) (1/8 in thick specim.)
Fluoroplastics		
Polychlorotrifluoroethylene (PCTFE)	4.5-6.0	2.5-5
Polytetrafluoroethylene (PTFE)	2.0-5.0	3
Polyfuoroalkoxy (PFA) fluoroplastic	4.0-4.3	No break
Fluorinated ethylene-propylene (FEP)	2.7-3.1	No break
Polyvinylidene fluoride (PVDF)	2.9-8.3*	2.5-80
Modified PE-polytetra fluoroethylene (TFE)	6.5	No break
PE-polymonochlorotrifluoroethylene (CTFE)	6.0-7.0	No break
Ionomer	2.5-5.4	7-No break
Ketones		
Polyaryletherketone	13.5	1.6
Polyetherether ketone (PEEK)	10.2-15.0	1.6
Phenolic	5.0-9.0	0.2-0.4
Polyamide (PA)		
Nylon 6	6.0-24.0	0.6-3.0**
Toughened	6.5**	16.4**
Copolymers and rubber modified compounds	6.3-11.0**	1.8-No break**
With molybdenum disulfide	11.5	0.9
Nylon 6,6	8.5-13.7**	0.5-1.5**
Toughened	7.0-11.0**	12.0**-19
Rubber modified compounds	7.5**	3-No break**
Nylon 6,6-6 copolymer	7.4-12.4**	0.7**
Nylon 6,9	8.5**	1.1**
Nylon 6,10	7.1-8.5*	0.9-2.3
Nylon 6,12	6.5-8.8**	1.0-1.9**
Toughened	5.5**	12.5**
Nylon 11	8.0**-9.5	1.8**-No break
Nylon 12	5.1-10.0**	1.0-No break
Aromatic polyamide (transparent)	7.6-14.0**	0.8-3.5**
Polyamide-imide (PAI)	16.2-22.0	1.2-2.7
Polybutylene (PB)	3.8-4.4	No break
Polycarbonate (PC)	9.1-10.5	12-16
Polyester copolymer	9.5-11.3	1.5-10
Impact modified PC/polyester	7.6-8.5	2-18
Polydicyclopentadiene	5.3-6.0	5.0-9.0
Polyester, thermoplastic		
Polybutylene terephthalate (PBT)	8.2	0.7-1.0
PCTA	5.9-9.0*	1.5-No break
Polyethylene terephthalate (PET)	7.0-10.5	0.2-0.7
PETG	6.3-7.1*	1.7-No break
Polyester/PC, high impact	4.5-9.0	12-19
Wholly aromatic (liquid crystal)	15.9-27.0	0.6-10

*: Tensile yield strength (it is higher than the tensile strength at break for this material, or it is the only available).

**: Dry, as molded (approximately 0.2% moisture content).

Table 9: (cont'd).

	Tensile strength at break (10^3 psi)	Izod impact strength (ft lb/in of notch) (1/8 in thick specim.)
Polyester, thermosetting		
Rigid	0.6-13.0	0.2-0.4
Flexible	0.5-3.0	>7
Polyetherimide (PEI)	15.2*	1.0-1.2
Polyethylene (PE)		
Low-density polyethylene (LDPE) and medium-density polyethylene (MDPE)		
Branched	1.2-4.6	No break
Linear copolymer	1.9-4.0	1.0-No break
Ethylene-vinyl acetate (EVA)	1.2-6.0*	No break
Ethylene-ethyl acrylate	1.6-2.1	No break
High-density polyethylene (HDPE)	3.8-4.8*	0.4-4.0
Copolymers	2.5-6.5	0.3-6.0
Ultra high MW	5.6-7.0	No break
Cross-linked	1.6-4.6	1-20
Polyimide (PI)		
Thermoplastic	10.5-17.1	1.5
Thermoset	4.3-22.9	0.6-15
Polymethylpentene (PMT)	2.0-4.7*	2-3
Polyphenylene oxide (PPO), modified	6.8-9.6	3-6
Impact modified	7.0-8.0	6-8
Polyphenylene sulfide (PPS)	7.0-12.5	<0.5
Polyphthalamide (PPA)	15.1*	1.0
Extra tough	10.8*	20
Polypropylene (PP)	4.5-6.0	0.4-1.4
Copolymer	4.0-5.5	1.1-14.0
Impact modified	3.5-5.0	2.2-No break
Polyallomer	3.0-3.8	1.7-3.8
Polystyrene (PS)	5.2-8.2	0.3-0.5
Rubber modified	1.9-6.2	0.9-7.0
Styrene-acrylonitrile (SAN)	9.9-12.0*	0.4-0.6
Olefin rubber modified	5.6-6.0*	13-15
Acrylic-styrene-acrylonitrile (ASA)	5.2-5.6*	9-11
ASA/PVC	6.3-6.7*	17-20
ASA/PC	6.6-6.8*	13
Styrene maleic anhydride (SMA)	5.2-8.1*	0.4-2.0
Impact modified	4.5-6.0*	2.5-6
SMA/PC	6.6-8.0*	10-12
Copolymers, high heat-resistant	7.1-8.1	0.4-0.6
Impact modified	4.6-5.8	1.5-4.0
PC blend	6.8-8.0	10-12
Styrene MMA	8.1-9.7	0.2-0.3

*: Tensile yield strength (it is higher than the tensile strength at break for this material, or it is the only available).

Table 9: (cont'd).

	Tensile strength at break (10^3 psi)	Izod impact strength (ft lb/in of notch) (1/8 in thick specim.)
Polyurethane (PU)		
Thermoset, liquid	0.2-10.0	25-Flexible
Thermoset, unsaturated	10.0-11.0	0.4
Thermoplastic	7.8-11.0*	1.5-1.8
PVDC copolymers	3.5-5.0	0.4-1.0
Barrier film resins	2.8-4.9	0.3-1.0
Silicone		
Silicone/nylon 6,6	10.1-12.5	0.8-0.9
Silicone/nylon 12	5.2-7.4	0.6-0.7
Silicone epoxy	0.5-8.0	0.3
Sulfone		
Polysulfone	10.2*	1.2
Polyarylsulfone	10.4-12.0*	1.6-12
Polyethersulphone (PES)	9.8-13.8	1.4-No break
Polyphenylsulfone	10.1	13
Modified Polysulfone	7.2-7.4*	7-No break
Thermoplastic elastomers (TPE)		
Polyolefin, low and medium hardness	0.6-2.5	No break
Polyolefin, high hardness	1.6-4.0*	5.0-16.0
Co-polyester	1.8-6.0	2.1-No break
Polyester	1.0-6.8	2.5-No break
Polyether-amide	2.0-7.0	4.3-No break
Styrene-butadiene or styrene-isoprene	3.7-4.4*	No break
Styrene-ethylene and/or butylene	0.6-3.0	No break
Silicone/PA	5.2-12.5	0.6-No break
Silicone/polyester	5.0	No break
Silicone/polyolefin	0.5-1.0	No break
Silicon/PS ethylene butadiene-styrene	1.0-3.3	No break
Silicone/PU	2.1-6.5	No break
Elastomeric alloys	0.6-4.0	No break
Vinyl		
Polyvinyl chloride (PVC), rigid	5.9-7.5	0.4-22
PVC, flexible	1.5-3.5	Wide range
Vinyl formal	10.0-12.0	0.8-1.4
Chlorinated polyvinyl chloride (CPVC)	6.8-9.0	1.0-5.6
Vinyl butyral, flexible	0.5-3.0	Wide range
PVC/acrylic	6.4-7.0	1-12

*: Tensile yield strength (it is higher than the tensile strength at break for this material, or it is the only available).

BIBLIOGRAPHY

BIBLIOGRAPHY

- Abate, G. F. and Heikens, *Polym. Commun.*, **24**, 137 (1983).

- Amdouni, N., Sautereau, H., Gerand, J. F., Fernagut, F., Coulon, G. and Lefebvre, J. M., *J. Mater. Sci.*, **25**, 1435 (1990).

- Argyropoulos, D., Nie, L. and Narayan, R.,presentation at AIChE 1991 Annual Meeting (1991).

- Bagley, E. B., Fanta, G. F., Burr, R. C., Doane, W. M. and Russell, C. R., *Polym. Eng. Science*, **17**, 311 (1977).

- Baker, W. E. and Saleem, M., *Polym. Eng. Sci.*, **27**, 1634 (1987).

- Ballegooie, P. V. and Rudin, A., *Polym. Eng. Sci.*, **28**, 1434 (1988).

- Barentsen, W. M., Heikens, D. and Piet, P., *Polymer*, **15**, 119 (1974).

- Barlow, J. W. and Paul, D. R., *Polym. Eng. Sci.*, **24**, 525 (1984).

- Broutman, L. J. and Sahu, S., *Mater. Sci. Eng.*, **8**, 98 (1971).

- Brown, S. B. and Orlando, C. M., in *Encyclopedia of Polymer Science and Engineering*, John Wiley & Sons, 1988, Vol. 14, p. 169.

- Campbell, J. R., Hobbs, S. Y., Shea, T. J. and Watkins, V. H., *Polym. Eng. Sci.*, **30**, 1056 (1990).

- Chang, F. C. and Hwu, Y. C., Polym. Eng. Sci., 31, 1509 (1991).

- Cheremisinoff, N. P., *Polymer Mixing and Extrusion Technology*, Marcel Dekker, 1987.

- Dekkers, M. E. J. and Heikens, D., *J. Mater. Sci.*, **18**, 3281 (1983a).

- Dekkers, M. E. J. and Heikens, D., *J. Appl. Polym. Sci.*, **28**, 3809 (1983b).

- Dekkers, M. E. J. and Heikens, D., *J. Mater. Sci.*, **19**, 3271 (1984).

- Dick, J. S., *Compounding Materials for the Polymer Industries*, Noyes Publications, 1987.

- Doane, W. M., *J. Coat. Technol.*, **50**, 88 (1978).

- Eastmond, G. C. and Mucciariello, *Polymer,* **23**, 164 (1982).

- Fanta, G. F., Bagley, E. B., in *Encyclopedia of Polymer Science and Technology,* John Wiley & Sons, Supplement, 1977, Vol. 2, p. 665.

- Fayt, R., Jérôme, R. and Teyssié, P., *J. Polym. Sci. Polym. Lett. Ed.*, **24**, 25 (1986).

- Fayt, R., Jérôme, R. and Teyssié, P., *Polym. Eng. Sci.*, **27**, 328 (1987).

- Flegler, L. S., Heckman, J. W., Jr. and Klomparens, K. L., *An Introduction to electron Microscopy,* MSU CEO, 1990.

- Francis, P. S. and Wambach, A. D., in *Engineering Materials Handbook*, ASM International, 1988, Vol. 2, p. 217.

- Gaylord, N. G., Ender, H., Davis, L. and Takahashi, A., in *Modification of Polymers*, ACS Symposium Series, 1980, p. 469.

- Goe, G. L., Hillstrom, G. F., Keay, J. G., McQuigg, D. W., Scriven, E. F. V. and Sowers, E. E., *Chemspec USA 90 Symposium* (1990).

- Griffin, G. J. L., in *New Approaches to Research on Cereal Carbohydrates*, Elsevier Science Publishers, 1985, p. 201.

- Hagarman, J., in *Modern Plastics Encyclopedia '92*, McGraw-Hill, 1991, p. 216.

- Han, C. D., *Multiphase flow in Polymer Processing*, Academic Press, 1981.

- Hojo, H., Toyoshima, W., Tamura, M. and Kawamura, N., *Polym. Eng. Sci.*, **14**, 604 (1974).

- Ide, F. and Hasegawa, A., *J. Appl. Polym. Sci.*, **18**, 963 (1974).

- Ishai, O. and Cohen, L. J., Int. *J. Mech. Sci.*, **9**, 539 (1967).

- Kienzle, S. Y., in *Polymer Blends and Alloys: Guidebook to Commercial Products*, Technomic Publishing, 1988, p. 1.

- Kim, J. H., Barlow, J. W. and Paul, D. R., *J. Polym. Sci. Polym Phys. Ed.*, **27**, 223 (1989).

- Kowalski, R. C., *ANTEC '90, Conf. Proc.*, 1902 (1990).

- Lavengood, R. E., Nicolais, L. and Narkis, M., *J. Appl. Polym. Sci.*, **17**, 1173 (1973).

- Leidner, J. and Woodhams, R. T., *J. Appl. Polym. Sci.*, **18**, 1639 (1974).

- Locke, C. E. and Paul, D. R., J. Appl. Polym. Sci., 17, 2791 (1973).

- MacKnight, W. J., Karasz, F. E. and Fried, J. R., in *Polymer Blends*, Vol. 1, Academic Press, 1978, p. 185.

- Manson, J. A. and Sperling, L. H., *Polymer Blends and Composites*, Plenum Press, 1976, p. 77.

- Meier, D. J., *Heterophase Polymer Systems*, Michigan Molecular Institute, Notes for Course 702, 1991.

- Mohanakrishnan, C. K., Narayan, R. and Nizio, J. D., presentation at AIChE 1991 Annual Meeting (1991).

- Nakamura, S. and Tobolsky, A. V., *J. Appl. Polym. Sci.*, **11**, 1371 (1967).

- Narayan, R., in *Emerging Technologies for Materials and Chemicals from Biomass*, ASC Symposium Series 476, 1991, p. 1.

- Neu, R. P., *The Use of Graft Copolymers as Compatibilizing Agents in the Cellulose Acetate - Polystyrene System*, M.S. Thesis, Purdue University, 1989.

- Olabisi, O., Robeson, L. M. and Shaw, M. T., *Polymer-Polymer Miscibility*, Academic press, 1979, p. 19.

- Otey, F. H., Westhoff, R. P. and Doane, W. M., *Ind. Eng. Chem. Prod. Res. Dev.*, **19**, 592 (1980).

- Paul, D. R., in *Polymer Blends*, Vol. 1, Academic Press, 1978a, p. 1.

- *Idib*, Vol. 2, 1978b, p. 35.

- Paul, D. R. and Barlow J. W., in *Polymer Compatibility and Incompatibility, Principles and Practices*, Harwood Academic Publishers, 1982, p. 1.

- Paul, D. R., Barlow, J. W. and Keskkula, H., in *Encyclopedia of Polymer Science and Engineering*, John Wiley & Sons, 1988, Vol. 12, p. 399.

- Paul, D. R., *Polymer Blends*, Michigan Molecular Institute, Notes for Course 1019, 1991.

- Phillips, D. C. and Harris, B., in *Polymer Engineering Composites*, Applied Science Publishers, 1977, p. 45.

- Rauwendaal, C., *Polymer Extrusion*, Hasner Publishers, 1986.

- Sawyer, L. C. and Grubb, D. T., *Polymer Microscopy*, Chapman and Hall, 1987.

- Sahu, S. and Broutman, L. J., *Polym. Eng. Sci.*, **12**, 91 (1972).

- Scott, C., Ishida, H. and Maurer, F. H. J., *J. Mater. Sci.*, **22**, 3963 (1987).

- Shaw, M. T., in *Polymer Blends and Mixtures, NATO ASI Series, Series E: Applied Sciences - No. 89*, Martinus Nijhoff Publishers, 1985a, p. 37.

- *Ibid.*, 1985b, p. 57.

- Spanoudakis, J. and Young, R. J., *J. Mater. Sci.*, **19**, 473 (1984).

- Subramanian, P. M. and Mehra, V., *Polym. Eng. Sci.*, **27**, 663 (1987).
- Taylor, G. I., *Proc. R. Soc. London, Ser. A*, **146**, 501 (1934).
- Thomas, E. L. and Talmon, Y., *Polymer*, **19**, 225 (1978).
- Toensmeier, P. A., *Mod. Plastics*, **65** (10), 62 (1988).
- Tsoganakis, C., *Adv. Polym. Technol.*, **9**, 321 (1989).
- Tsubokawa, N. and Kogure, A., *J. Polym. Sci. Polym. Chem. Ed.*, **29**, 697 (1991)
- Walker, B. M., in *Handbook of Fillers for Plastics*, Van Nostrand Reinhold Company, 1987, p. 420.
- Westhoff, R. P., Otey, F. H., Meltretter, C. L. and Russell, C. R., *Ind. Eng. Chem., Prod. Res. Dev.*, **13**, 123 (1974).
- Wu, S., in *Polymer Blends*,Vol. 1, Academic Press, 1978, p. 243.
- Wu, S., *Polymer*, **26**, 1855 (1985).
- Wu, S., *Polym. Eng. Sci.*, **27**, 335 (1987).
- Young, A. H., in *Starch: Chemistry and Technology*, Academic Press, 1984, p. 249.
- Young, R. J., in *Structural Adhesives: Developments in Resins and Primers*, Elsevier Applied Science Publishers, 1986, p. 163.
- Xanthos, M., *Polym. Eng. Sci.*, **28**, 1392 (1988).
- Xanthos, M., Young, M. W. and Biesenberger, J. A., *Polym. Eng. Sci.*, **30**, 355 (1990).

MICHIGAN STATE UNIV. LIBRAR
31293017069810